非補強レンガ積みの曲げ、せん断およびねじり挙動に対するポリプロピレンバンドの補強効果

STRENGTHENING EFFECT OF POPYPROPYLENE BANDS ON BENDING, SHEAR, AND TORSIONAL BEHAVIORS

非補強レンガ積みの曲げ、せん断およびねじり挙動に対するポリプロピレンバンドの補強効果

by

TA QUY HUNG

A Dissertation Submitted in Partial Fulfillment

of the Requirements for the Degree of

Doctor of Philosophy

Division of Engineering

MURORAN INSTITUTE OF TECHNOLOGY

Muroran, JAPAN

-March, 2024-

ACKNOWLEDGEMENTS

Foremost, I wish to express first of all deep gratitude to my supervisor Professor Mizoguchi Mitsuo for the continuous support of my Doctoral Course study and research, for this patience, motivation, enthusiasm, immense knowledge and sharing his experience. His guidance helped me in all the time of research and writing of this thesis. I could not have imagined having a better advisor and mentor for my Doctoral Couse study.

Beside my supervisor, I would like to thank to the professors in my committee members for their encouragement, insightful comments, and hard questions. Absolutely, their comments and advises have helped me to improving the quality of the research.

My completion of this project could not have been accomplished without the support from Japanese Government. The author also especially thanks to Japanese Government for providing scholarship to support me finishing this research.

I would like to thank to Mr.Endo, Ms.Noda, Ms.Chiba and of all members have been working at Center for International Relations because making my life at Muroran became actually agreeable and comfortable. They were always enthusiastically of helping in every situation when I need them.

I thank to Assoc.Prof Yamaji Naoko, Assoc.Prof Ono Masatsugu, who helped me to improvable ability Japanese language. Therefore, I can better understand the unique culture and character of Japanese people.

I would like to say thanks to Dr. Duong Quang Hung, who had recommended and his guidance into the proceeding making documents created a great opportunity for me could be continue the studying way.

I thank my fellow labmates: Mr.Yano, Ms.Matsubarashi, Mr.Miyoshi for the simulating discussions, for the sleepless nights we were working together before deadline, and for all

the fun we have had together. Especially, I also thanks to Mr. Kochan, who is my tutor he was helped me so much in during Master course time of living at Muroran.

Last but not the last, my family: dad, mom and younger sister because of you guys, my word is always pleasant and my journey is never impossible when receiving the encouragement from them it is a large motive with me to overcome all challenges and difficulties. I think of that was not occurred may be my studying become more difficult. From my heart, I acknowledge that good things.

LIST OF TABLES

LIST OF FIGURES

ABSTRACT

Vietnam is a country, with most of its territory facing the sea. Earthquakes are not considered high-priority disaster. However, severe winds from typhoons and tropical storms are responsible for extensive damage. Typhoon alone account for 80% of all disaster-related damage in the country. In addtion, the strength and frequency of typhoons have been gradually increasing in recent years, which creates more risks to humanity and the economy. In the types of houses were damaged by typhoon, studies have pointed out that 70% of them are semi-permanent house with break structures. We researched a strengthening method using Polypropylen (PP) band to prevent housing damage caused by strong winds. In this study, we have developed a new method of fixing PP band to brick. The PP band is sandwiched between two flat steel washers and fastened with a steel screw to plastic plug embedded in the side of the brick. A total of 49 specimens used to study the influence of PP band on flexural, shear, and torsional behavior of brick masonry. Nine prism specimens to the flexural failure test. Thirty triplet specimens were used in the shear behavior test and in torsion behavior test was ten specimens. The results show that PP band using our proposed method of fastening was significantly effective in increasing the bending behavior and ductility, as well as improving the shear and torsional strength of the specimens. In order to provide further insights into behavior, preliminary nonlinear numerical simulations are also implemented, using the parameters obtained from the tests. The numerical models employ simplified micro-modelling approach. The accurary in the main behavioral characteristics and failure modes is ascertained.

CHAPTER 1. INSTRODUCTION

1.1. General

Most of the residential houses are conducted with unreinforced brick masonry in many typhoon regions. These structures are not safe against wind loading. Recent climate change has caused serious damage to people and masonry houses in most countries, especially developing countries. Earthquakes and typhoons occur more frequently and with increasing intensity. Putting people in constant danger. In Vietnam, earthquakes are not considered the main factor causing serious consequences but typhoons are. The length of Vietnam's territory is more than 3,240 km, all adjacent to the sea. Every year, there are on average about four to six storms, two or three of which are high intensity typhoons that can destroy houses. Therefore, research measures to strengthen houses to resist strong winds is a necessary issue. Currently, there are many ways to strengthen houses made from masonry bricks such as reinforced concrete, mortar layer, vertical reinforcement, external post-tensioned technique, and external FRP reinforcement methods. However, these methods are not suitable for application in developing countries like Vietnam due to technical requirements, high price. PP band has emerged as an effective material for reinforcement, feasibility in construction and ease of use. In the literature, some researchers have studied the use of PP band to reinforce masonry house structures, but most of them are in earthquake conditions and there has been no research related to the effects of typhoon. That is also the main reason for us to conduct this study.

In addition, in those studies, the method of fixing PP bands on the specimens can be improved to maximize more the tensile strength of PP bands. Therefore, a new immobilization method was proposed.

1.2. Overview of the current typhoon situation

There are 58 provinces and five centrally governed cities in Vietnam. In this survey, the provinces and municipalities are divided into the following six major regions and eight sub-regions.

a) Northern region (North-West/ North-East)
b) Red river delta region
c) Central region (North-Central/South-Central)

d) Central Highland region

e) South-East region (Dong Nai river basin)

f) Mekong river delta region

Figure 1.1. Regional map in Vietnam. Source: Wikipedia

The central region and the central highland region do not overlap. The regions are divided into more detailed regions as necessary. Figure 1.1 demonstrates the division described above. **Table 1.1** indicates the provinces according to the defined regions.

Region	Sub-region	Province or municipality
North	North-West	Hoa Binh, Son La, Dien Bien, Lai Chau, Lao Cai, Yen Bai
	North-East	Phu Tho, Ha Giang, Tuyen Quang, Cao Bang, Bac Kan, Thai Nguyen, Lang Son, Bac Giang, Quang Ninh
Red River Delta		Vinh Phuc, Ha Noi, Bac Ninh, Ha Nam, Hung Yen, Hai Phong, Hai Duong, Thai Binh, Nam Dinh, Ninh Binh.

Central	North-Central	Thanh Hoa, Nghe An, Ha Tinh, Quang Binh, Quang Tri, Thua Thien Hue
	South-Central	Da Nang, Quang Nam, Quang Ngai, Binh Dinh, Phu Yen, Khanh Hoa, Ninh Thuan, Binh Thuan
Central Highland		Kon Tum, Gia Lai, Dak Lak, Dak Nong, Lam Dong
South-East		Ho Chi Minh, Ba Ria Vung Tau, Binh Duong, Binh Phuoc, Dong Dai, Tay Ninh.
Mekong Delta		An Giang, Bac Lieu, Ben Tre, Ca Mau, Can Tho, Dong Thap, Hau Giang, Kien Giang, Long An, Soc Trang, Tien Giang, Tra Vinh, Vinh Long.

Source: Prepared by JICA survey team based on annual statistic data of MARD

Table 2.2. shows the risk level of natural disasters in each region published by the Government of Vietnam. The risk levels of storms and floods in the coastal area are relatively high. The risk levels of drought in high altitude regions such as the North-West, Central Highlands and South-Central regions are high. The risk levels of seawater intrustion, inundation and landslide (which may include coastal erosion and land subsidence) in the Mekong Delta region are high because of the low plain and large-scale rivers.

Table 1.2. Risk level of natural disasters in each region

Disaster type	North Mountain	North-East (Red river)	North-Central	South-Central	South-East	Central Highland	Mekong Delta	Other coastal
Storms	+++	++++	++++	++++	+++	++	+++	++++
Floods	-	++++	++++	+++	+++	+++	++++	++++
Flash floods	+++	-	+++	+++	+++	+++	+	+++
Typhoons	++	++	++	++	++	+	++	++
Drought	+++	+	++	+++	+++	++	+	+++
Desertification	-	-	+	++	++	++	+	++
Saline Intrusion	-	+	++	++	++	+	+++	++
Inundation	-	+++	++	++	++	-	+++	+++
Landslides	++	++	++	++	++	+	+++	++

Storm surges	-	++	++	++	++	++	+++	++
Forest fires	++	+	++	+++	+++	-	+++	+++
Environmental and industrial disasters	-	++	++	++	+++	+++	++	+++

Note: ++++; extreme danger; +++: danger; ++: moderate danger; +: less danger; -: safety

Source: UNDP, 2015 (Original: UNISDR, 2004)

Located in the tropical monsoon area of the northwestern Pacific, Vietnam is well known as one of the most likely to disaster happen in the world. Period researched was included war for independent (1964 – 1975), so damages in that may be exaggerated.

Based on database source of CRED, EM-DAT, period from 1964 to 2014 more than 254 disasters occurred have caused 84,836,083 people affected including deaths (27,329 people), injured (15,422 people), homeless (4,766,345 people). It can be important seen that Vietnam has been suffered dramatically by natural disasters 189 natural disasters recorded nearly three times to technology disasters (65 events) and were root of 25,097 deaths (91,83% in total). Besides that the damages were calculated $10,619,282 affected (80,054,316 people).

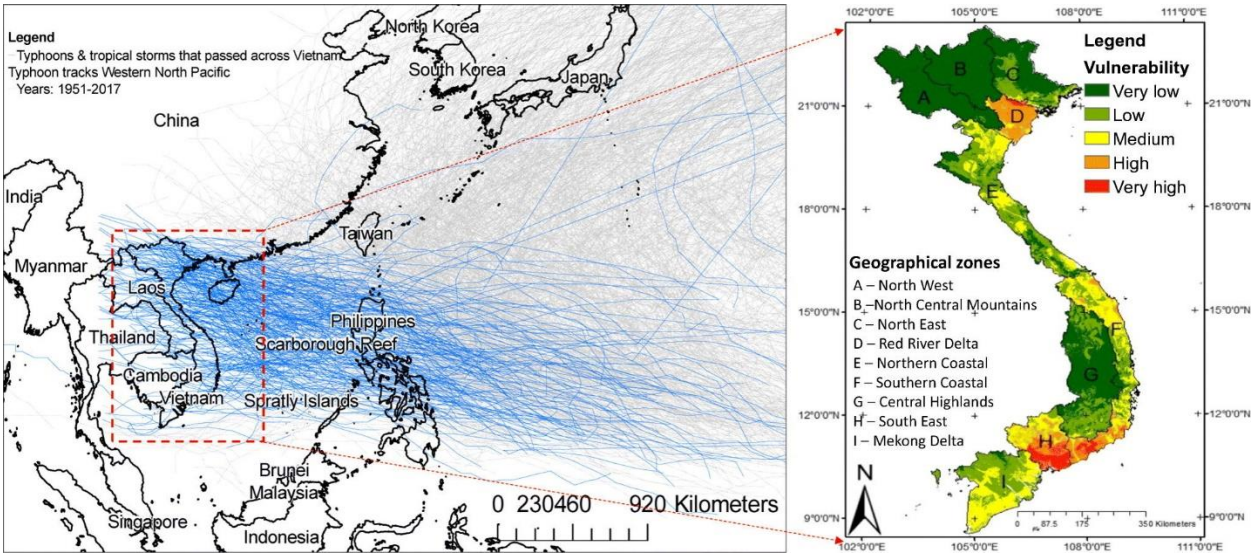

Figure 1.2. Track of storms landed Vietnam region

Vietnam is located in the tropical monsoon area, considered one of five storm hubs of Pacific Asia, and is regularly faced with various disasters such as: flood, flash flood, storm, storm

surge, tropical depression, and inundation, whirlwind, coastline erosion, hail rain, drought, landslide, forest fire.

Trend of natural disasters occur: As can be seen from statement from the Report: Country Disaster Response Handbook, author expressed because of increasing significantly of climate change in Vietnam in recent years, hazard natural has intensified not only magnitude, frequency but also volatility such as rising rainfall events, very high frequency of floods and flash floods, seasonal river floods and coastal floods in almost regions of this country. And on the report of Government 2004 also mentions that global climate change rose dramatically disaster events from late 1990s, and leading loss of live, livehoods, and property. In general, on the whole country catastrophe hazards natural occur heavily on water related disasters such as flood and flash flood or storm and drought. Moreover, each region in the country has suffered more different disasters such as: in the Northern mountain (the Red river) was subjected to extensive landslides, fire, silting, whirlwind, inundation as 80 percent areas is covered by hill and mountain's terrain combined; in the Coastal central provinces with narrow plains separated, sloping topography were subjected to salt penetration, whirlwind, inundation, fire, industrial and environmental hazard; in the Southern Delta (Mekong river) with large areas mangroves were enduring with whirlwinds, landslides, forest fires, sea water intrusion, prolonged deep inundation, river bank erosion; opposite to above areas, in the Central high regions with almost mountain surrounding were faced to forest fires, landslides, whirlwinds and industrial and environmental hazard significantly.

1.2.1. Typhoons in the past

Eighty-six typhoons made landfall in the 25 years from 1997 to 2022 (Table 1.3). It means 3.3 typhoons per year on average. Among them, Typhoon Linda that struck the Mekong delta caused historical damage in 1997. Typhoon Linda and the recent typhoons are listed below.

Table 1.3. Typhoons in the past 20 years

Year	No	Name	Affected area
2022	1	Typhoon Noru	Thua Thien Hue, Da Nang
	2	Tropical storm Sonca	Da Nang, Quang Ngai

2021	1	Tropical storm Koguma	Thanh Hoa
	2	Tropical storm Conson	Da Nang
	3	Tropical storm Dianmu	Thua Thien Hue, Binh Dinh
	4	Low tropical depression	Thua Thien Hue, Khanh Hoa
2020	1	Tropical storm Sinlaku	Nghe An
	2	Tropical storm Noul	Quang Tri, Thua Thien Hue
2019	1	Tropical storm Mun	Thanh Hoa
	2	Tropical storm Wipha	Quang Ninh
	3	Tropical storm Podul	
	4	Tropical storm Kajiki	Thua Thien Hue
	5	Tropical storm Matmo	Quang Ngai, Binh Dinh
	6	Tropical storm Nakri	
2018	1	Tropical storm Son Tinh	Thanh Hoa, Nghe An
	2	Tropical storm Bebinca	Nghe An
	3	Tropical storm Toraji	Khanh Hoa
	4	Tropical storm Usagi	Can Tho
2017	1	Typhoon No.2 (Talas)	Thanh Hoa – Quang Binh
	2	Typhoon No.4 (Sonca)	Ha Tinh – Quang Tri
	3	Typhoon No.10 (Doksuri)	Nghe An – Thua Thien Hue

	4	Typhoon No.12 (Damrey)	Khanh Hoa, Dak-lak, Lam Dong
	5	Typhoon No.14 (Kirogi)	Off-shore of Ninh Thuan – Ba Ria Vung Tau
2016	1	Typhoon No.1 (Mirinae)	Thai Binh – Ninh Binh
	2	Typhoon No.2 (Dianmu)	Hai Phong – Thai Binh
	3	Typhoon No.4 (Rai)	Da Nang – Quang Ngai
	4	Low tropical depression	Quang Tri - Da Nang
2015	1	Typhoon No.1 (Kujira)	Nam Dinh, Thai Binh, Hai Phong, Quang Ninh
	2	Typhoon No.3	Quang Nam, Quang Ngai
2014	1	Typhoon No.2 (Rammasun)	Cao Bang, Lang Son
	2	Typhoon No.3 (Kalmaegi)	Quang Ninh, Lao Cai, Yen Bai, Ha Giang
	3	Typhoon No.4 (Sinlaku)	Binh Dinh, Phu Yen
2013	1	Typhoon No.2 (Bebinka)	Hai Phong, Ha Tinh
	2	Typhoon No.5 (Jebi)	Quang Ninh
	3	Typhoon No.6 (Mangkhut)	Thanh Hoa
	4	Typhoon No.8(Noname)	Thua Thien Hue, Quang Nam
	5	Typhoon Wutip	Ha Tinh, Quang Binh, Quang Tri
	6	Typhoon No.11 (Nari)	Da Nang, Binh Dinh

	7	Typhoon No.14 (Haiyan)	Quang Ninh
	8	Typhoon No.15 (Podul)	Khanh Hoa, Ninh Thuan
2012	1	Typhoon No.4	Northern mountainous area
	2	Typhoon No.5 (Kai-tak)	Quang Ninh
	3	Typhoon No.7(Gaemi)	Binh Dinh, Phu Yen, Gia Lai
	4	Typhoon No.8 (Sontinh)	Quang Ninh, Hai Phong
	5	Typhoon Pakhar	Binh Thuan, Ca Mau
2011	1	Typhoon Nock-ten	Thanh Hoa
	2	Typhoon Nesat	Quang Ninh, Hai Phong
	3	Typhoon Haitang	Quang Tri, Thua Thien Hue
2010	1	Typhoon Basyang	Hai Phong, Thai Binh, Nam Dinh
	2	Typhoon Mindulle	Nghe An, Quang Binh
2009	1	Typhoon Soudelor	Quang Ninh, Hai Phong
	2	Typhoon Mujigae	Thai Binh, Thanh Hoa
	3	Typhoon Ketsana	Quang Nam, Quang Ngai
	4	Typhoon Parma	Quang Ninh, Nam Dinh
	5	Typhoon Mirinae	Da Nang
2008	1	Typhoon Kammuri	Quang Ninh
	2	Typhoon Mekkahla	Ha Tinh, Quang Binh
	3	Typhoon Noul	Khanh Hoa, Ninh Thuan
2007	1	Typhoon Toraji	Quang Ninh
	2	Typhoon Lekima	Ha Tinh, Quang Binh
2006	1	Xangsane	Da Nang, Quang Nam, Quang Ngai, Thua Thien Hue
	2	Durian	Ba Ria Vung Tau, Ben Tre, Tien Giang, Vinh Long, Bac Lieu,..

2005	1	Typhoon Damrey	Quang Ninh, Thanh Hoa
	2	Typhoon Vicente	Nghe An, Quang Binh
2004	1	Typhoon Chanthu	Quang Ngai
	2	Typhoon Muifa	Ca Mau, Bac Lieu, Kien Giang
2003	1	Typhoon Koni	Quang Ninh, Thanh Hoa
	2	Typhoon Krovanh	Quang Ninh, Thanh Hoa
	3	Typhoon Nepartak	Quang Ninh, Thanh Hoa
	4	Low tropical depression	Nghe An, Quang Binh
2001	1	Typhoon Usagi	Nghe An, Quang Binh
	2	Typhoon Lingling	Binh Dinh, Ninh Thuan
	3	Typhoon Kajiki	Quang Tri, Quang Ngai
2000	1	Typhoon Wukong	Nghe An, Quang Binh
	2	Typhoon Kaemi	Quang Tri, Quang Ngai
1999	1	Typhoon Eve	Quang Binh
	2	Low tropical depression	Binh Thuan, Ca Mau
	3	Low tropical depression	Binh Dinh, Ninh Thuan
1998	1	Typhoon Chip	Ninh Thuan
	2	Typhoon Dawn	Khanh Hoa
	3	Typhoon Elvis	Binh Dinh, Phu Yen
	4	Typhoon Faith	Phu Yen, Khanh Hoa
1997	1	Typhoon Zita	Quang Ninh, Thanh Hoa
	2	Typhoon Fritz	Quang Tri, Quang Ngai
	3	Low tropical depression	Quang Ngai, Binh Dinh
	4	Typhoon Linda	Binh Thuan, Ca Mau

Source: MONRE HP

1. **Typhoon Linda (November 1997)**

Typhoon Linda which struck the Mekong delta on November 1 to 2, 1997 brought historical damage to the area. The southernmost province, Can Tho, recorded 233 mm of rainfall and suffered from inundation widely spreading into farmland. A huge number of fishermen died in the sea because they hadn't experienced such a devastating typhoon and couldn't evacuate adequately. A fishing village lost most of the adult men. The damage included not only river flooding and inundation but also collapse of houses and felled trees caused by strong wind.

- Death/missing: 3,111 people
- Affected people: over 1 million people
- Collapsed house: 77,000 house
- Shipwreck/capsized: 3,078 boats
- Total economic loss: VND 7,180 billion

2. **Typhoon Doksuri (September 2017)**

On September 15, 2017 Typhoon Doksuri landed in Central Vietnam and hit Ha Tinh and Quang Binh provinces. It raised the sea level due to low-pressure and tidal waves generated by strong wind (maximum wind speed: 135 km/h) broke coastal dikes in many places. Costal dikes were broken along the coast extending from Hai Phong province to Thua Thien Hue province, a length of 55 km in total.

3. **Typhoon Damrey (November 2017)**

Typhoon Damrey landed on Khanh Hoa province on November 4, 2017 and severely damaged the central region. Damage in Khanh Hoa, Phu yen, Binh Dinh, Quang Ngai, Thua Thien Hue, Quang Nam and Da Nang provinces was relatively enormous. A lot of power poles fell due to the strong storm that caused prolonged blackout.

- Human damage: Deaths 10, missing 19, evacuation 35,000.
- Houses: Inundated/partially destroyed 137,836 houses, fully destroyed 3,483 houses.
- Agriculture: 33,153 ha including 9,163 ha of paddy and 20,783 ha of vegetables
- Infrastructure: Canals/dikes: 128 km

1.2.2. Disaster trend analysis

1.2.2.1. Trend of climate

A time series of annual total number of storms and tropical depressions that approached Vietnam in the past 30 years (1988-2017) is shown in Figure 1.3. Annual total number of approach and the total number of approached strong typhoons remains on the same level.
A previous study using climate model predicts that the number of typhoons approaching Vietnam will decrease in the future. Comparing the trends for each typhoon intensity, however, the number of weak-moderate storms will decrease but severe storms will increase.

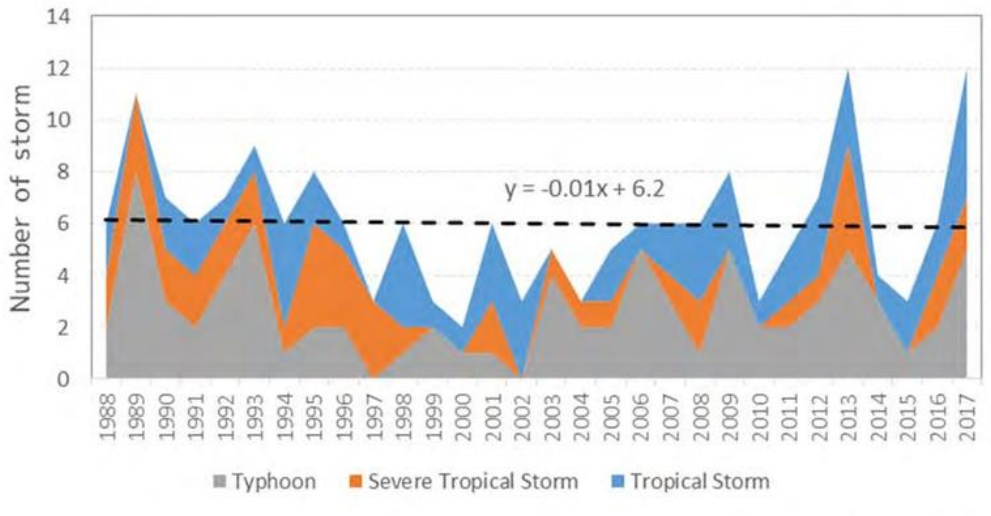

Figure 1.3. Annual total number of storms and tropical depressions

1.2.1.2. Methodology for wind and surge hazards

Cyclones are classified according to wind speeds in their circulation and these classifications vary from country to country. In Vietnam, Deaufort Wind Scale is used as tool to evaluate

Table 1.4. Beaufort Wind Scale

Force	Wind (Km/h)	WMO Classification	Appearance of wind effects
			On Land
0	Less than 1.9	Calm	Calm, smoke rises vertically

1	1.9-5.6	Light Air	Smoke drift indicates wind direction, still wind vanes
2	7.4-11.1	Light Breeze	Wind felt on face, leaves rustle, vanes begin to move
3	13-20.4	Gentle Breeze	Leaves and small twigs constantly moving, light flags extended
4	20.4-29.6	Moderate Breeze	Dust, leaves, and loose paper lifted, small tree branches move
5	31.5-38.9	Fresh Breeze	Small trees in leaf begin to sway
6	40.7-50	Strong Breeze	Larger tree branches moving, whistling in wires
7	51.9-61.1	Near Gale	Whole trees moving, resistance felt walking against wind
8	63-74.1	Gale	Twigs breaking off trees, generally impedes progress
9	76-87	Strong Gale	Slight structural damage occurs, slate blows off roofs
10	88.9-102	Storm	Seldom experienced on land, trees broken or uprooted, "considerable structural damage"
11	103.7-116.7	Violent storm	
12	118.5+	Hurricane	

1.2.3. Trend of number of deaths and missing

A time series of the number of deaths and missing caused by natural disasters in Vietnam is shown in Figure 1.4. The most severe storm event in this record is “Linda” in 1997. “Linda” caused more than 3,000 deaths and missing in the country. Furthermore, a severe storm in 1996 and flood in 1999 in the Central region caused a considerable number of deaths and missing. The annual total number of deaths and missing not attributed to “Linda” is ca. 200-500; however, the numbers have been decreasing especially after the 2000s.

Majority of deaths and missing caused by floods and storms are from the Central region that is vulnerable to storms and monsoon rainfall (Figure 1.5). According to interviews at An Giang province, many people were killed by drowning accidents when they were moving inundated areas and fell into less-visible ditches rather than accidents that happened to

residents when they drifted away with the rapid flow of water. The major conceivable causes of injury are strong winds which destroy houses and make objects fly. A lot of death and missing in Ca Mau and Kien Giang, the south-end of the Mekong Delta, was caused b the storm "Linda" in 1997. "Linda" caused more than 1000 missing fishing boats in the southern sea area and a lot of destroyed houses. A report pointed out that the local people did not recognize the risk of storms because there had not been any direct storm damage in the region for a long time.

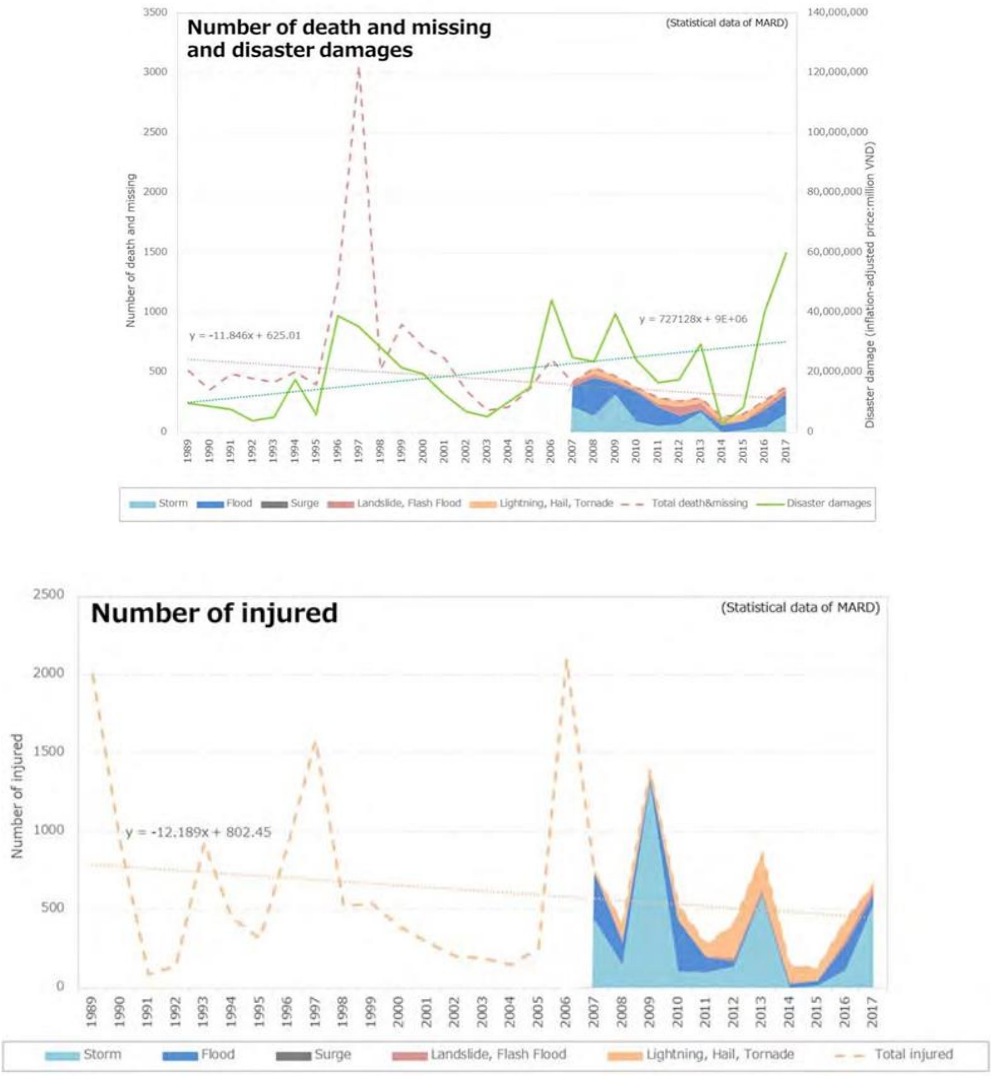

Figure 1.4. Number of death and missing (upper) and injured (lower) in 1989-2017. Note: regression line does not include storm "Linda" in 1997

Source: Prepared by JICA survey team based on annual statistical data (1989-2017) of MARD

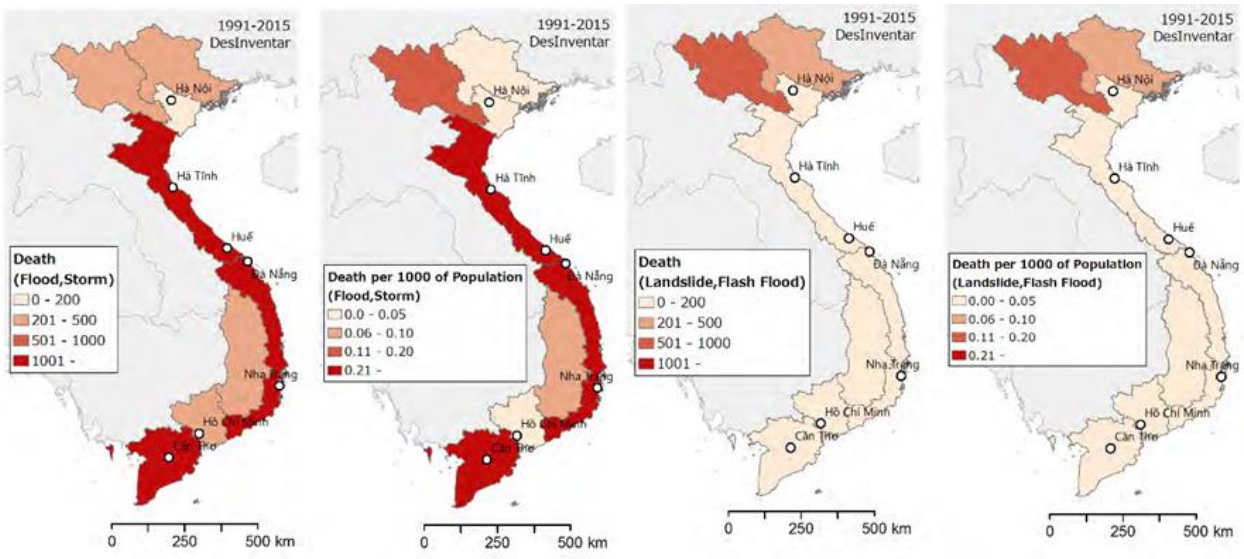

Figure 1.5. Distribution of death and missing (total number and number per 1000 capita caused by floods, storms, landsides, and flash floods)

1.2.4. Trend of disaster damage on Economy

Figure 1.6 shows a time series of disaster damage and GDP in Vietnam. The disaster damage on the economy has increased in the recent 30 years accompanying economic growth. The amount of disaster damage in 2016 is ca. 1% of GDP. The damage amount due to floods and storms (including parts of surge and landslide damage) accounts for a large portion of the each year disaster damage. The disaster damage due to drought in 2015-2016 is also large, which accounts for approximately 38% of the disaster damage in the two years.

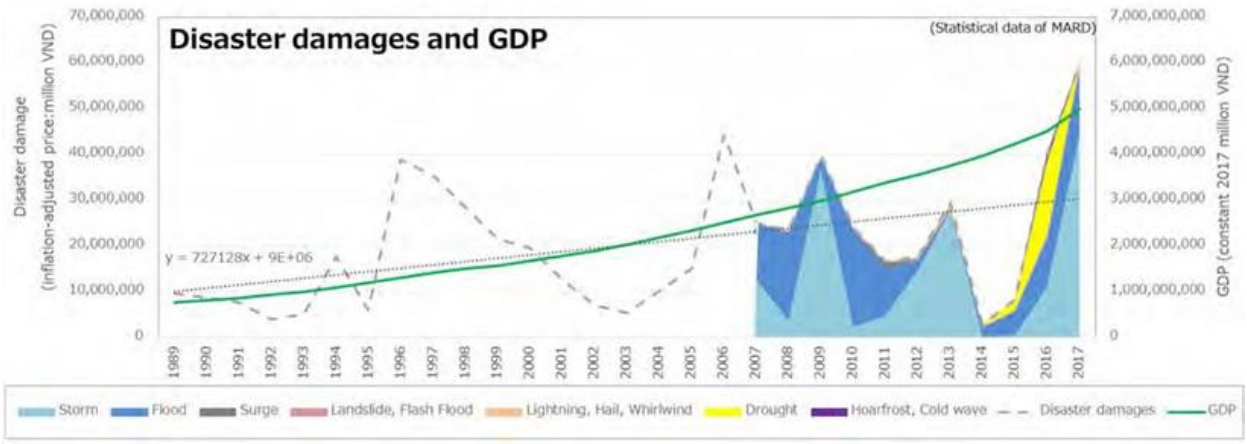

Figure 1.6. Trend of disaster damage and GDP in Vietnam (1989-2017)

1.3. Overview of the brick masonry building

According to the 2009 housing classification, there are four types of shelter in Vietnam. These are categorized based on number of secure parts (foundation, walls and roof) there are in the structure:

- Permanent
- Semi-permanent
- Less permanent
- Simple

A permanent house comprises all three secure parts whereas semi-and less permanent houses consist of the two and one secure parts respectively. A simple house has no secure parts in its structure. In urban areas, semi-permanent and permanent housing account for 49 % and 31.7 % of housing respectively (GSO, 2009) (Figure 1.7). Less permanent and simple house account for 9.5 % and 9.8 % respectively. According to damage statistics for recent disasters such as typhoon Xangsane (2006) and Ketasna (2009), semi-permanent housing is the worst affected, with roofs and walls suffering the most critical damage (ADPC, 2007)

Table 1.5. Housing classification based on construction materials in the 2009 Population housing census.

Classification	Main material of supporting columns	Main material of roof	Main Provinces Affected
Sturdy	+ Steel-reinforced + Concrete + Brick/Stone + Iron/steel/solid wood	+ Steel-reinforced concrete + Tile (cement/terra-cotta)	+ Steel-reinforced concrete + Brick/stone masonry + Wood/metal
Flimsy	+ Scrap wood/bamboo + Other	+ Sheeting (fibrocement/metal) + Leaves/straw/tar paper + Other	+ Mud/lime/straw + Slabs/bamboo screen/ planks + Other

Source: Central Population and Housing Census Steering Committee, Socialist Republic of Vietnam, the 2009 Vietnam Population and Housing Census Major Findings, 2009, Table 9.2, 122.

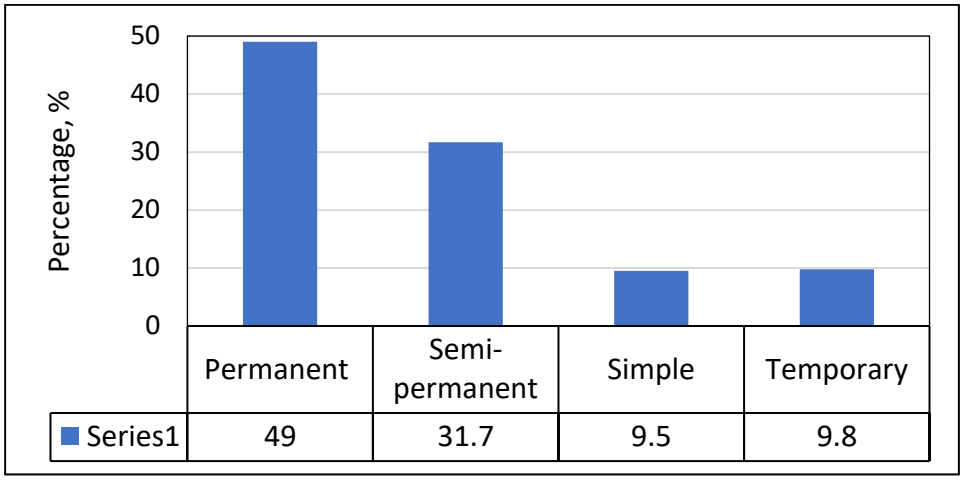

Figure 1.7. Percentages of housing types in urban areas of Vietnam

Table 1.6. Proportion of household with dwelling by type of house, urban/rural, socio-Economic region and province/city, 01/4/2019. Unit: %

	Total	Proportion by type of house			
		Building status		Type of dwelling/flat	
		Permanent and semi-permanent	Less permanent and temporary	Apartment building	Single detached house
Entire Country	100,0	93,1	6,9	2,2	97,8
+ Urban	100,0	98,2	1,8	5,8	94,2
+ Rural	100,0	90,3	9,7	0.3	99,7
Socio-economic region + Northern Midlands and Mountains	100,0	84,4	15,6	0.3	99,7

+ Red river Delta	100,0	99,3	0.7	4,6	95,4
+ North and South Central Coast	100,0	97,3	2,7	0.6	99,4
+ Central Highlands	100,0	90,3	9,7	0.2	99,8
+ Southeast	100,0	98,4	1,6	4,6	95,4
+ Mekong River Delta	100,0	80,8	19,2	0.2	99,8

Poorly constructed houses and inappropriate construction methods are considered to be the main causes of uncontrolled housing damage (Davis, 1987; Chantry and Norton, 2008; Charlesworth, 2011). In Vietnam, there is a rising trend in housing damage due to climate-related disasters despite efforts by local government, agencies and affected communities to implement disaster risk reduction strategies. In 2006 for example, typhoon Xangsane hit Central Vietnam, causing more than 24000 houses to collapse. Over 325000 houses were damaged (CCFSC, 2011). In the same year, following typhoon Xangsane, typhoon Durian then hit the region and caused more loss and damage. Nearly 50000 houses were totally destroyed, and almost 200000 houses were inundated and badly damaged. In the following year, typhoon Lekima hit Central Vietnam, causing over 1850 houses to collapse; 111770 houses were damaged badly. In 2008, a big flood partially destroyed over 180200 houses and totally destroyed 183 houses. Notably in September 2009, typhoon Ketsana landed in eleven provinces of Central Vietnam (with the greatest impacts seen in Hue, Da Nang, Quang Nam and Quang Ngai) and destroyed about 21700 houses totally and more than 473500 houses partially (CCFSC). Following these disasters, damage was usually more severe in masonry structures than in non-masonry ones and frequently affected low-income groups. This growing tendency of housing damage poses a real concern about the effectiveness of current housing construction methods and how to develop appropriate housing strategies for this region.

Over 70 % of houses built during this period lack hazard-mitigation measures and structure with non-reinforced walls and roofs are increasingly common. During big disasters such as typhoons Xangsane (2006) and Ketsana (2009), damages were unexpectedly huge with low-income groups being the worst affected.

In an era of climate change, climate-related disasters in Vietnam are expected to increase in frequency and intensity (Hoang 2011; MONRE, 2012), particularly greater floods and typhoons (EM-DAT, 2012) (Figure). Housing in urban areas of central Vietnam tend to be modernized, built with new load-bearing structures and construction materials, such as reinforced concrete for structure, brick masonry for walls, and clay tiles and iron sheets for roofs (Ly et al 2010). However inappropriate uses of these innovations increase the risks to housing risks during adverse climate events.

For these reasons, this research has focused on low-income housing in the highly vulnerable area of the two most disaster-pone cities of Central Vietnam: Hue and Da Nang. Semi-permanent hosing was selected for this study as it is the most common type of housing in Vietnam and it most at risks from climate hazards. Examining semi-permanent low-income housing through the lens of post-disaster housing reconstruction and climate resilience should help us to better understand climate-resilient housing and improve the likelihood of developing a resilient housing system for central Vietnam.

1.4. Objectives of research

The purpose of the study is to strengthen existing masonry house structures in strong wind conditions caused by typhoons, using the proposed method that PP band is sandwiched between two flat steel washers and fastened with a steel screw to plastic plug embedded in the side of the brick. This reinforcement helps increase the strength and prolong the destruction time of the wall. From the above meanings, ensure everyone's safety and have enough time to escape before the destruction of the house occurred. That is extremely important.

The detail objectives of this research are:

1. Evaluate the correctness of the proposed method and the suitability of using two steel plates to clamp the PP band.

2. To study the applicability of PP strips on small samples.

3. Verify the destruction model using numerical modeling. Then, draw conclusions

1.5. Outline of thesis

This thesis consists of six chapters followed by references as follows:

Chapter 1. Introduction

Context and reasons for conducting the research and the necessity of this research in practice. In addition, it is desirable to conduct experiments to check the correctness of the method.

Chapter 2. Provide an overview of the impact of storms on house structures in Vietnam. Issues such as number of storms occur every year, the level of storms that can destroy a house, type of house most affected, and number of destroyed houses will be mentioned.

Chapter 3. Provide a comparison between the PP band fixation method in previous studies and the current proposed method to demonstrate the feasibility and ease of application of this method.

Chapter 4. Contains discussion and analysis of results of the prism specimens. The results include load-deflection relationship, shear stress-slip curves, and failure loads and crack patterns. Additionally, numerical modelling works will carry out in details.

Chapter 5. Contains summary and conclusions in detail for all studies explained in Chapter 4.

CHAPTER 2. OVERVIEW OF METHODS FOR FIXING PP BAND TO BRICK

2.1. Method using tensioner and sealer

Susanta Banerjee et al (2018), Past earthquakes witnessed the poor performance of unreinforced masonry (URM) structures resulting into huge economic loss and large number of casualties. In this context, the present paper is aimed to investigate the shear behaviour of a series of masonry wallets (unretrofitted and retrofitted) under diagonal compressive loading. To improve the wallet behaviour in shear, polypropylene band (PP-band) and steel wire mesh (WM) are used as retrofitting material. Both faces of wall are wrapped to get full tightening effect during loading. Bricks having standard size and half scale size are used to construct the full-scale wallet and small-scale wallet, respectively. It has been observed that retrofitted wall exhibits significant improvement in terms of load carrying capacity, displacement ability. Failure mode for both unreinforced masonry (URM) and strengthened specimens are reported and shear strength is computed using analytical formulations. It was observed that both the strengthening materials not only increase the load carrying capacity but also helps in changing the failure mode from brittle to ductile in some extent. From the study, it may be concluded that use of PP band and steel wire mesh are effective in improving the shear behaviour of masonry structures for both the types of wallets.

(Enhancing shear capacity of masonry wallet using PP band and steel wire mesh)

Susanta Banerjee et al (2019), The collapse of the masonry wall occurs mainly due to inadequacy of load transferring mechanism of out-of-plane behaving wall during earthquake, and is the cause for huge loss of property and life of inhabitants. Hence, an experimental program was carried out to investigate the efficiency of masonry wall in flexural loading. Total 32 specimens were tested. Some specimens were unreinforced and others were reinforced. In India, both clay brick and fly-ash brick are commonly used to construct the masonry wallets. Hence, these walls, were tested under four-point loading method as per ASTM E518-10 recommendations to investigate the influence of different brick composition in out-of-plane behaviour of wall. In addition, comparative study was also made between traditional full-size and half-scale bricks to check its suitability for the construction of scale-down models. Cost effective materials such as polypropylene (PP) band

and steel wire mesh (WM) were used to strengthen these walls. The result shows that both the strengthening techniques are effective in delaying the collapse of the structure, also enhancing the flexural strength and ductility, and this paper presents these outcomes. This paper also presents the cracking load, load-displacement behaviour, stiffness and energy dissipation capacity. Finally, an analytical formulation has also been developed to validate the cracking load of the wall with experimental results

(Enhancing the flexural behavior of masonry wallet using PP band and Steel wire mesh)

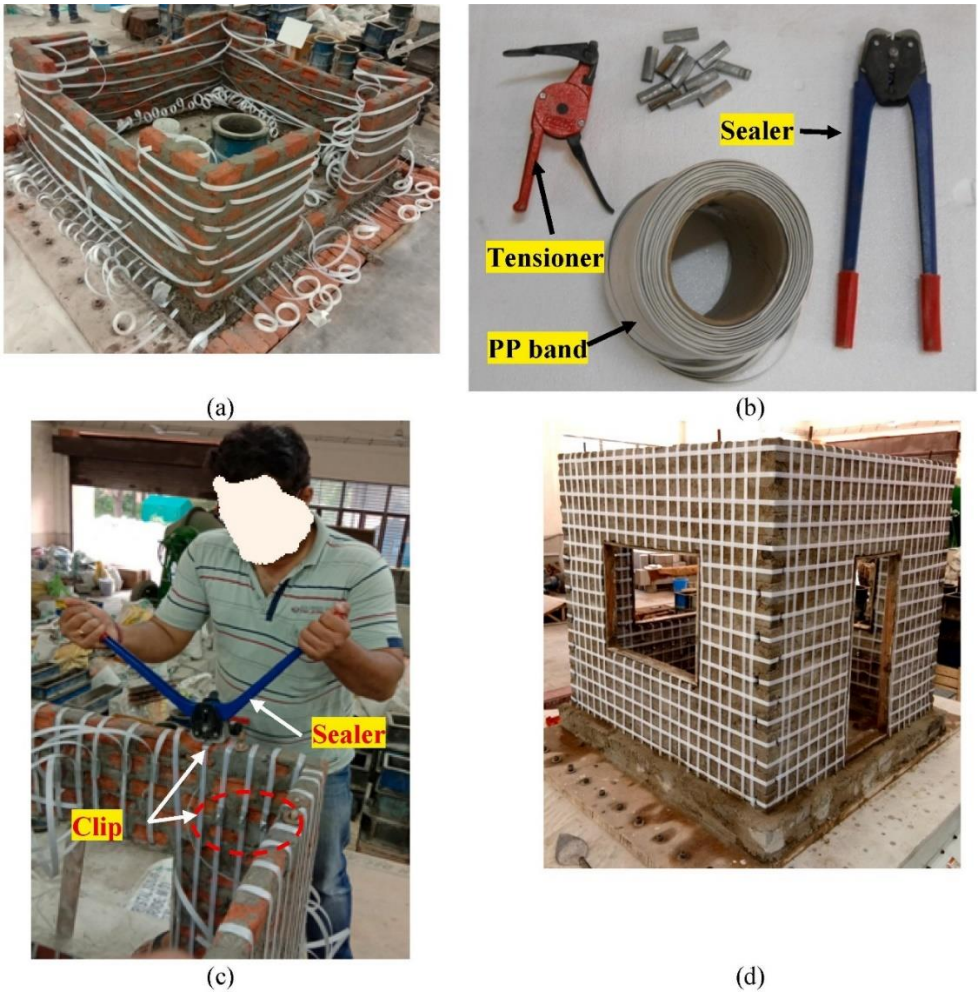

Figure 2.1. Strengthening stages of building model: a. arranging the PP band; b. tightening items of PP band; c. sealing process of a clip with the band; d. final stage after PP band strengthening.

Susanta Banerjee et al (2020), The seismic vulnerability of unreinforced masonry (URM) structures was observed during the past seismic events, which caused a huge loss of life and property. However, URM buildings are quite common in developing countries like India as they offer cheap shelters to people with low income. An easily implementable strengthening technique with cost-effective materials for enhancement of the seismic behaviour of URM building is of utmost importance. Hence, this study was carried out to develop a technique to improve the strength and ductility of URM buildings. Clay bricks and eco-friendly fly-ash bricks were used for the construction of the building models. Brick sizes were reduced to half so that the scale-down building model can be constructed for testing. The building models were tested in a uni-directional shaking table using swept sine motions. The experimental investigation was categorized in three phases. In the first phase, the effect of diaphragm action on seismic behaviour of masonry building was investigated by providing the flat reinforced concrete slab and pitched timber truss as a roof on top of the building. The second phase focused on the enhancement of the seismic behaviour of the URM wall by strengthening with two cost-effective materials, such as polypropylene (PP) band and steel wire mesh (WM). In the third phase, cracked (damaged) URM walls were repaired and retrofitted with wire mesh. It was observed that both the strengthening materials were effective in improving the ductility of the URM buildings.

(Augmenting the seismic performance of masonry models using polypropylene band and steel wire mesh through shaking table testing)

Susanta Banerjee et al (2021), the present study aims to enhance the seismic performance of single-storied scaled-down building models by strengthening with two cost-effective materials; polypropylene (PP) band and steel wire mesh. This is a quick and straightforward process which was followed for the strengthening purpose. Half-scale size of clay and fly-ash bricks were used for making the test specimens. Both URM and strengthened building models were subjected to bi-directional swept sine motion. Each damaged state of building models was reported during the loading sequence. The crack progressions and failure characteristics of the building models were thoroughly observed. Furthermore, arias intensity, acceleration amplification factor, and performance evaluation indices were determined forabetter understanding of the seismic response of the models. It

was noticed that both the strengthening materials were effective and economical in improving the performance (strength, global stiffness, damage tolerance) of masonry building models adequately.

(Seismic performance enhancement of masonry building models strengthened with the cost-effective materials under bi-directional excitation)

Sanket Nayak and Sekhar Chandra Dutta (2015), A previous study using a scaled-down model of single-room masonry structures tested on a shaking table has shown that strength may be considerably increased by tying up the masonry walls by polypropylene (PP) bands, wrapping the walls using steel wire mesh, and providing horizontal L-shaped reinforcing bars at corners. The effectiveness of the same economic approaches and their combinations has been studied for similar scaled-down models with proportionate openings representing doors and windows, as a logical further scope of the previous study testing these models on a shaking table. As the presence of openings influences the crack and damage propagation leading to failure, the present study may give a more realistic picture of the seismic behavior of masonry structures with openings. Experiments have shown that PP bands were more effective than horizontal L-shaped reinforcing bars in arresting cracks and preventing collapse of the models, even those severely damaged. Further, the most important aspect of the study is that the technique is economical and can be implemented without involvement of any technical manpower or sophisticated equipment. The interesting observations regarding the effectiveness of such economical strengthening measures obtained from the study may be helpful for seismic strengthening of real-life masonry structures with door and window openings, leading to broad guidelines in this direction.

(Improving seismic performance of masonry structures with openings by polypropylene bands and L-shaped reinforcing bars)

Sanket Nayak and Sekhar Chandra Dutta (2016), Masonry structures have exhibited their extreme vulnerability even in the event of past minor to moderate earthquakes. Junction failure followed by out-of-plane collapse of the wall orthogonal to the direction of strong shaking is the reason of failure of small masonry building structures as shown in a

recent literature. In this context, present study makes an attempt to examine the efficacy of a few strengthening techniques of such structures verified through testing a large number of small-scale models on shake table. Techniques being cost effective and easy to implement may prove useful in improving seismic performance. Large number of experimental results presented in this study may help in choosing one of the suitable techniques depending on specialties of a particular local condition.

(Failure of masonry structures in earthquake: A few simple cost-effective techniques as possible solutions)

Jamshid Zohreh Heydariha et al (2019), Unreinforced masonry (URM) buildings exhibited extreme vulnerability during past earthquakes though these are shelters of majority population in many earthquakes prone developing countries. Most of the current retrofitting techniques used for such structures are either expensive or requires highly skilled labor or sophisticated equipment for implementation. On the other hand, the retrofitting technique proposed in this paper is economical and easy-to-apply. This paper aims at examining the performance of the retrofitting technique using polypropylene (PP) band. The monotonic load-displacement behaviors of URM wall and the wall retrofitted with PP band are compared. It was found that URM wall retrofitted by PP band improves the ductility and energy absorption capacity by three times, and two times, respectively. Performance of a full-scale masonry building retrofitted with PP band in Nepal during last Gorkha earthquake of April 25, 2015, has also been presented in this paper. Its was observed that the PP band retrofitted masonry building survived while the nearly many buildings experienced severe damage and some of them collapsed. This study demonstrates the efficacy and practicability of use of PP band for improving seismic resistance of URM structure.

(Experimental and field performance of PP band-retrofitted masonry: evaluation of seismic behavior)

S. Ebrahimzadeh and K. Nasrollahzadeh (2023), This paper proposes a strengthening method for improving the seismic performance of Unreinforced Masonry (URM) brick walls. What is noteworthy regarding the proposed technique is the low price and easy application

of polypropylene (PP) bands, which are widely used in the packaging industry. Three half-scale specimens were tested under cyclic lateral loading simultaneously upon imposing a constant vertical load. First, the URM wall was tested up to a certain drift in which a reduction in lateral capacity was recorded. According to the crack pattern observed on the wall surface, a repair strategy was taken to upgrade the damaged wall in the shortest possible time and with minimum manpower. In doing so, horizontal PP bands were employed to wrap the wall. The repair technique stopped the spread of cracks and prevented reduction in lateral capacity. Besides, the third specimen, which is identical to the URM wall but is strengthened by PP bands, was tested and it developed a superior performance by changing the failure mode and increasing the maximum strength, the strength at maximum displacement, and maximum displacement by 88%, 38%, and 185%, respectively, compared to URM wall.

(Experimental study on performance of repaired and strengthened unreinforced masonry walls using polypropylene bands)

Zhao Wenyang et al (2023), Since masonry structures are prone to collapse in earthquakes, a novel joint reinforcement method with a polypropylene band (PP-band) and cement mortar (CM) has been put forward. Compared with the common reinforcement methods, this method not only facilitates construction but also ensures lower reinforcement cost. To systematically explore the influence of joint reinforcement on the seismic performance of masonry walls, quasi-static tests were carried out on six specimens with different reinforcement forms. The test results show that the joint action of PP-band and CM can significantly improve the specimen's brittle failure characteristics and enhance the integrity of the specimen after cracking. Compared with the specimen without reinforcement, each of the seismic performance indexes of the joint reinforced specimen had obvious improvement. The maximum increased rate about peak load and ductility of the joint reinforced specimen is 100.6% and 233.4%, respectively.

(Experimental study on the seismic performance of masonry wall reinforced by cement mortar and polypropylene band)

2.2. Method using a portable ultrasonic welder, straw, and steel wire

Synthetic organic polymer grids, i.e. those having carbon in their backbone structure, are an alternative option for external strengthening of adobe masonry walls against earthquake actions. Polypropylene (PP) band meshes have been proposed and shown to be effective plastic reinforcement systems for seismic strengthening (Tolles at al 2002). Because of their common use for packaging, PP bands are available worldwide and ensure high resistance, low cost, ease of installation and durability. As described for other techniques, PP band should be placed in critical zones of the wall, basically following the patterns of cracks expected under in-plane seismic actions. Horizontal, vertical and/or diagonal PP bands can be connected to both sides of adobe masonry walls by means of plastic wires or other materials. Afterwards, the adobe wall is plastered with mud mortar to allow a satisfactory bond between the mesh and the wall, protection of the mesh from environmental actions and a good appearance of the retrofitted wall.

Mayorca and Meguro (2008), Past earthquakes have shown that the collapse of seismically weak adobe/masonry structures is responsible for most of the fatalities in developing countries. It is, thus, urgent to improve their seismic performance in order to reduce future casualties and to protect the existing housing stock. To encourage seismic retrofitting, inexpensive and easy to implement technical solutions are desirable. Retrofitting by polypropylene band (PP-band) meshes satisfies these requirements. These bands, commonly used for packing, are resistant, inexpensive, durable and worldwide available. Experiments and advanced numerical simulations have shown that PP-band meshes can dramatically increase the seismic capacity of adobe/masonry houses. Nevertheless, a simple yet accurate design method is still needed to optimize the mesh arrangement and assess its performance. PP-band meshes increase the structure ductility and energy dissipation capacity through controlled cracking. However, large deformations during seismic events are expected and therefore, the design method must take this into account. In this paper, a methodology to design PP-band mesh retrofitted structures is outlined and discussed. (A step towards the formulation of a simple method to design PP band mesh retrofitting for adobe/ masonry houses)

Mayorca and Meguro (2009) proposed a design method for optimal arrangement of PP band meshes for seismic strengthening of single-storey adobe masonry buildings with flat roofs. Those researchers developed a displacement-based design procedure where the ductility demand to be absorbed by the strengthening system is estimated from the lateral strength deficit. The latter is the additional strength reduction factor required to with stand the design base shear provided the seismic code. Such a methodology relies upon the outcome of previous experimental test that showed approximately the same values of cracking lateral force and stiffness for the unreinforced and PP band-strengthened adobe walls (Sathiparan et al.2008). Therefore, the external strengthening system is regarded as a solution that provides additional displacement ductility to the adobe wall, without changing its initial (elastic) properties. Effective design parameters are the mesh density and plaster layer properties, which have a major influence on displacement ductility demand given a lateral strength deficit. The strengthening system is designed so as to get the required displacement capacity against in-plane lateral actions and a safety verification against out-of-plane capacity of adobe walls and limit their lateral deformations.

Sathiparan, Mayroca, Meguro (2010), This paper introduces a technically feasible and economically affordable PP-band (polypropylene bands) retrofitting for low earthquake resistant masonry structures in developing countries. Results of the material tests and shaking table tests on building models show that the PP-band retrofitting technique can enhance safety of both existing and new masonry buildings even in worst case scenario of earthquake ground motion like JMA7 seismic intensity. Therefore proposed method can be one of the optimum solutions for promoting safer building construction in developing countries and contribute earthquake disaster mitigation in future (Experimental study on static and dynamic behavior of PP band mesh retrofitted adobe masonry structure)

Navaratnarajah Sathiparan, Meguro (2012), This paper introduces a technically feasible and economically affordable PPband (polypropylene bands) retrofitting for low earthquake resistant masonry structures in developing countries. Results of the basic material tests and shaking table tests on building models show that the PP-band retrofitting technique can enhance safety of both existing and new masonry buildings even in worst case scenario of earthquake ground motion like JMA 7 seismic intensity. Therefore, proposed

method can be one of the optimum solutions for promoting safer building construction in developing countries and can contribute earthquake disaster mitigation in the future. (Shaking Table Tests on ¼ Scale PP-band Retrofitted Model of Low Earthquake Resistant Masonry Houses)

Sathiparan, Meguro (2013), This paper investigates a recently developed retrofitting technology specifically aimed at preventing or prolonging the collapse of stone masonry buildings under strong earthquakes. This technology uses common polypropylene packaging straps to form a mesh, which is then used to prevent or prolong collapse. This paper examines the findings from static and dynamic testing of the proposed retrofit. It is shown that the proposed technique effectively prevents brittle masonry collapse and the loss of debris (Experimental investigation on the seismic performance of PP band strengthening stone masonry house)

Sathiparan, Meguro (2013), This paper presents an innovative retrofitting method for masonry houses, which consists of polypropylene bands (PP-band) arranged in a mesh fashion. The PP-band technology aims to prevent or, at least, put off wall collapse by providing both sides with the mesh made of a cheap packthread and keeping the integrity of the walls. In order to verify the suitability of the proposed method, a series of masonry wallettes, with and without retrofitting, was tested under in-plane and out-of-plane loads. Although the retrofitted wall peak strength was almost the same as that of the bare wall, its postpeak strength was larger and sustained for lateral drifts. In order to investigate the proposed retrofitting features for different material properties and mesh configurations, tests on a number of masonry wallettes were performed (Shear and flexural bending strength of masonry wall retrofitted using PP band mesh)

Sathiparan, Meguro (2014), This paper discusses on the shaking table test results of two 1:4 scale model of two-story masonry structure typically used in constructing low-rise residential buildings. This test is performed to provide a better understanding of the seismic behavior of the PP-band (polypropylene band) mesh retrofitted adobe masonry house. The test structure is subjected to a series of different levels of harmonic motion that applied along the longitudinal direction. The results of the shaking table tests on building models show

that the PP-band retrofitting technique can enhance the safety of masonry buildings, even during severe ground motion. (Seismic evaluation of earthquake resistance and retrofitting measures for two story masonry houses)

Dar, Umair, Meguro (2014), Popypropylene band retrofitting has been proposed as the retrofitting method for masonry structure in many under developing countries. For this method, the PP band is connected at every intersection of the mesh on the masonry wall. If we can reduce the number of connecting points of PP band mesh, this method will be more effective. In this paper, we can reduce the effects of reduced numbers of connecting points of PP band mesh by ¼ scale-models on shake table test. The fully connected (PPF) and the non-connected cases (PPN) were compared. The PPN model showed the effectiveness as for the retrofitting method. (Reduction of PP band mesh connectivity for masonry structure retrofitting)

Sathiparan and Meguro (2015), extended their experimental program to adobe houses with a vaulted roof, assessing the combined effects of PP band mesh and tie bars. The latter were implemented to reduce/eliminate horizontal thrust forces on load-bearing walls supporting a roof consisting of a barrel vault. Three quarter-scale house models were tested on a shaking table. The input motion was a harmonic excitation with increasing intensity in each successive test run. Regardless of the presence of tie bars, the PP band strengthening ensured wall integrity up to large deformations, allowing load redistribution throughout the specimen. Tie bars produced only a small increase in displacement ductility, lateral load-carrying capacity or stiffness. Nonetheless, the presence of tie bars improved the control of permanent deformations and energy dissipation capacity. This strengthening approach is expected to allow additional time for evacuation of adobe houses by increasing the collapse displacement. (Strengthening of adobe houses with arch roofs using tie-bars and polypropylene band mesh)

Strengthening of adobe house with arch roofs using tie-bars and polypropylene band mesh. Integrity up to large deformations, allowing load redistribution throughout the specimen. Tie bars produced only small increase in displacement ductility, lateral load-carrying capacity or stiffness. Results show that a potential use FRP in combination with PP

band is a good alternative as it significantly enhances the shear capacity, energy dissipation as well as the ductility of URM masonry structure at a very low retrofitting cost. An experimental study was conducted to evaluate the potential improvements in the in-plane and out-of-plane strength of masonry wallets. These strengthening materials are also helpful in attributing higher ductility by containing the broken fragments of the masonry. On the other hand, the strengthening measures also can significantly improve the strength and ductility of masonry wallets under both shear and flexural loads and prevent brittle failure.

(a) PP-mesh Fabrication

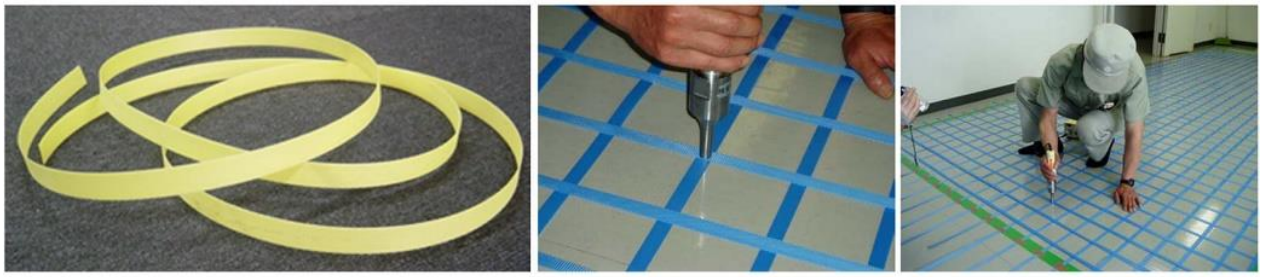

(b) Tools for PP-Mesh Fabrication & Installation

Plastic welder | Steel Wire | Pliers | Twisting tool

(c) Prepare connecting holes

(d) PP-Mesh Installation

(e) Connecting plate installation

(f) PP-band retrofitted house before and after plastering

Figure 2.2. PP band mesh retrofitting procedure for masonry house

SM Umair, M Numada, Meguro (2015), In the current research work, an attempt is made to increase the seismic capacity of unreinforced masonry (URM) structures by proposing a new composite material which can improve shear strength and deformation capacity of URM wall systems. Fiber Reinforced Polymer (FRP) having high tensile and shear stiffness can significantly increase in-plane and out-of-plane strength of masonry walls, but, inherently, FRP strengthened wall systems exhibit brittle failure under extreme seismic loading. Polypropylene (PP-band) is a low cost material with sufficient ductility and deformation capacity. Keeping in view the behavior of FRP and PP-band, a composite of FRP and PP-band is proposed for retrofitting of URM walls. Mechanical behavior of the proposed composite material is assessed by carrying out an in-plane diagonal compression test and an out-of-plane bending test on twenty-five 1/4-scaled masonry wall panels. Experimental plan for each panel, URM, PP-band retrofitted, FRP retrofitted and FRP + PP-band retrofitted masonry, is diagonal compression test and three-point bending test. Experimental results have determined that FRP + PP-band composite increased, not only the initial peak strength, but also the ductility, deformation capacity and residual strength of URM wall systems. (Fiber reinforced polymer and Polypropylene composite retrofitting technique for masonry structures)

M.Umair Saleem et al. (2016), Current research work presents the seismic response of brick masonry houses retrofitted by different composite materials under dynamic shake table tests. Tests were performed on 1:4 scaled unreinforced masonry (URM), Polypropylene (PP-band) retrofitted, Glass Fiber Reinforced Polymer (FRP) retrofitted and FRP + PP-band retrofitted house models. A minimum reinforcement ratio of FRP was selected to use with PP-band as FRP + PP-band composite. Results show that URM is highly brittle and can hardly withstand an ordinary ground motion, whereas PP-band retrofitting has increased the ability of URM houses to withstand a severe ground motion with intense cracking and separation of wall segments. However, despite no collapses, PP-band retrofitted house model had lost its serviceability when subjected to strong input ground motion. Unlike PP-band, FRP retrofitted houses were collapsed suddenly without giving any warning with respect to ductility and energy dissipation. The sudden failure of FRP houses is attributed to very low FRP reinforcement ratio (0.0006), as it is an expensive material and its sole use in

higher amounts would result in significant increase of retrofitting costs. Results show that a potential use of FRP in combination with PP-band is a good alternative as it significantly enhances the shear capacity, energy dissipation as well as the ductility of URM masonry structure at a very low retrofitting costs (Seismic response of PP band and FRP retrofitted house models under shake table testing).

Pranoy Debnath, Sekhar Chandra Dutta (2023), An experimental study was conducted to evaluate the potential improvements in the in-plane and out-of-plane strength of masonry wallets. Four different strengthening materials, namely, wire meshes, PP bands, used cement bags and waste textiles, are used to strengthen the masonry wallets. The effect of strengthening due to the use of steel wire mesh is well-accepted and understandable. However, the other three materials are either environmental waste or cause long-run environmental pollution. If these can be effectively used for strengthening and the extent of strengthening can be compared with whatever is observed for steel wire mesh and if found to be suitable, then the use of such material would have the advantage of maintaining a cleaner environment. Test results showed that English and Flemish bonds exhibit superior strengths than the other masonry bond types. On the other hand, the strengthening measures also can significantly improve the strength and ductility of masonry wallets under both shear and flexural loads and prevent brittle failure. These strengthening materials are also helpful in attributing higher ductility by containing the broken fragments of the masonry. Further, the improvement in strength is considerable, as presented in detail in the paper. The increase in strength and ductility is in the order of 231%–171% and 7.75 to 1.69, respectively. Using the PP bands, used cement bags and waste textiles may be beneficial for their availability leading towards the reduction of waste materials. (In plane and out of plane strength of different masonry bonds along with the effect of some waste materials for strengthening masonry wallets)

Navaratnarajah Sathiparan and Kimiro Meguro (2011), This paper introduces a technically feasible and economically affordable PP-band (polypropylene bands) retrofitting for low earthquake resistant masonry structures in developing countries. Results of the basic material tests and shaking table tests on building models show that the PP-band retrofitting technique can enhance safety of both existing and new masonry buildings even in worst case

scenario of earthquake ground motion like Japan Meteorological Agency (JMA) seismic intensity scale 7. Therefore, proposed method can be one of the optimum solutions for promoting safer building construction in developing countries and can contribute earthquake disaster mitigation in the future.

(Seismic behavior of low earthquake resistant arch shaped roof masonry houses retrofitted by PP band meshes)

Navaratnarajah Sathiparan et al (2013), The collapse of stone masonry is one of the greatest causes of death in major earthquake events around the world. This paper investigates a recently developed retrofitting technology specifically aimed at preventing or prolonging the collapse of stone masonry buildings under strong earthquakes. This technology uses common polypropylene packaging straps to form a mesh, which is then used to prevent or prolong collapse. This paper examines the findings from static and dynamic testing of the proposed retrofit. It is shown that the proposed technique effectively prevents brittle masonry collapse and the loss of debris.

(Experimental investigation on the seismic performance of PP band strengthening stone masonry houses)

Pranoy Debnath, Sekhar Chandra Dutta (2023), An experimental study was conducted to evaluate the potential improvements in the in-plane and out-of-plane strength of masonry wallets. Four different strengthening materials, namely, wire meshes, PP bands, used cement bags and waste textiles, are used to strengthen the masonry wallets. The effect of strengthening due to the use of steel wire mesh is well-accepted and understandable. However, the other three materials are either environmental waste or cause longrun environmental pollution. If these can be effectively used for strengthening and the extent of strengthening can be compared with whatever is observed for steel wire mesh and if found to be suitable, then the use of such material would have the advantage of maintaining a cleaner environment. Test results showed that English and Flemish bonds exhibit superior strengths than the other masonry bond types. On the other hand, the strengthening measures also can significantly improve the strength and ductility of masonry wallets under both shear and flexural loads and prevent brittle failure. These strengthening materials are

also helpful in attributing higher ductility by containing the broken fragments of the masonry. Further, the improvement in strength is considerable, as presented in detail in the paper. The increase in strength and ductility is in the order of 231%–171% and 7.75 to 1.69, respectively. Using the PP bands, used cement bags and waste textiles may be beneficial for their availability leading towards the reduction of waste materials.

(In-plane and out of plane strength of different masonry bonds along with the effect of some waste materials for strengthening masonry wallets)

Zhao Wenyang et al (2023), In order to study the enhancement effect of polypropylene band (PP-band) on the bending performance of brick masonry, the bending tensile test was carried out on 216 brick masonry specimens. Combined with numerical simulation, the influences of masonry mortar strength, coating mortar strength and PP-band mesh with different mesh sizes on the bending performance of brick masonry were studied. The results show that the strength of masonry mortar has the greatest influence on the peak bending load of brick masonry. Compared with M1 strength, when the strength of masonry mortar increases to M2.5, M5, M7.5 and M10, the corresponding peak bending load amplification of continuous section brick masonry is 15.87%, 31.11%, 37.60% and 44.45%, respectively, and that of the dentiform section brick masonry is 28.95%, 46.16%, 55.19% and 56.76%, respectively. The strength of coating mortar has little influence on the peak bending load, and its main function is to enhance the bond between PP-band and brick masonry surface. The joint action of high-strength coating mortar and PP-band can effectively improve the deformation resistance ability of brick masonry. The size of PP-band mesh mainly affects the amplitude of load recovery after the fracture of brick masonry. Compared with the mesh size of 12.5 cm, when the mesh size is reduced to 7.5 cm and 5 cm, the amplification of load recovery peak value of continuous section brick masonry can reach 63.42% and 130.38%, and that of the dentiform section brick masonry can reach 73.29% and 127.66%. The PP-band reinforcement method can provide reference for seismic reinforcement of masonry structures, especially in rural areas.

(Study on bending tensile performance of brick masonry reinforced with PP band)

Santhosh. L. S et al (2019), Masonry structures have exhibited their extreme vulnerability even in event of the past minor to moderate earthquakes. This paper investigates a recently developed retrofitting technology specifically aimed at preventing or prolonging the collapse of the masonry buildings under strong earthquakes. On the other hand, the retrofitting technique proposed in this paper is economical and easy to apolypropylenely. This paper aims at examining the performance of retrofitting technique using the polypropylene (Polypropylene) band. In this paper the monotonic load displacement behaviors of a URM wall and the wall retrofitted with Polypropylene band are compared. It was observed that the Polypropylene band–retrofitted masonry building survived, whereas many nearby buildings experienced severe damage and some of them collapsed. This study demonstrates the efficacy and practicability of use of Polypropylene band for improving seismic resistance of a URM structure.

(Review on performance of polypropylene band-Retrofitted masonry: Evaluation of seismic behavior)

Naveratnarajah Sathiparan, Kimiro Meguro (2013), One of the main causes of casualties in major earthquakes around the world is the collapse of low earthquake resistant masonry structures. Retrofitting of these types of structures is the key issue for earthquake disaster mitigation in developing countries, because it is the only way to reduce significantly casualties in future earthquakes. This paper presents an innovative retrofitting method for masonry houses, which consists of polypropylene bands (PP-band) arranged in a mesh fashion. The PP-band technology aims to prevent or, at least, put off wall collapse by providing both sides with the mesh made of a cheap packthread and keeping the integrity of the walls. In order to verify the suitability of the proposed method, a series of masonry wallettes, with and without retrofitting, was tested under in-plane and out-of-plane loads. Although the retrofitted wall peak strength was almost the same as that of the bare wall, its post-peak strength was larger and sustained for lateral drifts. In order to investigate the proposed retrofitting features for different material properties and mesh configurations, tests on a number of masonry wallettes were performed.

(Shear and flexural bending strength of masonry wall retrofitted using PP band mesh)

2.3. Proposed method by authors

In the studies mentioned above, there are two ways of strengthening the PP band. In the first method, PP band was tightened together by clip using tensioner and sealer. This method was effective in strengthening small brick masonry patterns. However, when considering using on walls, it is difficult to attach the PP band mesh to the wall. Almost all the walls were restrained at three or four edges. Therefore, the PP band mesh cannot wrap the wall at the intersection between the wall and column. In the second method, PP band mesh was created by using a portable ultrasonic welder. Afterwards, holes were drilled through the mortar layers in the wall and small straws/pipes were left embedded at the joints. PP band mesh can be applied to both faces of the wall with the help of connectors which can be a steel wire, PP band. Using a steel wire to fasten the PP band mesh on the wall, as shown in Figure 4.2(a), the hardness at the connection position was low. Additionally, when observed from the form of destruction in Figure 5.1, it was found that the surface between the mortar-brick or in mortar layer was often where the cracks first appeared, and continued to expand until failure. This raises the problem of damage to the connection position. It effectively reduces the tension ability of the PP band mesh owing to the simultaneous displacement of both fixed position and the mesh. Therefore, to clarity this issue, we have developed a suitable PP band fixation method to enhance the hardness at the connection position, Figure 4.3(b).

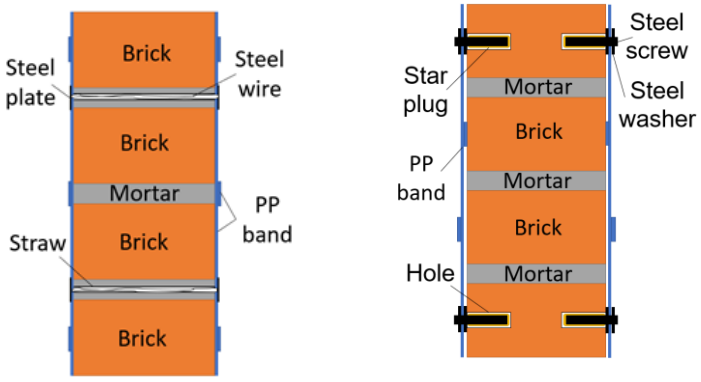

(a) Sathiparan et al. 2015 (b) Recent studies

Figure 2.3. Methods of PP band strengthening

2.3.1. Strengthening materials

The specimens were strengthened using a PP band (popularly used as a carton packaging material). We evaluate the tensile properties of PP band with dimensions 15.5 × 0.5 × 500 mm (width × thickness × length) according to JIS Z1527:2002. Figure 4.4 exhibits the setup used for the tensile test. The properties of the PP band used in this investigation are listed in Table 2.1.

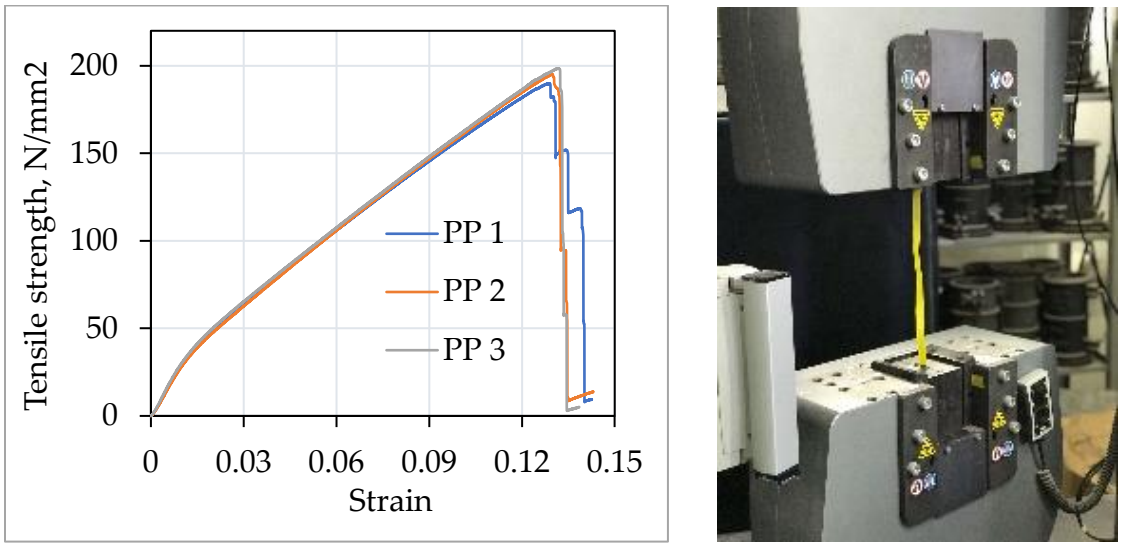

Figure 2.4. Direct tensile strengths of PP bands

Table 2.1. Parameter for PP band

Type of material	Properties	Values
PP band	Width	15.5 mm
	Thickness	0.5 mm
	Density	0.9 g/cm^3
	Tensile strength	194.6 N/mm^2
	Cut-off strain	13.0 %
	Modulus of elasticity	1500 N/mm^2

2.3.2. PP band fixing method to brick test

The installation process is straightforward and does not require skilled labor. The preliminary assessment of the proposed method in the direct tension test was performed on three cases: (1) Using only steel screw (5 × 25 mm) (Figure 2.5(a)), (2) Using one steel

washer and PP band placed between the steel washer and brick joined using a steel screw (Figure (2.5(b)), (3) Using two steel washers with the PP band placed between them, and joined by a steel screw (Figure 2.5(c)). Each case consists of three specimens with dimensions showed in Figure 2.5(d). The length of PP band and loading method were selected in accordance with JIS Z1527:2002. First, we drilled 6 mm holes in the bricks using an electric drill. The diameter of the hole was sized to ensure a tight fit with the star plug (6 × 25 mm). The tightening force applied to each steel screw was adequate to hold the PP band firmly in the plane. Figure 2.5(e) is presented the layout of specimen.

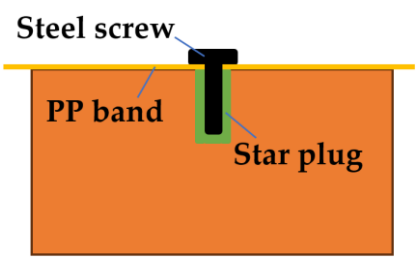

(a) Case 1

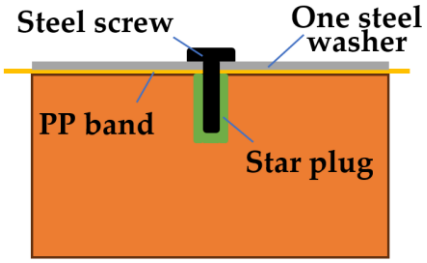

(b) Case 2

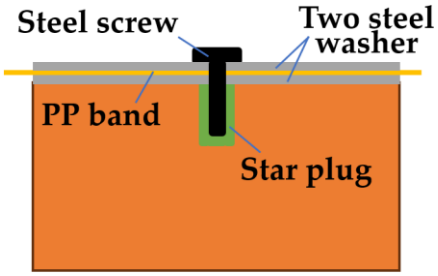

(c) Case 3

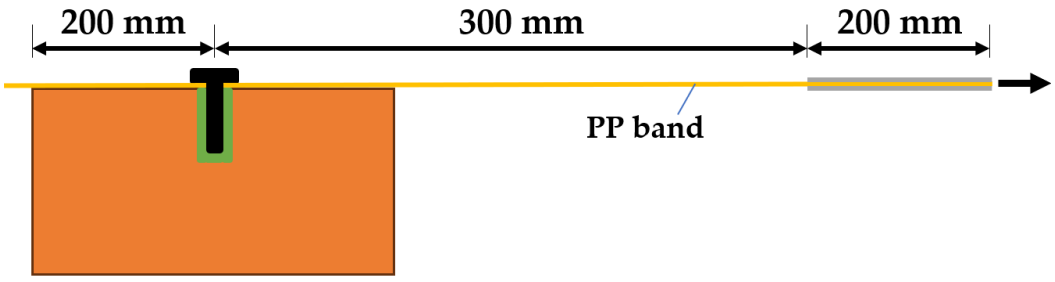

(d) Specimen dimensions

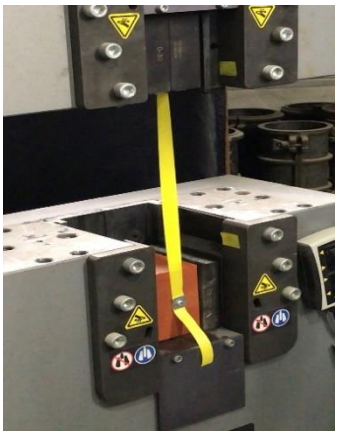

(e) Layout of specimen

Figure 2.5. Direct tensile tests at the fixed positions of the PP bands

The tensile stress-strain curves for the different cases are presented in Figure 4.5(a-c). It observed that in case (1), the average tensile strength and strain were lowest at 36.5 N/mm^2 and 0.013, respectively (Table 4.2 and Figure 4.6(a)). The PP band was damaged and separated from the steel screw. Case (2) showed good bonding ability of the PP band and rough brick surface under the effect of the initial twisting force. The slide in strength of the PP band on the steel washer is also observed in Figure 4.6(b), at a strain range of 0.024 to 0.036. However, in terms of tensile strength and strain, it was still lower than that in Case (3). In case (3), the average tensile strength and strain were the highest at 81 N/mm^2 and 0.046 (Table 4.2 and Figure 4.6(c)). It was observed that the connection in Case (3) was the best compared to the other cases. The deformation at the linking part between the steel washer and PP band does not occur suddenly but is sustained awhile. At the position where is the edge of the undamaged hole. Therefore, it is advisable to use two steel washers to strengthen the specimens.

Table 2.2. Result of the tensile test in cases

Case	Sample	Load, N	Tensile strength, N/mm^2	Strain	Average of tensile strength, N/mm^2	Average of strain
1	OW-1	262	33.7	0.011	36.5	0.013
	OW-2	272	35.1	0.012		
	OW-3	317	40.7	0.016		

	OWPP-1	442	57.0	0.025		
2	OWPP-2	452	58.3	0.027	61.6	0.028
	OWPP-3	538	69.4	0.031		
	TWPP-1	628	81.0	0.055		
3	TWPP-2	607	78.3	0.038	81.0	0.046
	TWPP-3	649	83.7	0.045		

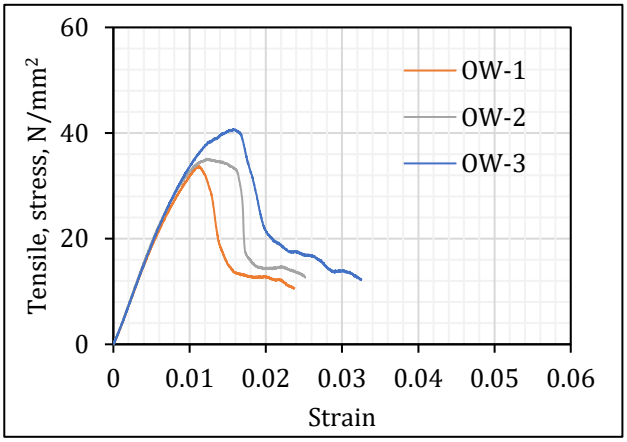

(a)

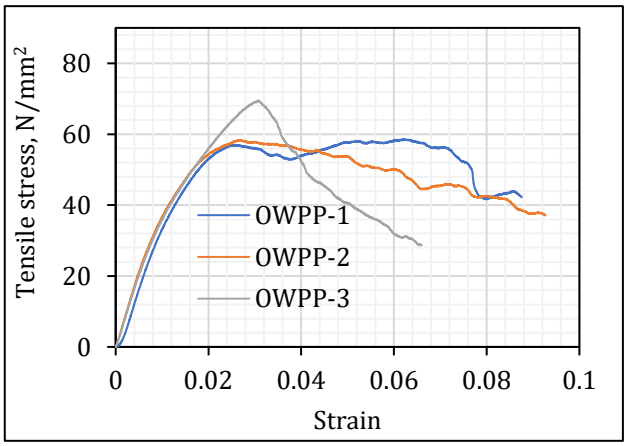

(b)

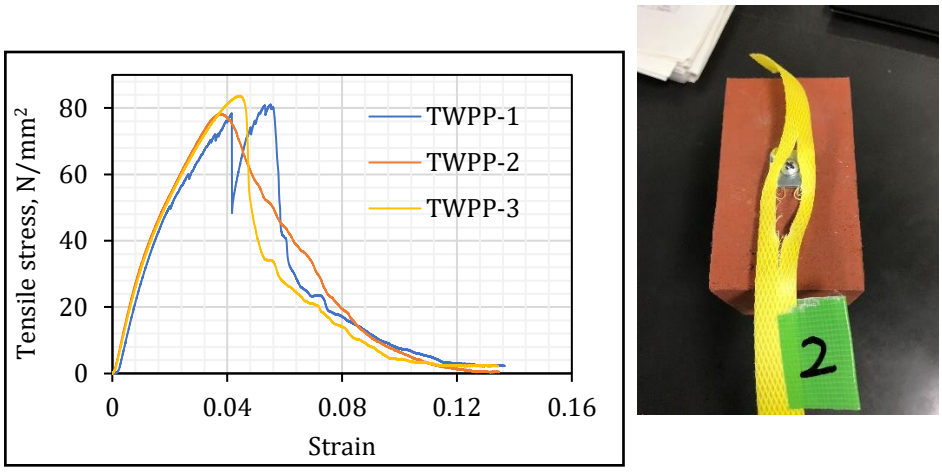

(c)

Figure 2.6. Tensile stress-strain curves and failure patterns in the investigated cases

2.4. Conclusions

This chapter has presented an overview of methods of fixing PP strips on walls. Three ways of fixing PP strips have been mentioned. Two of the three methods were investigated in previous studies. In addition to the advantage of these two methods, which is that they are easy to implement, the disadvantage is that they do not fully utilize the pulling ability of the PP strip. The first method, by using pipe A and steel fibers to fix to the wall, will cause the fixed position to have low stiffness, causing the PP strip network and the wall to not move at the same time when subjected to load. The second way can create traction in the PP strip, but the connection of the PP strip network with the wall is not good. From the above observation, the third fixation method proposed by the author in this study is intended to increase strength at the fixed position as well as create tensile force in the PP strip when conducting reinforcement work. Three cases of PP strip fixation were studied in this chapter. The results presented that using two steel plates gives the greatest tensile strength. The destruction does not occur immediately but lasts over a long period of time. It has an important meaning as it will increase the collapse time of masonry structures when applied in practice.

CHAPTER 3. TEST ON SMALL BRICK MASONRY

3.1. Experimental program

Derived from the proposed PP strip fixation method. In this chapter, experiments on small samples are outlined to verify the correctness of the proposed method. The three bending, shear and torsion behaviors of masonry were tested based on actual observations from storm wall damage as shown in Figure 3.1.

3.1.1. Introduction

It is well known that an earthquake is one of the leading cause of the collapse of masonry structure, and the two major seismic induced damage and collapse models of masonry walls are the in-plane and out-of-plane collapse mechanisms. The URM structures are much weaker in the out-of-plane direction than in the in-plane direction. Out-of-plane loading (perpendicular to the loading direction) is created by wind gusts in typhoons, leading to the collapse of houses. It is more dominant than the in-plane failure of URM wall. However, most masonry walls involved in real semi-permanent houses are supported on three or four sides. These boundary conditions lead to the assumption that the walls are subjected to bi-axial flexion when subjected to out-of-plane loads. The failure models of two-way spanning walls depend on the panel dimensions and support conditions. Consequently, the wall undergoes a combination of horizontal, vertical, and diagonal flexion, which must be investigated (Figure 3.1)

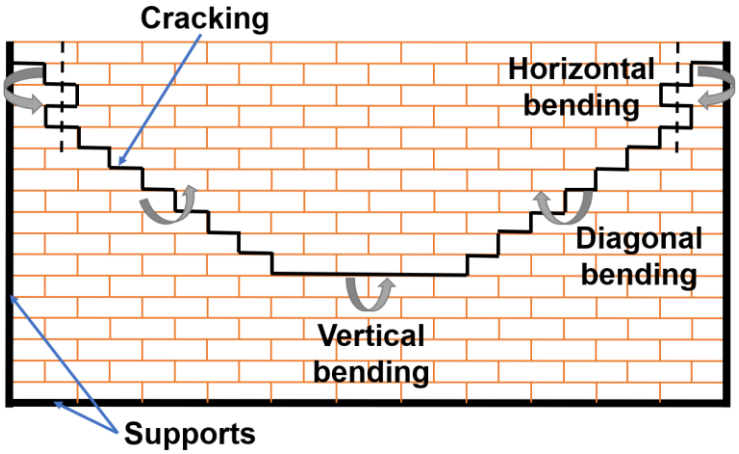

Figure 3.1 Two-way bending failure modes on three edges supported

3.1.1.1. Overview of one-way horizontal bending behavior

Horizontal bending strength is a fundamental parameter for masonry design. While it is uncommon for a wall to undergo pure horizontal flexure due to out-of-plane loading, some practical situations where the condition is approached include:

- A wall that is free along its top edge, that is simply supported along its vertical edges, and has flashing with a low coefficient of friction at its base.
- For a similar wall, but with no flashing, the top horizontal strip is predominantly in pure horizontal flexure if the wall is tall compared to it span

- Line failure:

For walls where the bond strength is relatively strong compared to unit strength, line failure may occur as a vertical through the brick units and perpend joints. Bending about an axis orthogonal to the bed joints is resisted by Figure 3.2(a).

(1) the flexural tensile strength of the perpend joint; and,

(2) the lateral modulus of rupture of the brick unit.

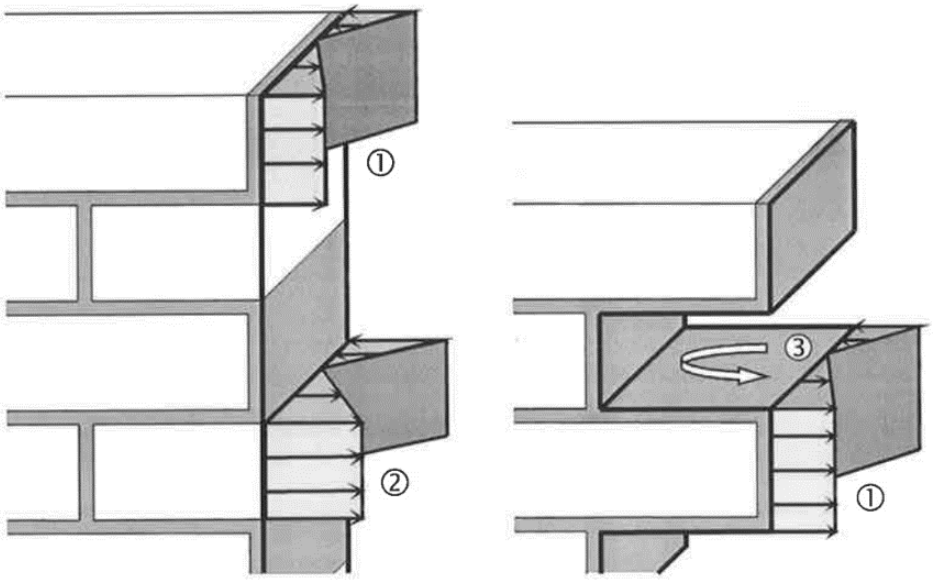

(a) Line failure (b) Stepped failure

Figure 3.2. One-way horizontal bending failure modes

- Stepped failure

Stepped failure is characterized by the propagation of a crack along a perpend joint then along half a horizontal joint (Figure 3.2(b)). Unlike one-way vertical bending, horizontal joint failure is most likely to be related to torsional shear and not tensile failure (Samarasinghe and Lawrence, 199; 1995), with frictional effects contributing to post-ultimate strength. Compressive stress due to self-weight and axial loading can substantially increase the torsional resistance developed on the horizontal joints (Baker, 1977; Samarasinghe and Lawrence, 1994). The failure mechanisms contributing to strength when failure occurs along a stepped crack line are (Figure 3.2(b))

(1) the flexural tensile strength of the perpend joint and

(3) torsional and frictional (post-ultimate) capacity of the horizontal joints.

- Load-deflection behavior

The one-way horizontal bending behavior of an URM section was discussed in with reference to the vertically oriented horizontal bending tests. The general load-deflection behavior is summarized here for completeness. To describe the horizontal bending response, eight key parameters of the load-deflection behavior were identified (Figure 3.3)

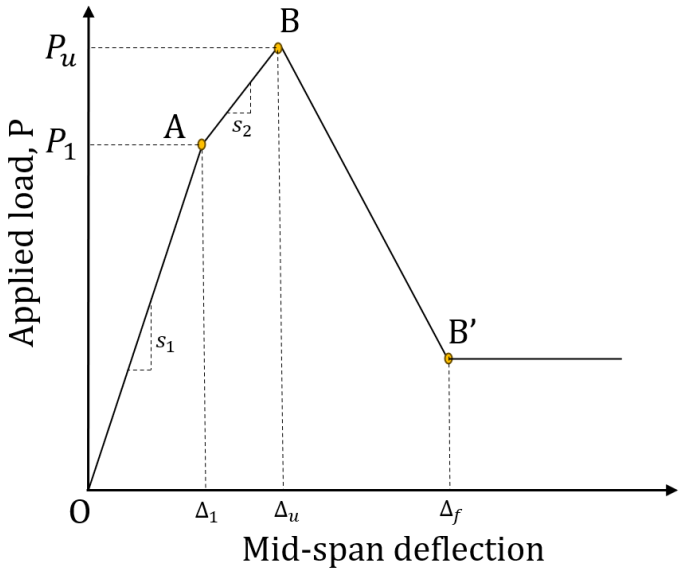

Figure 3.3. One-way horizontal bending behavior

- Primary slope, s_1
- Load at change slope, P_1
- Deflection at change of slope, Δ_1
- Secondary slope, s_2
- Ultimate load, P_u
- Deflection at P_u, Δ_u
- Frictional load resistance, P_f,
- Deflection at which P_u is reached, Δ_f

The typical moment-curvature behavior for masonry subjected to flexure parallel to the horizontal joints (Figure b) exhibits a significant decrease of stiffness before the ultimate strength is attained. Base and Baker (1973) reported a distinct change in stiffness during loading for small wall specimens subjected to horizontal bending. Lawrence (1983) attributed this to the gradual decrease of stiffness of the perpend joints. For the load-deflection behavior, the primary slope, s1, is linear, indicating elastic response. The load, P1, is the load where cracking of the perpend joints first occurs, corresponding to a marked change in slope (Lawrence and Morgan, 1975a; Lawrence, 1983; 1995). At this load, the level of deflection is low, hence the amount of torsional strain, and therefore stress, on each horizontal joint is also low. As a result, section strength is initially governed by the flexural strength of the perpend joints. For increases beyond the deflection at change of slope, Δ_1, the perpend joint cracking progresses (Lawrence, 1983; 1995), causing the load-deflection behavior to become increasingly governed by the torsional behavior of the horizontal joints. The load continues to increase at a less steep rate until the ultimate strength of the section, Pu, is reached at Δ_u. At this point, a mechanism develops due to torsional failure of horizontal joints or flexural failure of brick units and the load reduces to the residual capacity, P_f at Δ_f. The residual capacity is predominantly due to the frictional resistance of the horizontal joints (Baker et. Al, 1980) and is proportional to the compressive stress on the section. For a pure line failure, no frictional resistance is offered. In practice, the change of slope at Δ_1 occurs progressively (Lawrence, 1983) over the response between Δ_1 and Δ_u since the perpend joints do not fail simultaneously.

3.1.1.2. Overview of diagonal bending behavior

Most walls are supported on three or four sides, resulting in biaxial bending conditions when subjected to out of plane loading. The failure modes for two-way spanning walls depend on the panel dimensions and support conditions (Figure 3.4). The diagonal crack lines, which emanate from horizontal cracks in vertical bending. Wall strength is strongly influenced by the bending capacity along diagonal crack lines. At ultimate strength, the failure mechanisms that potentially contribute to the moment capacity, M_d, along a diagonal crack line are (Figure 5.4):

(1) The flexural tensile strength of the perpend joints;
(2) The torsional capacity of the bed joints
(3) The torsional capacity of the perpend joints
(4) The flexural tensile strength of the bed joints

Due to two-way action, prior to cracking, the torsional and flexural mechanisms occur simultaneously on each mortar joint. After cracking, resistance is governed by the frictional capacity of the joints. In reported results on full-scale wall panels, brick failure rarely occurs.

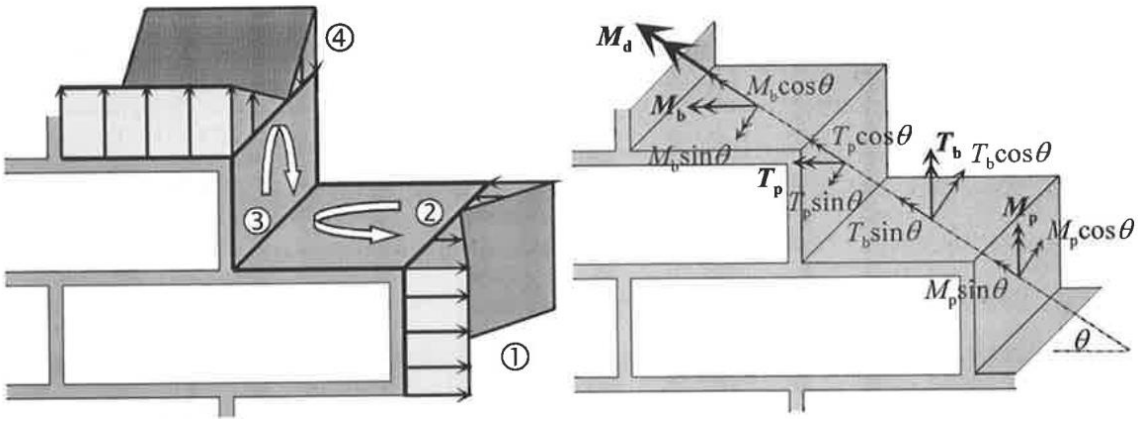

Figure 3.4. Diagonal bending failure mechanisms

where:

M_b is moment developed by each bed joint

M_p is moment developed by each perpend joint

T_b is torque developed by each bed joint

T_p is torque developed by each perpend joint

θ is angle of diagonal crack line to horizontal

3.1.1.3. Overview of one-way vertical bending behavior

For one-way vertical bending to occur, a wall must be supported at its upper and lower edges, and free along its vertical edges. An example of this type of wall is an internal URM partition wall without returns. Figure 3.5 shows a one-way vertically spanning URM wall subjected to an out of plane load, w, and undergoing a mid-height deflection, Δ. The wall is subjected to a vertical axial load, P, and is cracked at its supports and mid-height with the wall halves acting as rigid bodies.

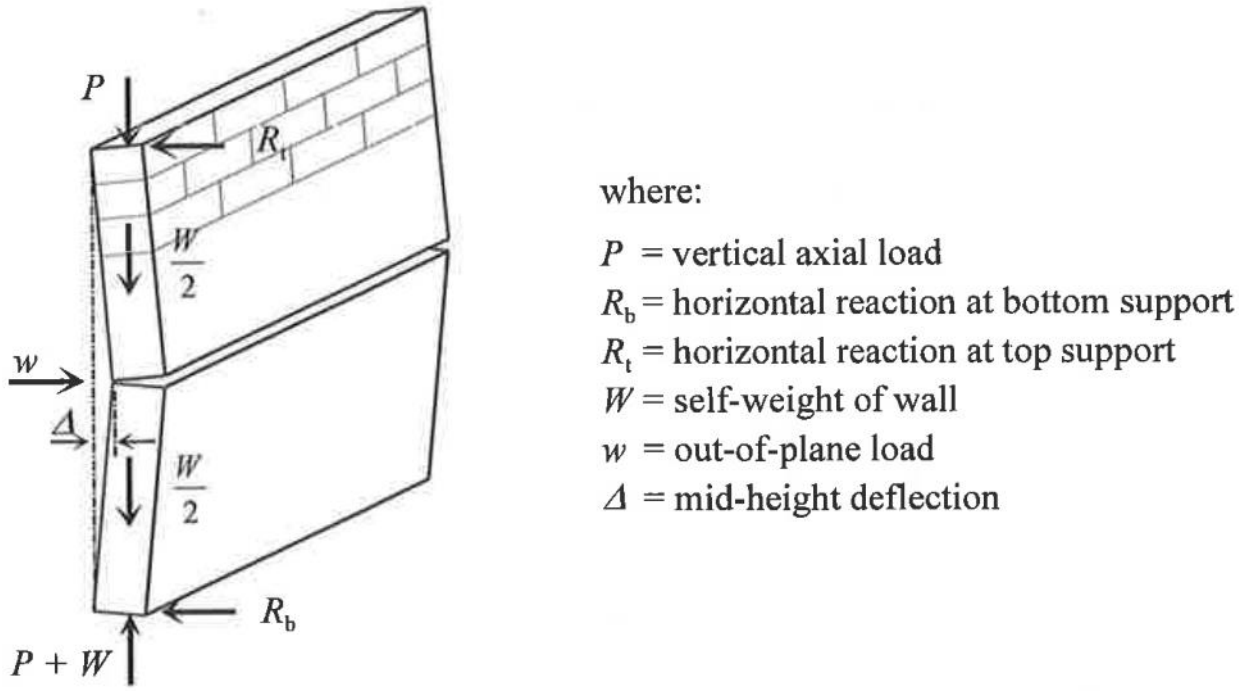

Figure 3.5. URM wall subjected to one-way vertical bending

The flexural capacity of a vertically spanning wall is highly dependent on the level of axial loading and bond strength f_{mt}. One the tensile stress in a bed joint due to out of plane loading exceeds the sum of the flexural tensile stress due to the unit-mortar bond plus the total compressive stress due to self-weight and axial loading, then cracking occurs in that joint.

The location of the crack generally occurs slightly above wall mid-height. Under static load-control conditions, collapse will not take place unless the out of plane is sufficient to cause formation of a collapse mechanism. Whereas, under deflection-control conditions, collapse will not occur until the mid-height deflection exceeds its point of instability (Priestley, 1985). Generally, the deflection at instability, Δ_u, is approximately equal to the wall thickness, t (Doherty et al., 2000)

The mechanisms are quite complex under the bending condition and the distribution of bending moment across the wall, which makes it difficult to assess failure mechanics completely on both the bed joint and head joint. Therefore, this study only focused on the failure behaviors of bed joints to investigate the effective strengthening of the PP band on bending, shear, and torsional behaviors using the method developed by author. The obtained results will be the necessary parameters to use for numerical modelling of actual walls in subsequent studies.

3.1.2. Material properties

Burnt bricks with dimensions of 210 × 100 × 60 mm (length × width × thickness) were used to construct the specimens, as per JIS R1250:2011. The mechanical properties of the bricks were determined by performing center-point bending, compression, and water absorption tests. The bricks were tested under uniaxial compressive loading (0.0075mm/s) along the horizontal directions. In further accordance to Vasconcelos and Lourenco, Young's modulus of brick (E_b) was also calculated by considering values between 30% and 60% of the compressive strength. A three-point bending test was also carried out on the brick unit at a rate 0.0075mm/s. The test results are summarized in Table 3.1.

Cement mortar was selected with the mix proportion of water/cement (C/S) and cement/sand (C/S) equal to 0.7 and 4.17, respectively. Tap water was used for mixing, and the water temperature was in the range of 25 ± 5°C. Cement, sand, and water were measured by weight in accordance with their respective proportions. Saturated surface dry sand with a grain size of less than 0.6 mm was used in each mix. The mechanical properties of mortar were evaluated by testing mortar prisms of 40 × 40 × 160 mm at the age of 28 days and experiment day. Molding was performed under laboratory conditions. The samples were

kept in the steel mold for 24h after casting, and the samples were removed from the molds after they were kept in the curing water until the date of testing. The flexural strength was measured by means of three-point bending tests, whereas the compressive strength was determined on the halves of the specimens after the bending tests. The mechanical properties of the mortar are listed in Table 3.1 together with the coefficient of variation (COV) in parentheses.

Figure 3.6. Compressive and flexural test for brick and mortar

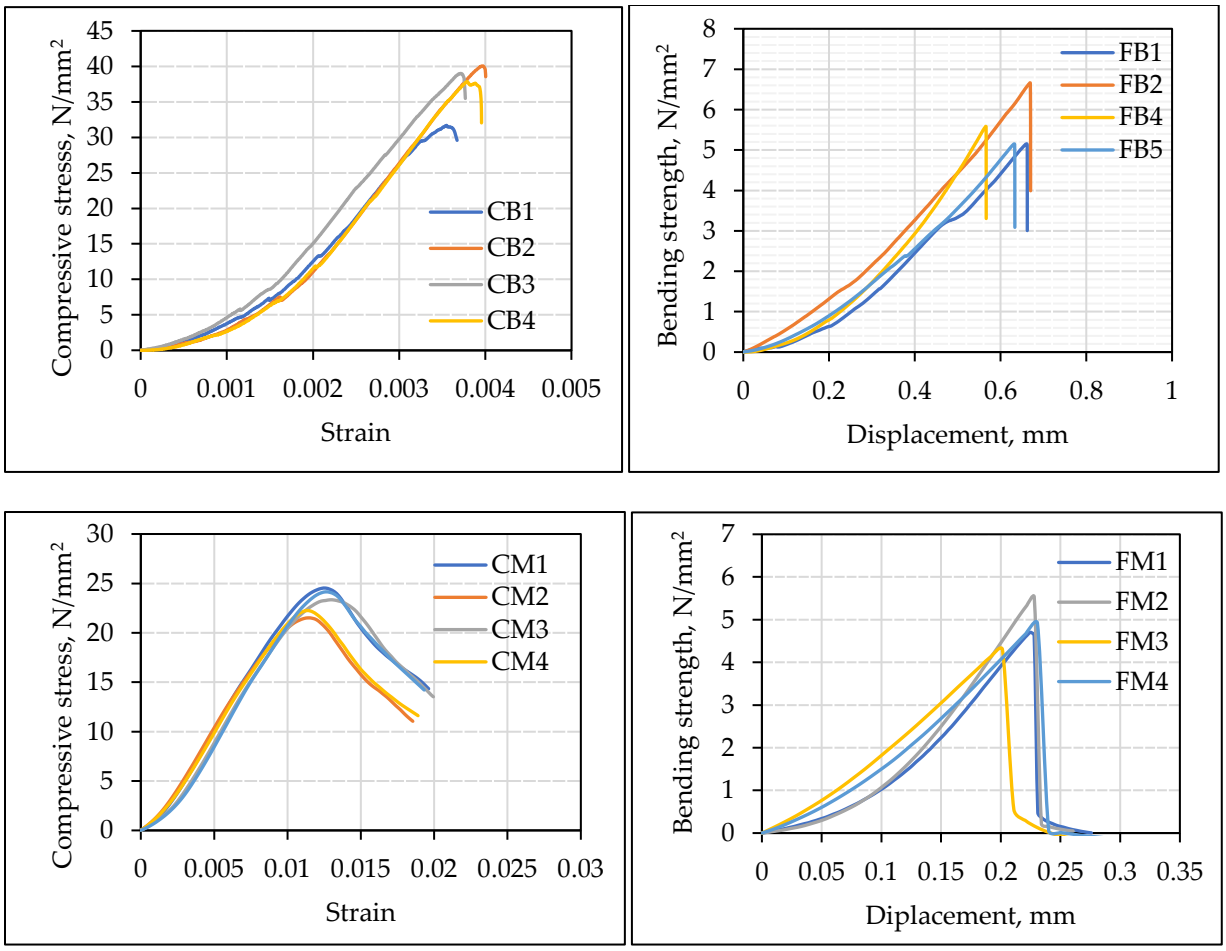

Figure 3.7. Mechanical properties of brick and mortar

Table 3.1. Mechanical properties of materials

Type of material	Properties		Values (COV)
Brick	Dimension, mm		210 × 100 × 60
	Density		1.98 g/cm³
	Water absorption		9 % (4.3%)
	Flexural strength		5.2 N/mm² (9.8%)
	Compressive strength		36 N/mm² (10.3%)
	Young's modulus		15700 N/mm²
Ordinary Portland Cement	Density		3.15 g/cm³
	Specific surface area		3490 cm²/g
Pit Sand	Density		2.61 g/cm³
Mortar	Flexural strength	28 days	3.6 N/mm² (10.4%)
	Compressive strength		17.4 N/mm² (11.5%)
	Young's modulus		2400 N/mm²
	Flexural strength	Experiment day	4.7 N/mm² (11.7%)
	Compressive strength		23 N/mm² (12.6%)
	Young's modulus		-

3.1.3. Flexural test

Nine prism specimens were subjected to the flexural failure test with seven bricklayers, and six layers of mortar joints, with dimensions of 480 × 210 × 100 mm (Figure 3.8). Four of the nine (FN-1 to FN-4) were not strengthened by the PP band to determine the flexural tensile strength of the joint, and the others (FP-1 to FP-5) were strengthened by the PP band. Table 5.2 listed the dimension of prism specimens and the distance between supports. The distance between the two fixed PP band positions was approximately equal to the distance between the two PP bands. The tensile force of PP band when strengthening was created by hanging scale with a value of 80 N for all specimens. A four-point bending test was performed according to the recommendation of ASTM E518:2010 [28]. The prism specimens were placed horizontally on the support, the distance between supports was maintained at 430 mm (L), and the two-line load was applied by two steel rods with dimensions of 120 × 22 mm (length × diameter), with a space of 142 mm, as illustrated in Figure 3.9. The flexural strength is calculated using Equation 3.1.

$$R_{um} = \frac{(P + 0.75P_s) \times L}{b \times d^2} \tag{3.1}$$

where R_{um} is the ultimate flexural strength, P_s is the self-weight of the prism (N), L is the span (mm), b is the average width of the prism (mm), and d is the average depth of the prism (mm).

In addition, mechanical properties, such as stiffness and ductility, were considered because they are critical parameters for determining the efficacy of any strengthening technique in flexural behavior. The initial stiffness is given by the ratio of the flexural strength to the deflection at the first crack, whereas the secant stiffness is obtained from the ratio of the ultimate flexural strength to the corresponding deflection. Ductility, which is the deformation capacity of a structure before collapse, is evaluated using Equation (3.2).

$$\mu_\Delta = \frac{\Delta_u}{\Delta_y} \tag{3.2}$$

where, Δ_u; Δ_y are the deflection at ultimate load P_u and cracking load P_y, respectively.

Table 3.2. Dimension of prism specimens and the distance between supports

Numbers		Weight W, N	Span L, mm	Wide b, mm	Depth d, mm
FN-1		200.3	426	210.0	100.0
FN-2	Non PP	199.8	427	209.5	100.5
FN-3	band	198.3	427	210.3	100.0
FN-4		198.1	427	209.7	99.80
FP-1		203.4	432	209.8	100.0
FP-2		200.4	427	211.5	101.2
FP-3	PP band	198.1	428	210.0	101.6
FP-4		201.6	430	210.5	100.0
FP-5		205.1	432	210.0	100.0

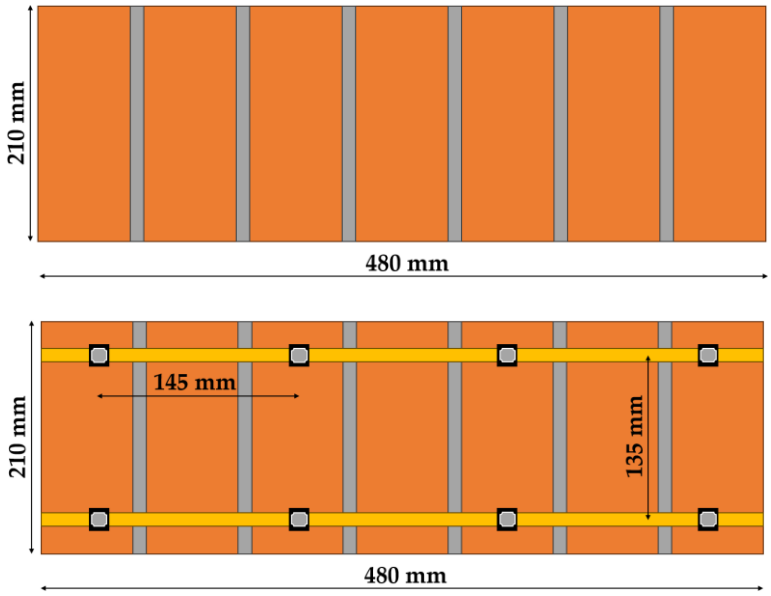

Figure 3.8. Unreinforced prism specimen and reinforced prism specimen

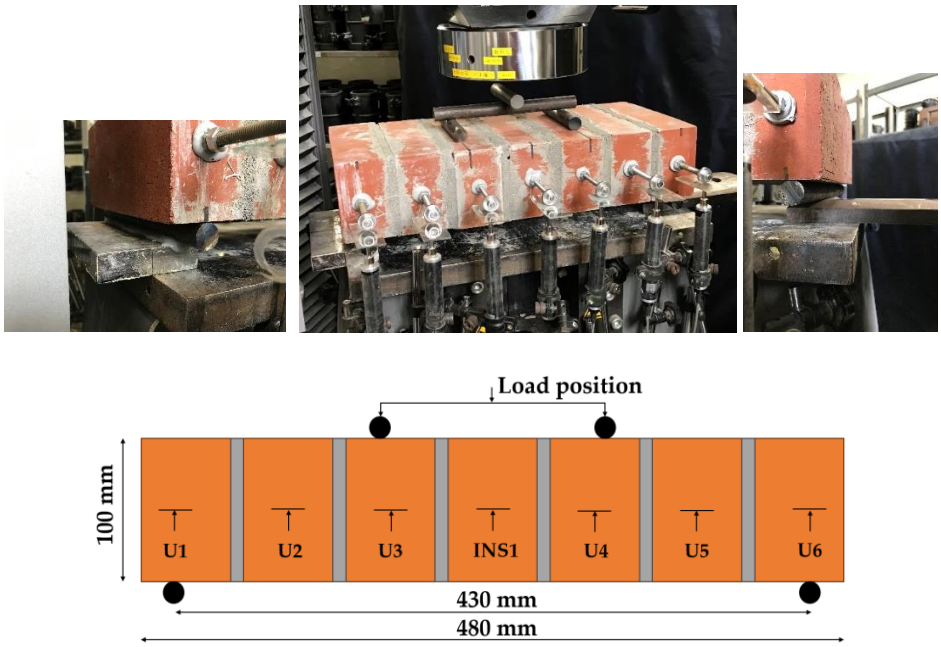

Figure 3.9. Flexural test set up

Fourteen linear variable displacement transducers (LVDT) (U1 to U12; INS1 and INS2) were installed on neutral line of the specimen at two sides to measure the prism displacement during the test, as shown in Figure 3.9. Two LVDTs (INS1 and INS2) at specimen center position and load cell were connected to the data acquisition system of universal testing machine (INSTRON). Due to limitations in the output of the system in Instron, only two LVDTs were used. The others were connected to fast data logger (U-CAM). The load rate for all prism specimens was kept at 0.005 mm/s. The timing synchronization between the U-CAM and Instron data will be performed.

3.1.4. Shear test

Thirty triplet masonry specimens were used in the shear behavior test. Each triplet specimen was created from three layers of brick and two layers of mortar with dimensions of 210 × 204 × 100 mm, as shown in Figure 3.10. Eighteen of 30 prisms without PP bands were used to determine the friction angle and cohesion of the mortar joint. Four different levels of pre-compression were used (0 N/mm^2, 0.2 N/mm^2, 0.4 N/mm^2, and 0.6 N/mm^2) in accordance with RILEM TC 127-MS:1996. The remaining triplet specimens will be used to estimate the effects of strengthening with the PP band in the shear behavior test. Furthermore, the stiffness of each specimen was ascertained from the stress-slip relationship curve. The

strengthening steps for the specimen with PP band were carried out similarly to that in the flexural test.

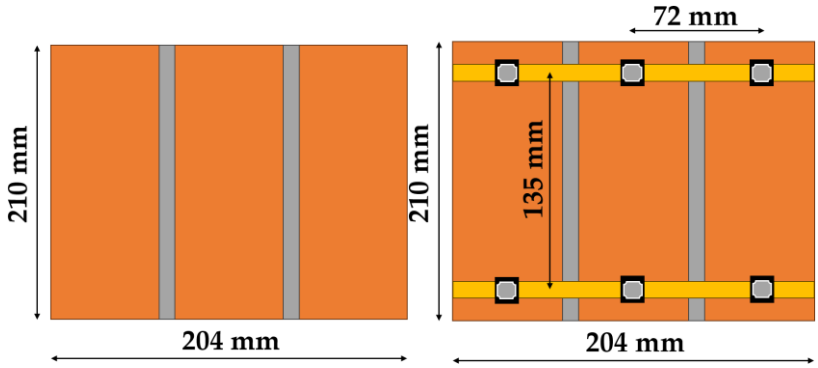

Figure 3.10. Non PP band triplet specimen and PP band triplet specimen

At first, the compressive stress was applied to the specimen via threaded bars before the shear load was applied. To obtain the pre-compression stress, the directional tensile tests of the two threaded bars were initially performed in the elastic region using four strain gauges. The primary purpose was to determine the force-strain relationship in each threaded bar (Figure 3.11). Prior to conducting the shear behavior test, four strain gauges were connected to the fast data logger (U-CAM) to measure the strain created by the wrench tightening force exerted by the handle, (Figure 3.12(a)), up to the desired level of axial pre-compression. Two nuts fixed the bottom steel plate and two threaded bars, and a wooden board and a layer of paperboard were placed at the center of the steel plate. The specimen was placed on a wooden board and compressed by a wrench tightening force using the other two nuts to influence the second steel plate. This ensured diffusion of the compressive load on the entire surface of the specimen. After the pre-compression value was obtained, the specimens were tested in a 500 kN universal testing machine operating (INSTRON) in displacement control at a rate of 0.0075 mm/s, (Figure 3.12(b)). The shear load was applied along the vertical direction to the intermediate brick, on an area of steel plate of 120 × 54 mm^2. The displacement of each brick was measured using ten LVDTs (U1 to U8; INS1 and INS2) positioned on four sides of the specimens, as shown in Figure 3.12(b).

Triplet specimens were placed such that the applied load acted parallel to the mortar joints. A load was applied as close as possible to the joints. Supports were provided below the triplet specimens at both end units. The shear strength was calculated using Equation (3.3).

$$\tau = \frac{P}{A_1 + A_2} \tag{3.3}$$

where A_1 and A_2 are the areas of the upper and lower mortar joints on the brick surface (mm^2), respectively; and P is the ultimate load.

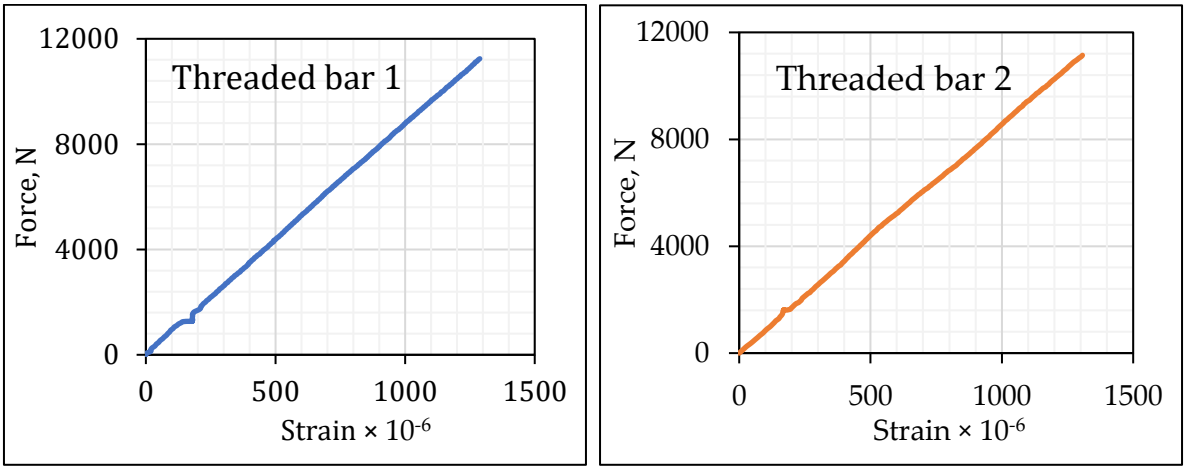

Figure 3.11. Directional tension of the threaded bar

The interface is governed by cohesive-frictional behavior, which was modeled using the Mohr-Coulomb failure criterion illustrated in Equation (3.4)

$$\tau = c + \sigma \tan \varphi \tag{3.4}$$

where c is the cohesion coefficient in N/mm^2, σ is the pre-compression in N/mm^2, φ is the friction angle in degrees.

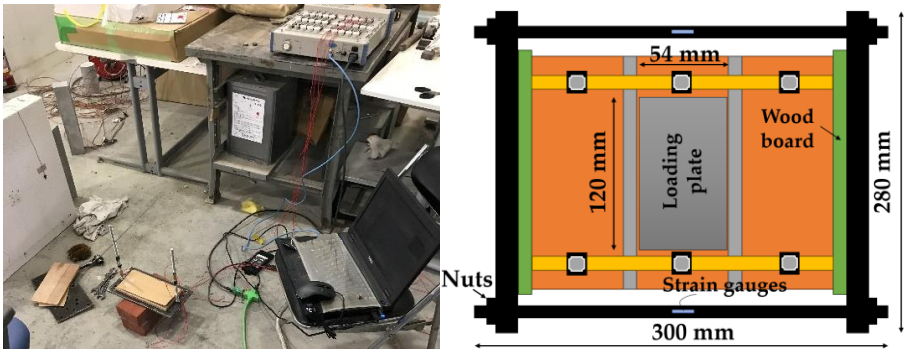

(a) Installation process

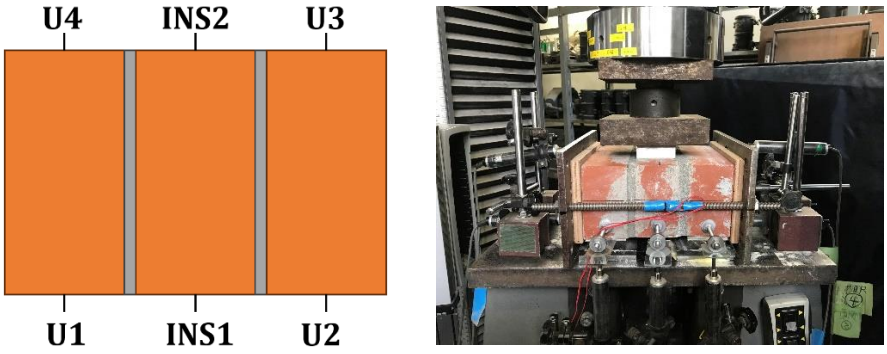

(b) Laying specimens on the machine

Figure 3.12. Test set up for shear test

3.1.5. Torsional test

Ten specimens were used for the torsional behavior test. Two layers of brick in each specimen were staggered (half-and-half) and one layer of mortar, as listed in Table 3.3. The PP band strengthened five specimens, the other five were not strengthened (Figure 3.13). Strengthening for the specimen with PP band was performed similarly to that in the flexural test. The ultimate torsional strength was calculated using Equation (3.5)[30, 31].

$$\tau = \frac{P \times L}{b^2 \times \left(a - \frac{b}{3}\right)} \tag{3.5}$$

where τ is the ultimate torsional strength (N/mm^2), P is the ultimate load (N), a is the length of the mortar joint (mm), and b is the width of the brick (mm).

Table 3.3. Specimen dimensions on torsion test

Numbers		Span L, mm	Length a, mm	Width b, mm
TN-1	Non PP band	262	105.0	100.0
TN-2		263	106.4	100.5
TN-3		260	105.3	100.0
TN-4		262	105.5	99.80
TN-5		266	105.2	100.0
TP-1	PP band	264	104.8	100.0
TP-2		263	105.0	101.2
TP-3		265	106.5	101.6

TP-4	266	106.0	100.0
TP-5	267	104.5	100.0

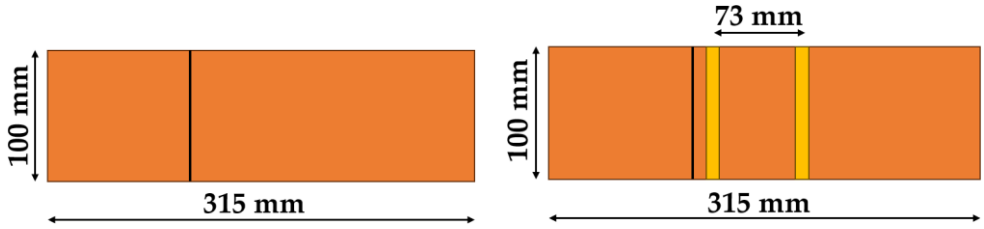

Figure 3.13. Non PP band specimen and PP band specimen

To measure the displacement of the specimen, two LVDTs (INS1 and INS2) were placed at the mid-span of the specimen at two lateral faces, as shown in Figure 3.14. They were connected to INSTRON. The load rate was kept at 0.005mm/s.

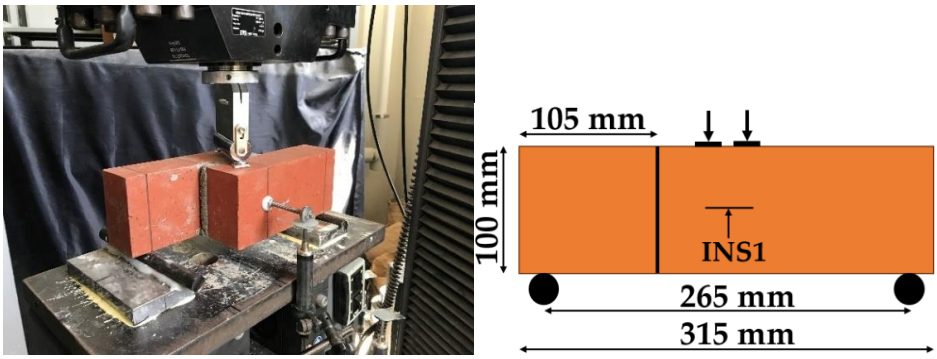

Figure 3.14. Test set up for shear test

3.1.6. Results and Discussions

3.1.6.1. Flexural test

Moment-deflection angle relationship of unreinforced specimens at center was displayed in Figure 3.15. Failure of the unreinforced prism specimens was sudden and brittle. Most prism specimens were split into two pieces (Figure 3.17). The failure of the specimen was caused by a crack that appeared near either side of the loading steel rod. The average peak flexural strength, average deflection, and average load-carrying capacity of the specimens at center were 0.343 N/mm^2, 0.026 mm and 0.163 kN.m, respectively (Table 3.4).

The experiment on PP band strengthened specimens showed that the PP band was effectively increased the collapse time of the specimens after the initial drop (Figure 3.16). The residual loading was observed in all specimens and improvements in the load-carrying capacity and deflection ability were observed for the reinforced specimen. The average load-carrying capacity at ultimate failure and deflection at first crack of the PP band specimens were 1.70 times and 1.62 times (Table 3.4) higher than that of Non PP band specimens. Similarly, the deflection ductility clearly increased, when compared to the Non PP band specimens, as listed in Table 3.4. The initial stiffness of the strengthened specimens was similar to that of unreinforced specimens. The secant stiffness showed a marked decrease. The first crack of FP-1, FP-3, and FP-4 specimens was initiated between the steel rod loading lines, while FP-2 and FP-5 specimens at outside of the steel rod loading lines (Figure 3.17(c,d)). The PP band took the resistance due to a further increase in load only. The test was terminated when the link between the PP band and the washer was completely ruptured (Figure 3.17(b)). We concluded that the proposed method produced the greatest improvement in the load-carrying capacity and the deflection. This proves the effectiveness of the proposed method, while Ref [16] has stated that the strength of wall did not increase with strengthening PP band.

Table 3.4. Mechanical properties of unreinforced and strengthened specimens in flexural test

Specimens	First crack		Ultimate failure		First crack	Ultimate failure	First crack	Ultimate failure	Deflection ductility, times	Average of improvement, times	
	Load, kN	Deflection, mm	Load, kN	Deflection, mm	Flexural strength, N/mm²		Flexural moment, kN.m			Deflection (First crack)	Moment (First crack and ultimate failure)
FN-1	1.53	0.041	-	-	0.34	-	0.163	-	1.0	-	-
FN-2	1.63	0.016	-	-	0.36	-	0.173	-	1.0		
FN-3	1.46	0.025	-	-	0.33	-	0.155	-	1.0		
FN-4	1.50	0.020	-	-	0.34	-	0.159	-	1.0		
Ave.	1.53	0.026	-	-	0.343	-	0.163	-			
FP-1	1.99	0.042	2.58	16.38	0.44	0.57	0.216	0.280	390	1.62	1.28 and 1.70
FP-2	1.85	0.040	2.61	9.53	0.39	0.55	0.198	0.279	238		
FP-3	2.23	0.035	2.49	14.65	0.46	0.51	0.234	0.262	419		
FP-4	1.82	0.039	2.83	22.09	0.40	0.61	0.196	0.304	566		
FP-5	1.77	0.054	2.32	6.55	0.40	0.52	0.194	0.254	121		
Ave.	1.93	0.042	2.57		0.418	0.552	0.208	0.276			

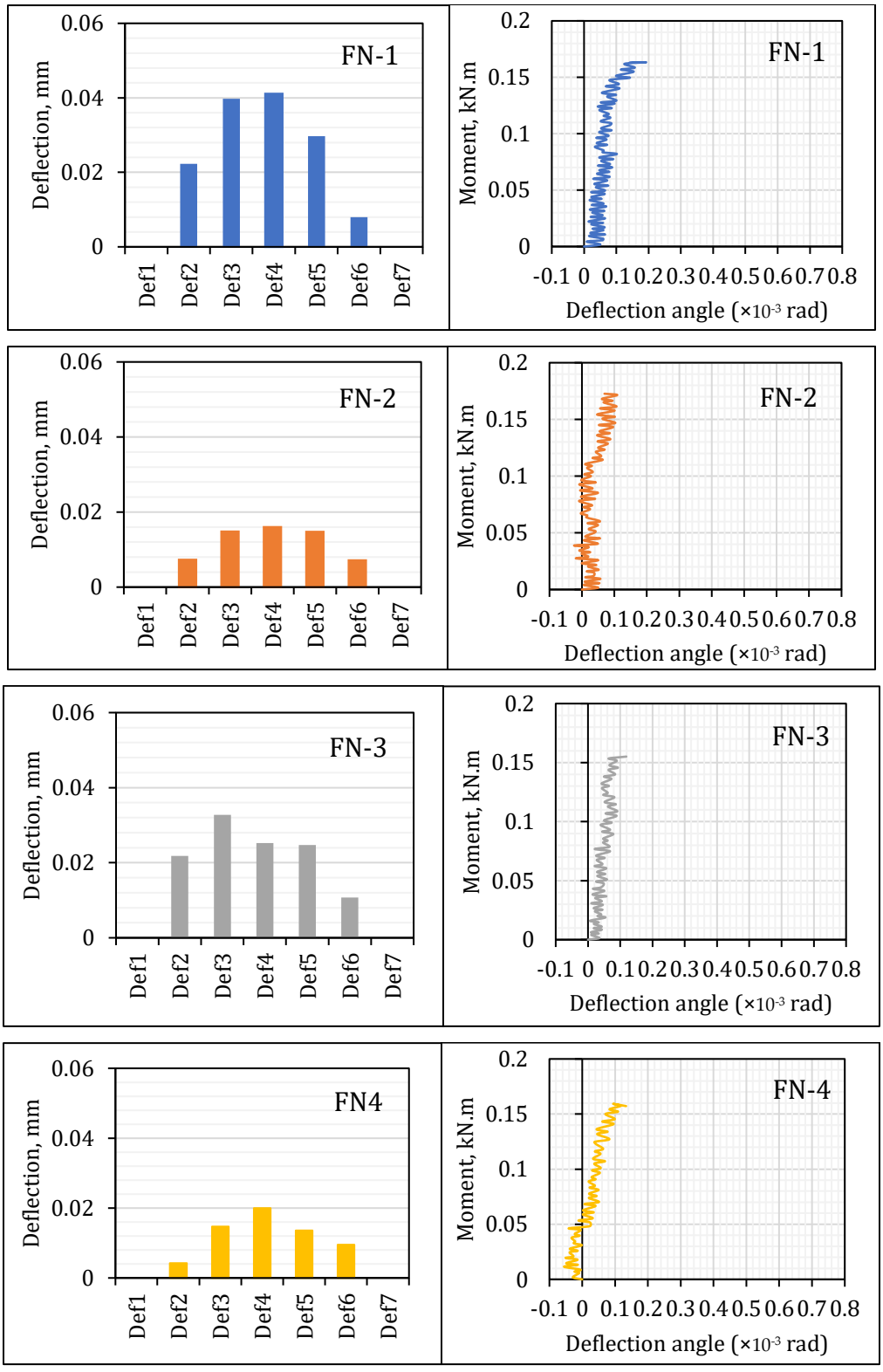

Figure 3.15. Moment-deflection angle relationships of the unreinforced

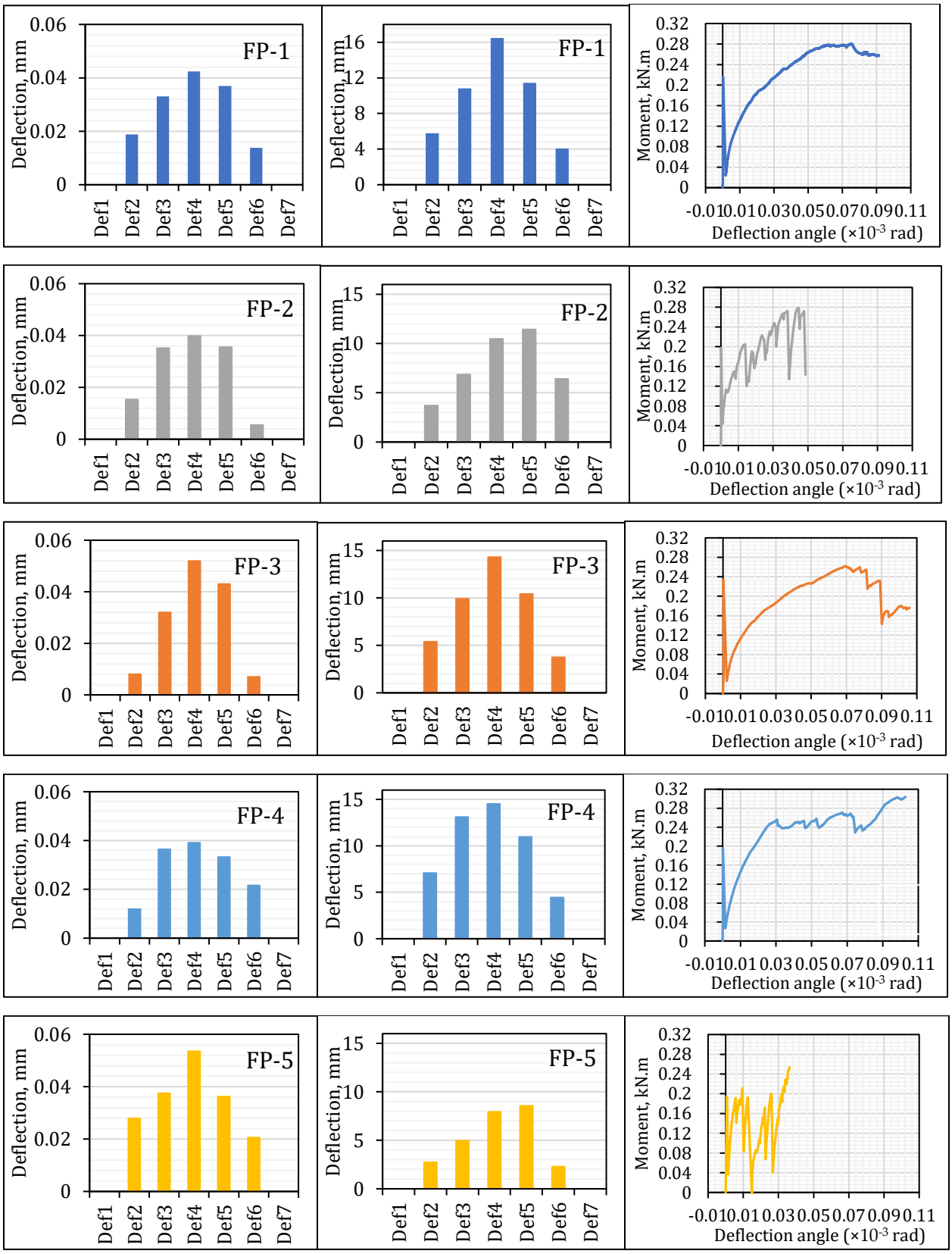

Figure 3.16. Moment-deflection angle relationships of reinforced specimens

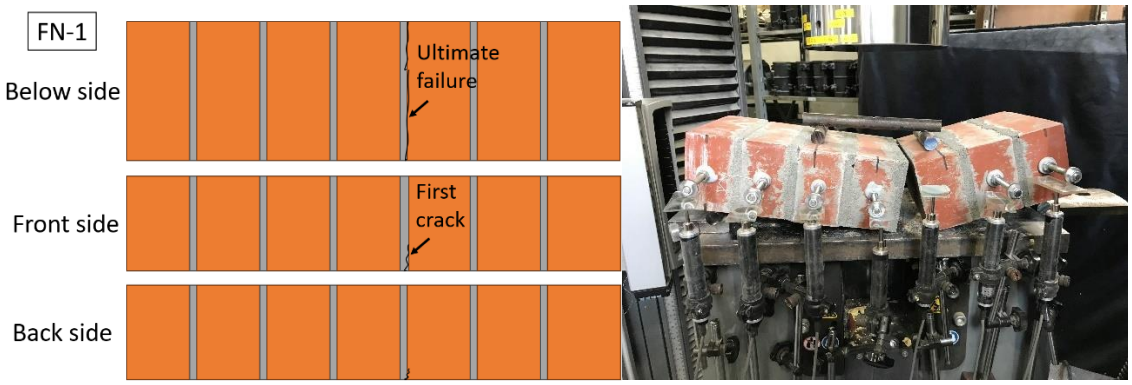

Non PP band specimen 1

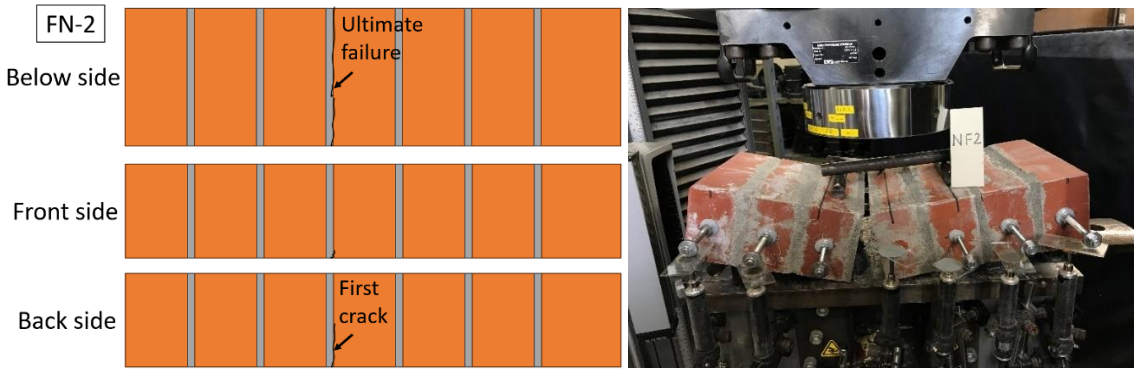

Non PP band specimen 2

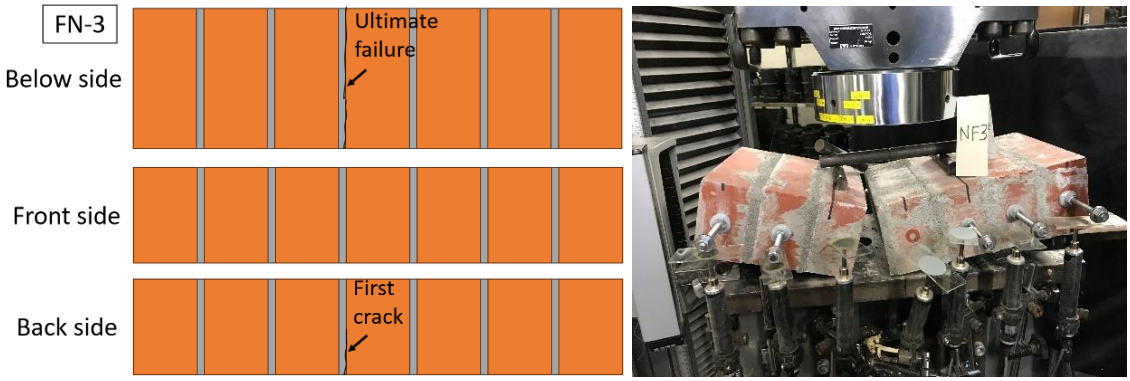

Non PP band specimen 3

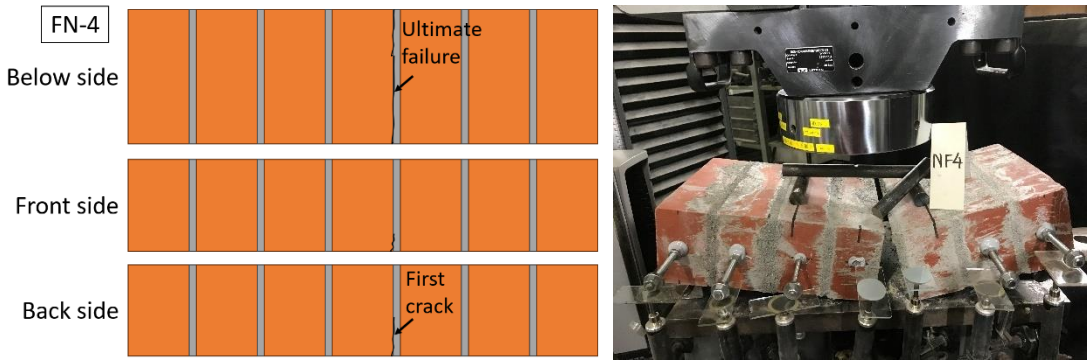

Non PP band specimen 4

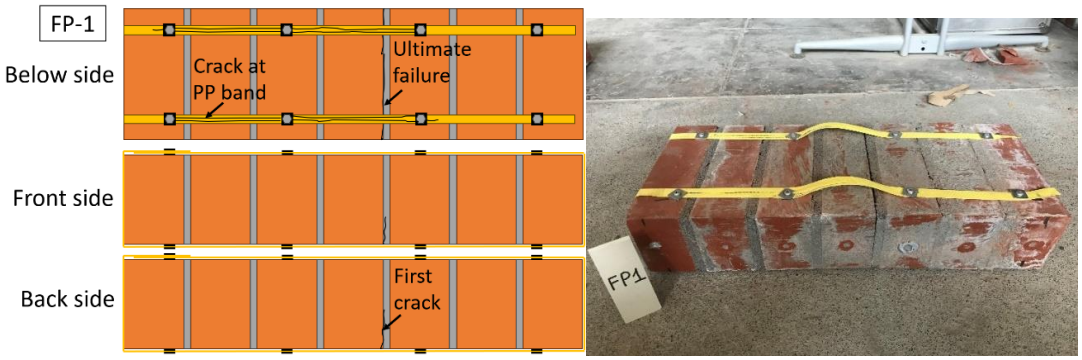

PP band specimen 1

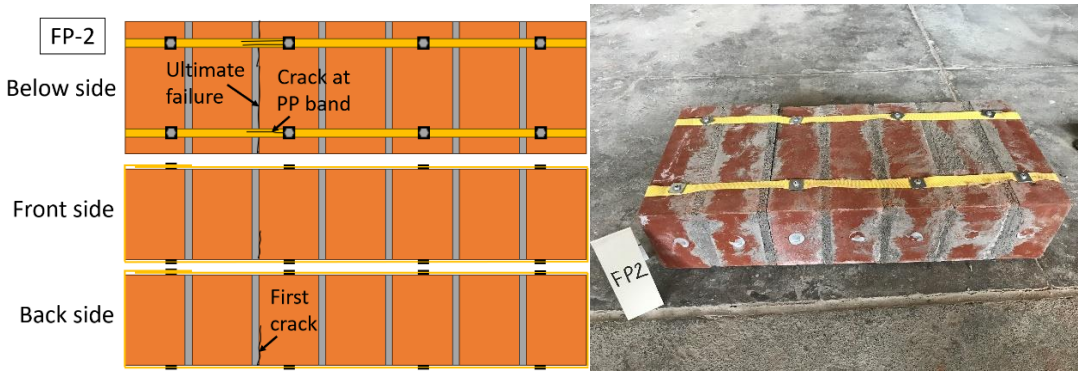

PP band specimen 2

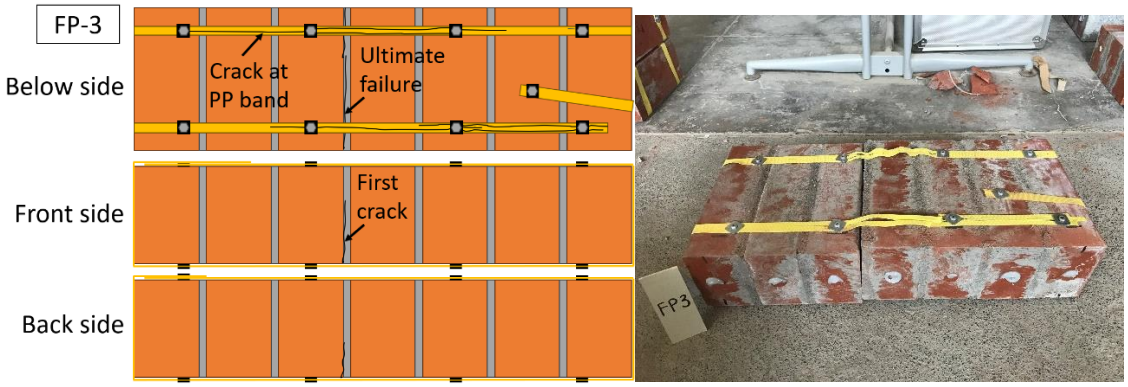

PP band specimen 3

In specimens without PP band, crack development begins on the back or front side of the specimen at the edge between the mortar and the brick. The load increases quickly then the crack widens further, causing the load to increase more slowly until it reaches the maximum load and the specimens is destroyed. In specimens with PP band, crack development similar to Non PP band specimens. First crack in PP band was started from the connection between

steel washer and steel plate, development at center of PP band. The position where fixed PP band on bricks was undamaged.

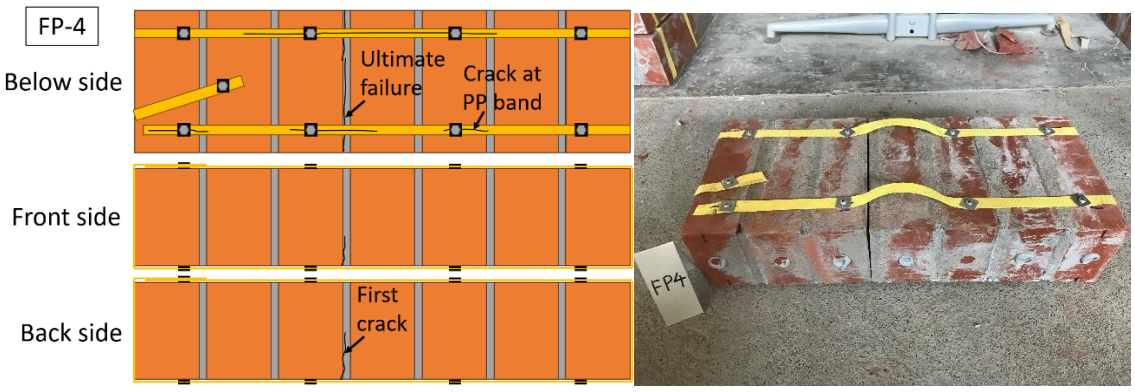

PP band specimen 4

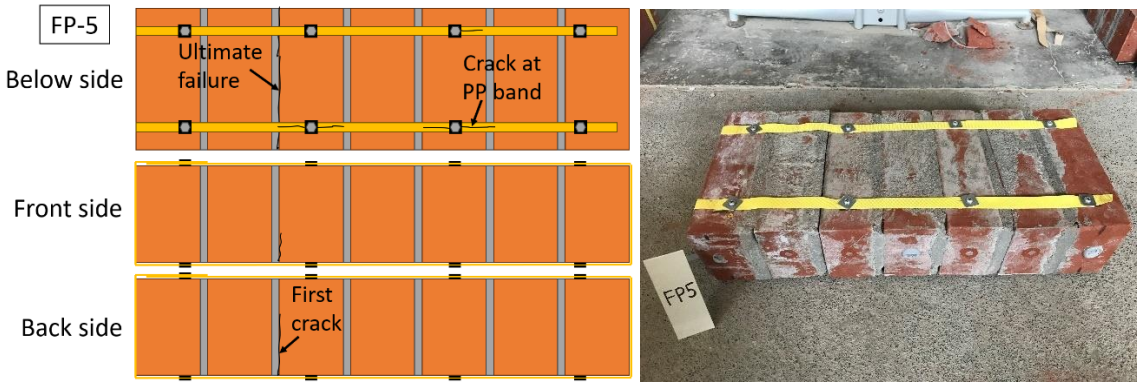

PP band specimen 5

Figure 3.17. Failure patterns of the specimens with PP bands and Non PP band

3.1.6.2. Shear test

Figure 3.19(a) illustrates the average shear strength-slip curves for various values of pre-compression (σ) for the unreinforced specimens. As observed, the shape of the curves depends on the level of pre-compression σ, with the shear strength τ increasing proportionally with σ. With each value of pre-compression (0, 0.2, 0.4, and 0.6 N/mm^2), the ultimate shear strength was obtained 0.39 N/mm^2, 0.51 N/mm^2, 0.95 N/mm^2, and 1.22 N/mm^2, respectively, as shown in Table 3.5. Tests on strengthened specimens (Figure 3.19(b)) showed an increase in shear strength for all pre-compression ranges of 0 – 0.6 N/mm^2, 0.57 N/mm^2, 0.96 N/mm^2, and 1.29 N/mm^2, respectively (Table 3.6). However, it

was not significant. The initial stiffness is not affected by the pre-compression level in both reinforced and unreinforced case.

Failure of the unreinforced and reinforced specimens is shown in two stages. In first stage, it will be destroyed at one of the four interfaces between the brick-and-mortar layer, where the bond between them was weaker. Afterwards, the load will continue to increase until the second interface between the brick and mortar is destroyed. The cause of increase was due to pressure from the two sides maintained during the experiment. In reinforced specimens, the two lateral bricks tended to move inward, which meant that the two PP band fixed points also moved, making the PP band slack. Consequently, we did not observe an increase more in load, and the load suddenly decreased. Hence, the role of the PP band in enhancing shear ability was not evident.

Table 3.5. Mechanical properties of unreinforced specimens in shear test

Sample	Load, kN	Slip, mm	Pre-compression σ, N/mm²	Shear stress τ, N/mm²	Average of shear stress τ, N/mm²	Average of slip, mm
SN0-1	17.87	0.084	0	0.43	0.39	0.078
SN0-2	14.78	0.072		0.35		
SN0-3	16.33	0.077		0.39		
SN02-1	19.98	0.094	0.2 (4.2kN)	0.48	0.51	0.102
SN02-2	24.47	0.101		0.58		
SN02-3	19.38	0.102		0.46		
SN02-4	22.01	0.116		0.52		
SN02-5	21.78	0.095		0.52		
SN04-1	39.29	0.128	0.4 (8.4kN)	0.93	0.95	0.128
SN04-2	37.17	0.121		0.89		
SN04-3	43.00	0.129		1.02		
SN04-4	41.72	0.132		0.99		
SN04-5	38.49	0.130		0.92		
SN06-1	49.65	0.185	0.6 (12.6kN)	1.18	1.22	0.207
SN06-2	52.60	0.235		1.25		
SN06-3	54.47	0.208		1.29		

SN06-4	54.07	0.194	1.19	
SN06-5	50.43	0.211	1.20	

Table 3.6. Mechanical properties of reinforced specimens in shear test

Sample	Load, kN	Slip, mm	Pre-compression σ, N/mm²	Shear stress τ, N/mm²	Average of shear stress τ, N/mm²	Average of slip, mm
SP02-1	26.94	0.126		0.64		
SP02-2	20.43	0.100	0.2	0.49	0.57	0.113
SP02-3	24.57	0.108	(4.2kN)	0.59		
SP02-4	23.61	0.116		0.56		
SP04-1	42.24	0.133		1.00		
SP04-2	38.72	0.121	0.4	0.92	0.96	0.124
SP04-3	41.54	0.128	(8.4kN)	0.99		
SP04-4	39.66	0.115		0.94		
SP06-1	55.62	0.223		1.32		
SP06-2	51.54	0.203	0.6	1.23	1.29	0.235
SP06-3	57.21	0.318	(12.6kN)	1.36		
SP06-4	53.34	0.196		1.27		

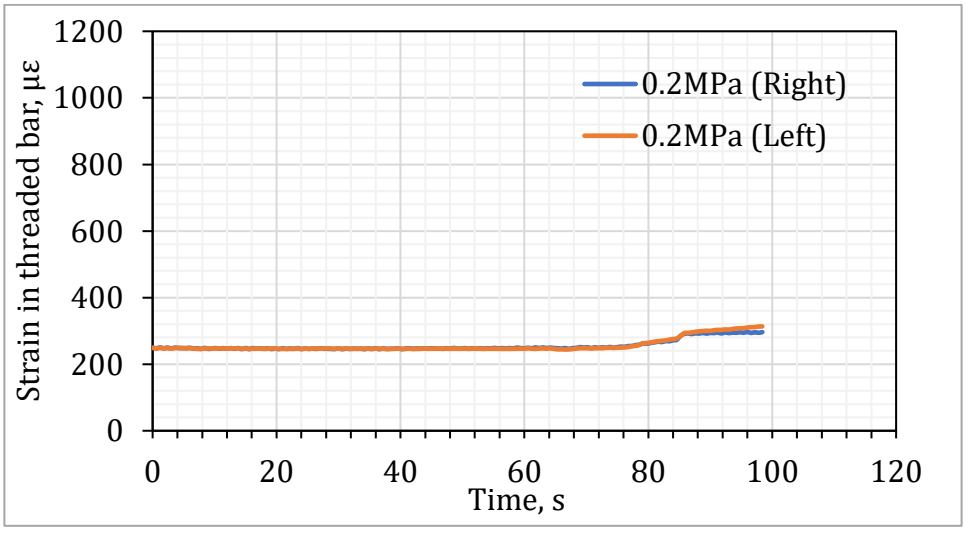

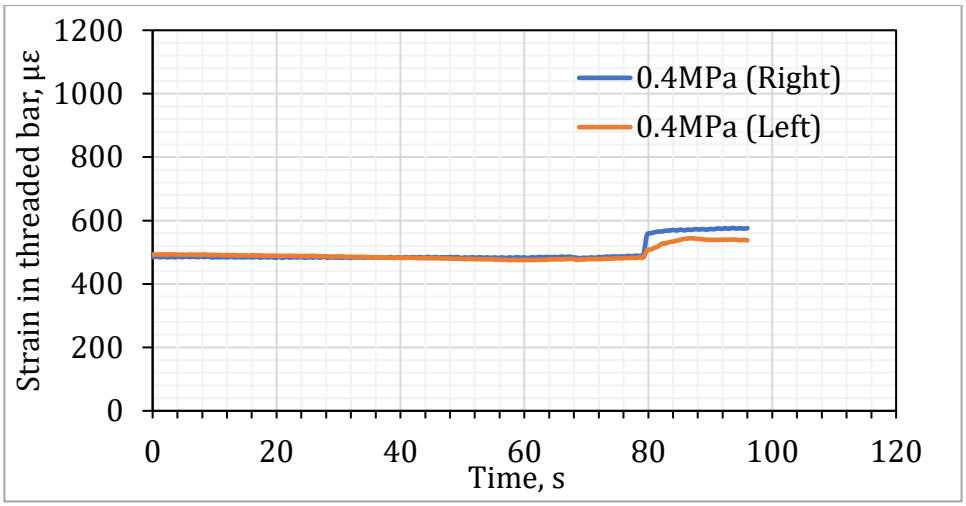

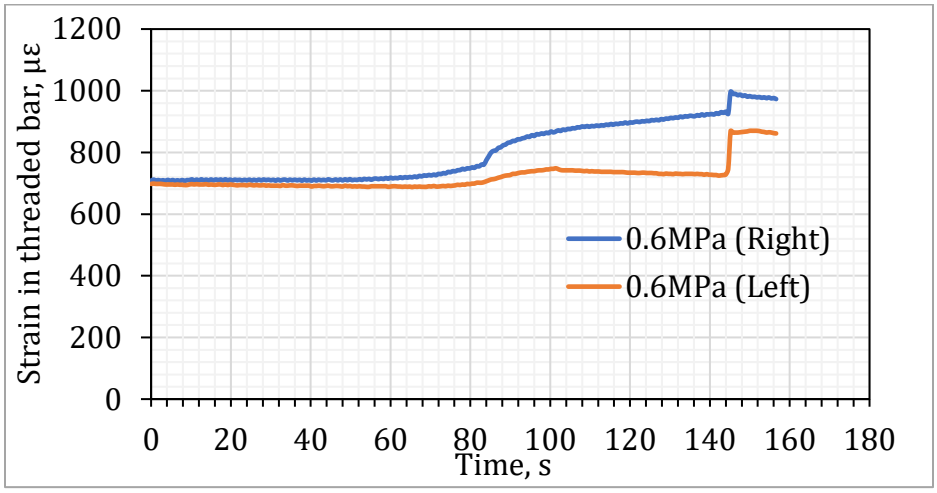

Figure 5.18. Relationship between strain-time in threaded bars

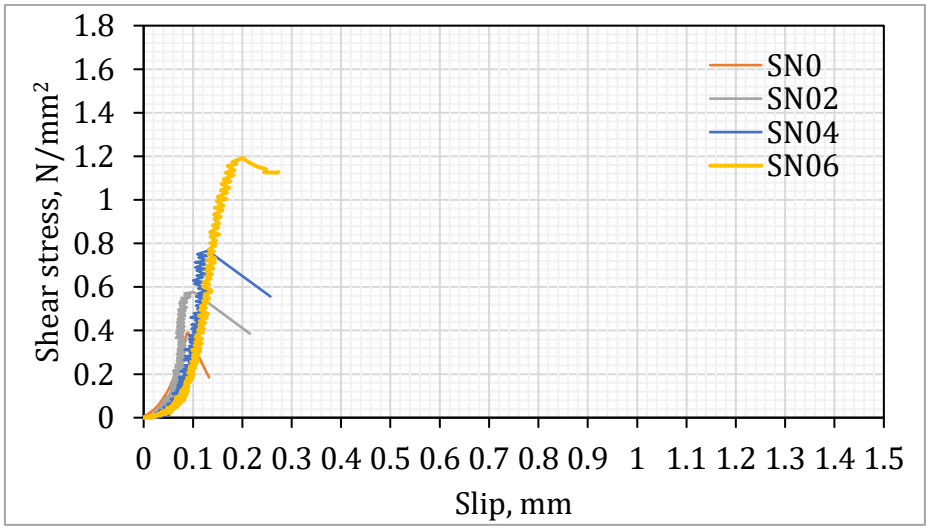

(a)

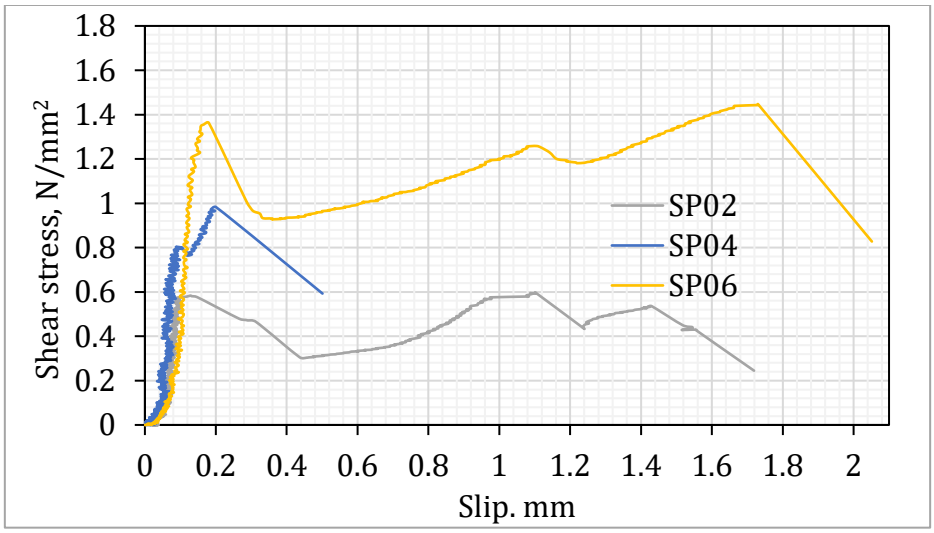

(b)

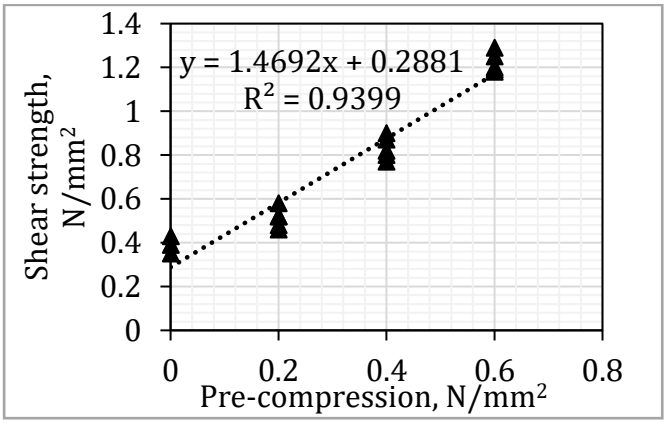

(c)

Figure 3.19. Shear stress-slip curve for unreinforced and reinforced specimens; Relationship between shear stress and pre-compression stress

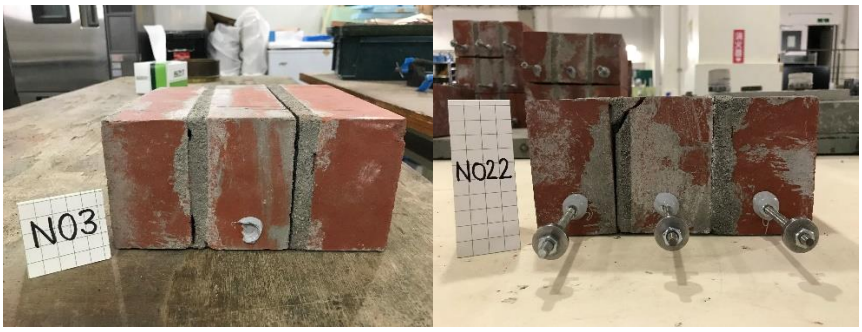

(a) SN0 (b) SN02

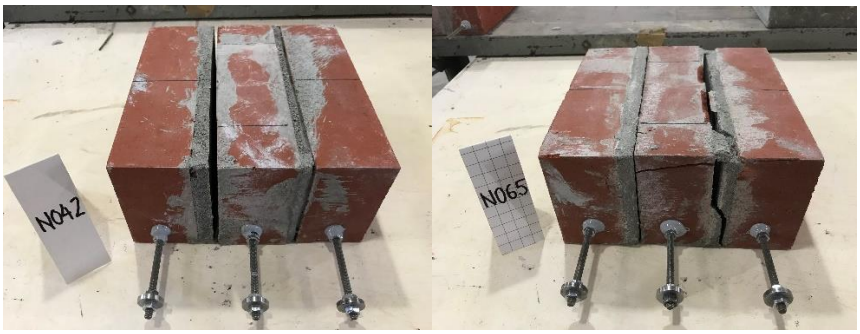

(c) SN04 (d) SN06

(e) SP02 (f) SP04

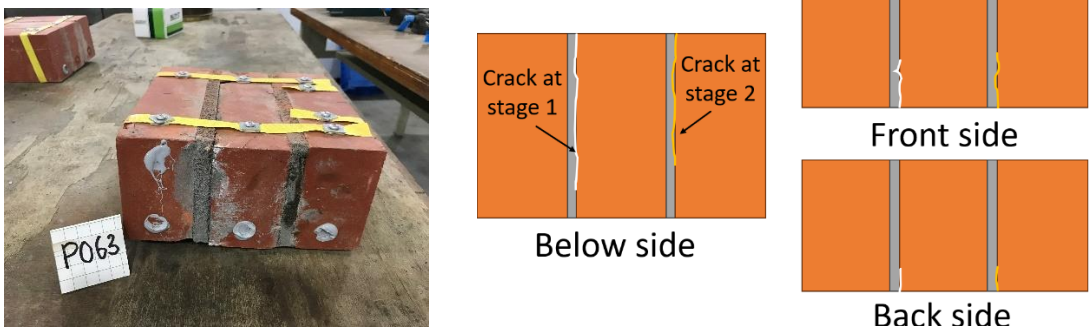

(g) SP06 (h) Development of crack in sides

Figure 3.20. Failure patterns of the shear specimens

Moreover, failure patterns of the unreinforced specimens are displayed in Figure 3.20(a-d). In cases of pre-compression (0, 0.2, 0.4 N/mm^2), cracks appeared at the mortar-brick interface. While with 0.6 N/mm^2, the observed failure mode was a combination of sliding along the mortar-brick interfaces and diagonal crack appeared near the interface through the mortar layer. A minor crack was also observed, propagating into the center brick at the peak load. The failure patterns of the reinforced specimens are also presented in Figure 3.20(e-g), it is observed that the reinforced specimens with PP band were not changed to

failure mode, cracks appeared in the mortar-brick interface of all cases of pre-compression. In case 0.6 N/mm^2, crack also observed in center brick.

The results in terms of pre-compression and shear strength at failure, together with parameters such as the friction angle and cohesion of the mortar joint were obtained from the linear interpolation in Figure 3.19(c). The cohesion value (c) is equal to 0.288 and the slope of the linear interpolation (tanφ) that indicates a friction coefficient of 1.469.

3.1.6.3. Torsion test

The load and deformation relationship of unreinforced and reinforced specimens are presented in Figure 3.21., and the results are summarized in Table 3.7. Failure of the unreinforced specimens was sudden and brittle. The improvements in the average load-carrying capacity and deformation ability at first crack were 1.21 times and 1.47 times, respectively. The load suddenly dropped and no longer increased. The ductility evidently increased. Crack occurred at the mortar-brick interface (Figure 3.22(a,b)). In the reinforced specimens, after failure, a slight increase in load observed in TP-2, TP-3, and TP-5 specimen until the PP band fixed position was ruptured (Figure 3.22(d)). But it was not exceeded the peak load. This circumstance was not the same as that in the flexural test. However, the PP band was effectively increased the collapse time of specimens. Unlike the cracks that appeared in TP-2, TP-3, and TP-5 specimen, cracks in TP-1 and TP-4 specimen appeared at both brick-and-mortar layer and bricks (Figure 3.22(c)). The cause of this is due to the strengthening method created a pre-tensioning force appears in the PP band, helping to increase reinforced specimen's load-carrying capacity.

Table 3.7. Mechanical properties of unreinforced and reinforced specimens in torsion test

Speci-mens	First crack		Ultimate failure		First crack	Ultimate Failure	Deflection ductility, times	First crack	Ultimate Failure	Average of improvement, times (First crack)	
	Load, kN	Deformation, mm	Load, kN	Deformation, mm	Torsional strength, N/mm^2			Torsional moment, kN.m		Deformation	Moment
TN-1	7.37	0.225	-	-	1.17	-	1.0	0.98	-		
TN-2	8.24	0.200	-	-	1.31	-	1.0	1.09	-		
TN-3	8.13	0.267	-	-	1.29	-	1.0	1.08	-		
TN-4	7.14	0.214	-	-	1.14	-	1.0	0.95	-	-	-
TN-5	7.89	0.207	-	-	1.25	-	1.0	1.05	-		
Ave.		0.223			1.23			1.03			

TP-1	9.98	0.393	-	-	1.59	-	-	1.32	-		
TP-2	9.18	0.346	5.89	19.09	1.46	0.94	55	1.22	0.78		
TP-3	8.07	0.319	4.82	21.09	1.28	0.77	66	1.07	0.75	1.47	1.21
TP-4	11.06	0.297	-	-	1.76	-	-	1.46	-		
TP-5	8.49	0.282	5.71	20.38	1.35	0.91	72	1.11	0.75		
Ave.		0.327			1.49	0.87		1.24	0.76		

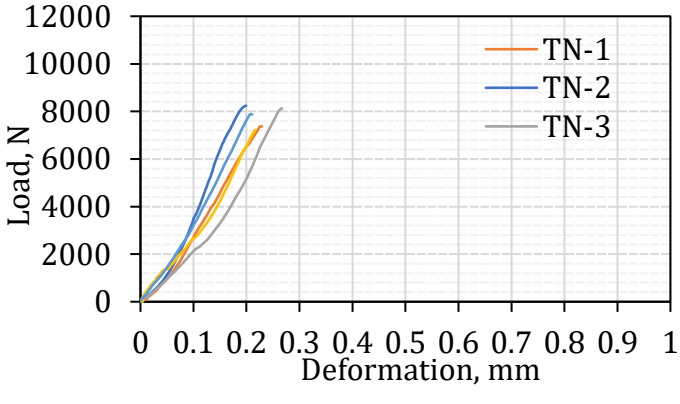

(a)

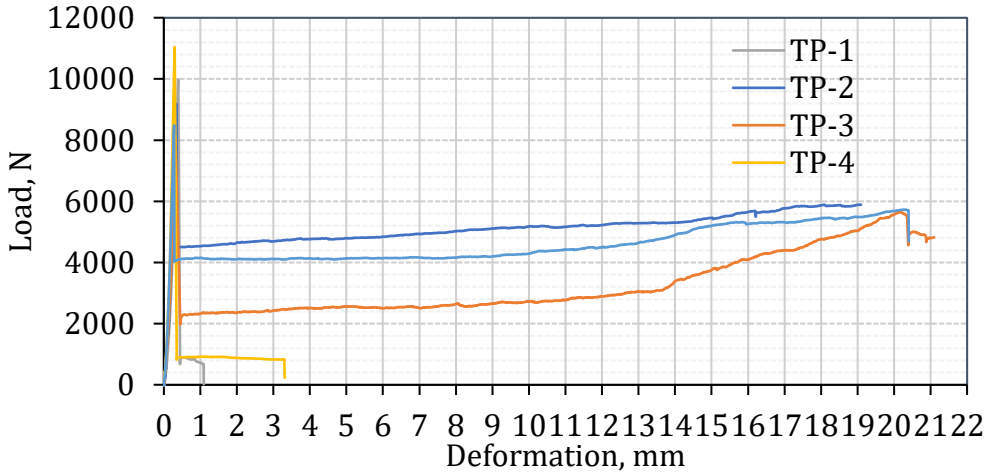

(b)

Figure 3.21. Load-deformation relationship of the unreinforced and reinforced specimens

(a)

(b)

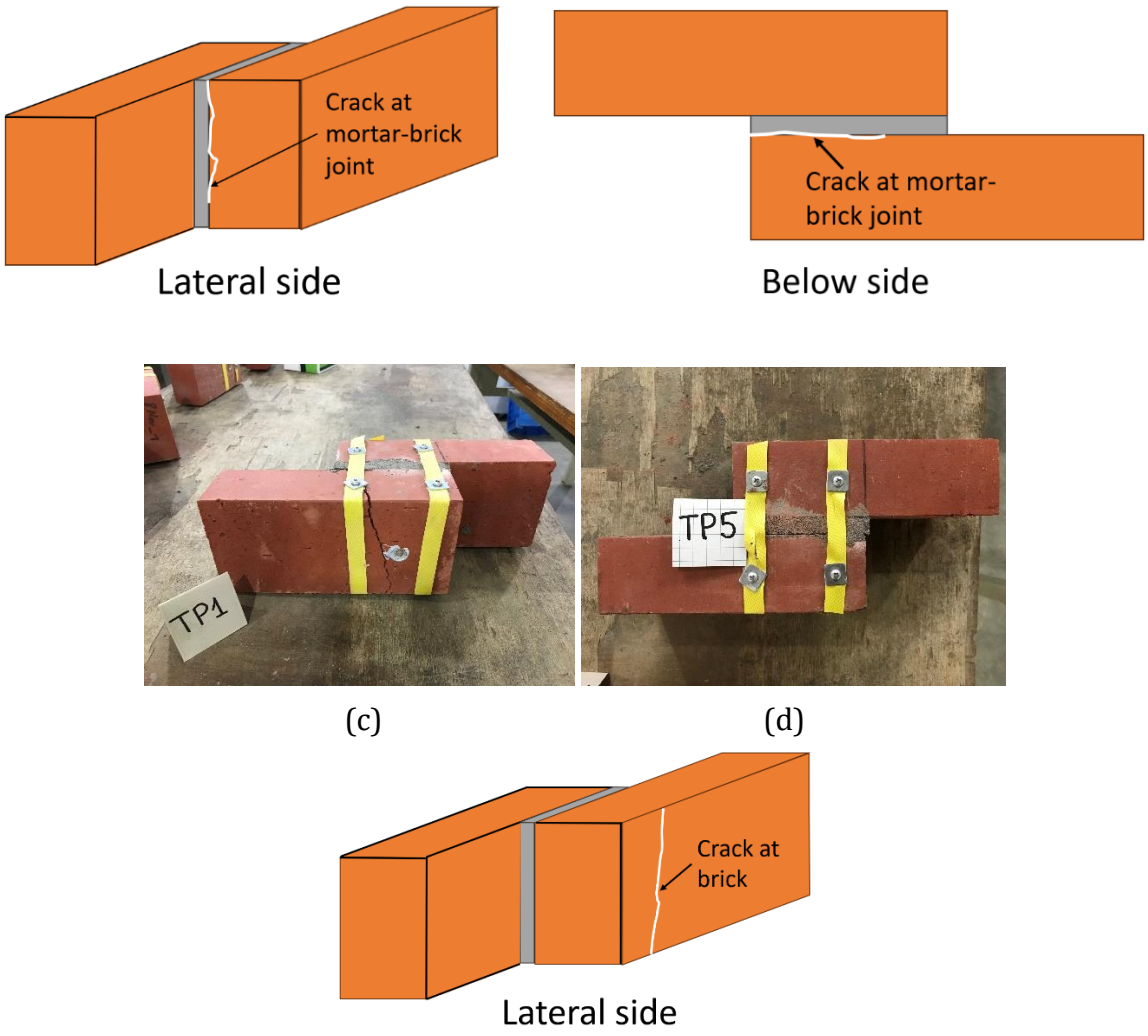

Figure 3.22. Failure patterns of the torsion specimens

3.1.7. Conclusions

A total of 49 specimens were tested to investigate the effectiveness of the PP band fixing method on flexural, shear, and torsion behaviors. In the flexural tests, the results show that the average load-carrying capacity at ultimate failure and deflection at first crack of the PP band specimens increased by 1.7 and 1.62 times, respectively, higher than those of Non PP band specimens. In the shear tests, the tests on the strengthened specimens showed an increase in the shear strength for all pre-compression ranges of 0.2 – 0.6 N/mm^2. However, it was not significant. Similarly, the initial stiffness is not significantly affected by the pre-compression level in both reinforced and unreinforced cases. In the torsion tests, the improvements in the average load-carrying capacity and deformation ability at the first

crack were 1.21 times and 1.47 times, respectively. In the reinforced specimens, at ultimate failure, a slight increase in load was observed, but it did not exceed the initial peak load.

CHAPTER 4. NUMERICAL ANALYSIS ON SMALL BRICK MASONRY

This section illustrates the simulation of the bending, shear and torsion test described in Section 3.1 carried out in the DIANA FEA Release 10.5, using a detailed micro-modelling approach.

4.1. Modelling approach

Several modelling strategies can be followed to analyse masonry structures, see Figure 4.23. An accurate model for simulating the mechanical behaviour of masonry should account for the main masonry failure mechanisms [49]. At a small scale, masonry failures are depicted in Figure 4.1. In particular, brick-mortar interface tensile failure (Figure 4.1(a)) and shear sliding (Figure 4.1(b)) are characterized by the failure of the bond between brick and mortar. Masonry crushing (Figure 4.1(d)), cracking (Figure 4.1(e)) and diagonal cracking (Figure 4.1(c)) are, instead, combined mechanisms involving bricks and mortar (Figure 4.1(d-e)) and bricks, mortar and brick-mortar interface (Figure 4.1(c)).

In the modelling approach herein proposed, the brick-mortar bond failures (Figure 4.1(a-b)) are accounted for by brick-mortar nonlinear cohesive interfaces, whereas the combined mechanisms involving also brick and mortar (Figure 4.1(c-e)) are accounted for by the nonlinear behaviour of brick-and-mortar FEs, see Figure 4.1(b). Therefore, brick and mortar crushing and cracking, although characterized by a complex evolution of micro-cracks, are represented by the inelastic behaviour of brick-and-mortar FEs.

Representative Elements composed by 3D solid FEs (Figure 4.2) with brick properties (red elements in Figure 4.2) and mortar properties (grey elements in Figure 4.2) are conceived and they are assembled by means of zero-thickness interfaces (green surfaces in Figure 4.2). For single leaf masonry panels, the RE concerns one brick as well as one head joint and one bed joint (Figure 4.2). Brick and mortar finite elements are characterized by distinct nonlinear plastic-damaging behaviour, both in tension and compression regimes.

Contact penalty method is enforced in the zero-thickness interfaces between the Representative Elements. Traditional point-against-surface contact method is considered [50]. The penalty stiffness is assumed to keep insignificant the penetration of the elements and to guarantee good convergence rates of simulations (compared, for example, with Lagrange multipliers methods [33]). In this study, penalty stiffness is assumed to be equal to

500 times the representative stiffness of underlying elements. In the pre-failure of interfaces, all the significant deformability of the system is addressed to the 3D FE part.

Dilatancy play an important role in the mechanical behaviour of masonry [51], although it is still currently object of investigation and debate [52, 53], and its characterization is complex as it is influenced by several mechanical factors (e.g. materials micro-structure, geometrical imperfections etc.). Experimental characterizations of dilatancy by van der Pluijm et al. [54] show that the dilatancy ratio is significantly influenced by the type of interface failure. Particularly, the magnitude of dilatancy turns out to be substantially higher when the crack crosses mortar (and/or units), compared to the dilatancy measured when detachment of the brick-mortar interfaces occurs (bond failure), which is considerably smaller.

In the modelling approach herein proposed, zero-thickness interfaces are conceived without a dilatant behaviour, whereas dilatancy is considered in the 3D nonlinear FEs in the framework of non-associated plasticity [55]. This approach, although simplified, appears to be consistent with the experimental outcomes pointed out in [55], i.e. significant dilatant behaviour only occurs when mortar (and/or units) undergoes failure.

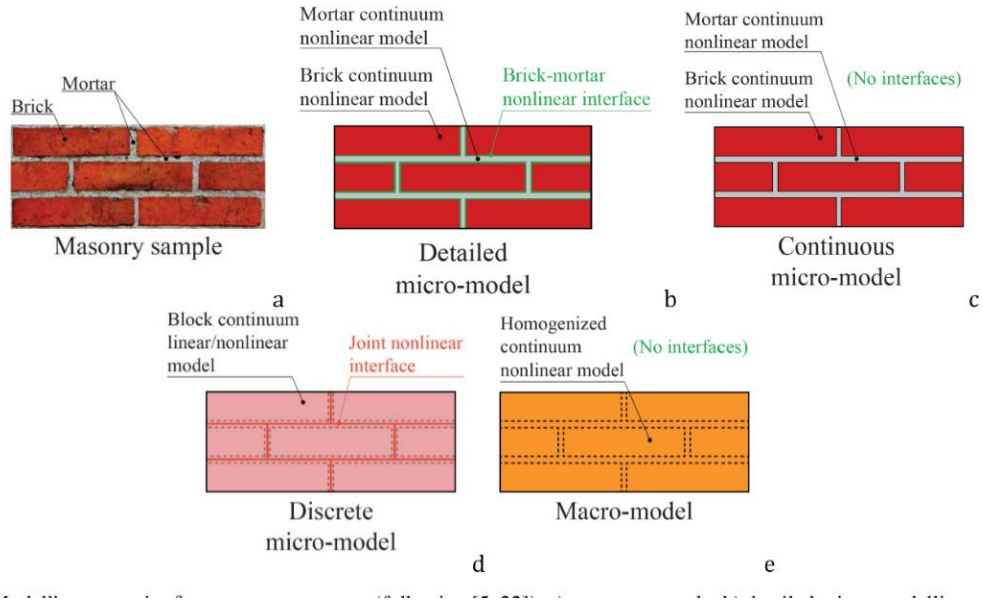

Figure 4.1. Modelling strategies for masonry structures (following [56, 57]): a) masonry sample, b) detailed micro-modelling, c) continuous micro-modelling, d) discrete-modelling and e) macro-modelling

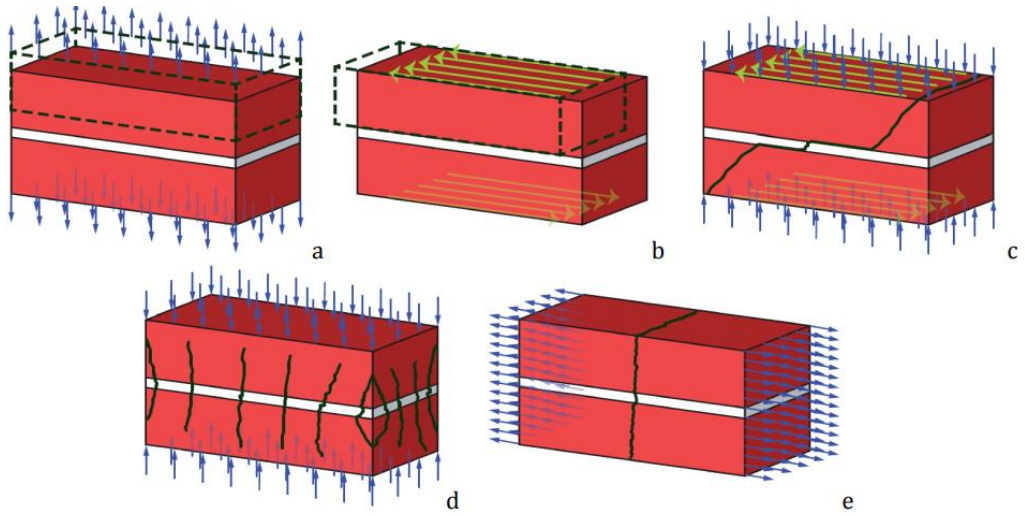

Figure 4.2. Masonry failure mechanisms (following [32]): a) brick-mortar interface tensile failure, b) brick-mortar interface shear sliding, c) diagonal masonry cracking, d) masonry crushing and e) brick and mortar tensile cracking

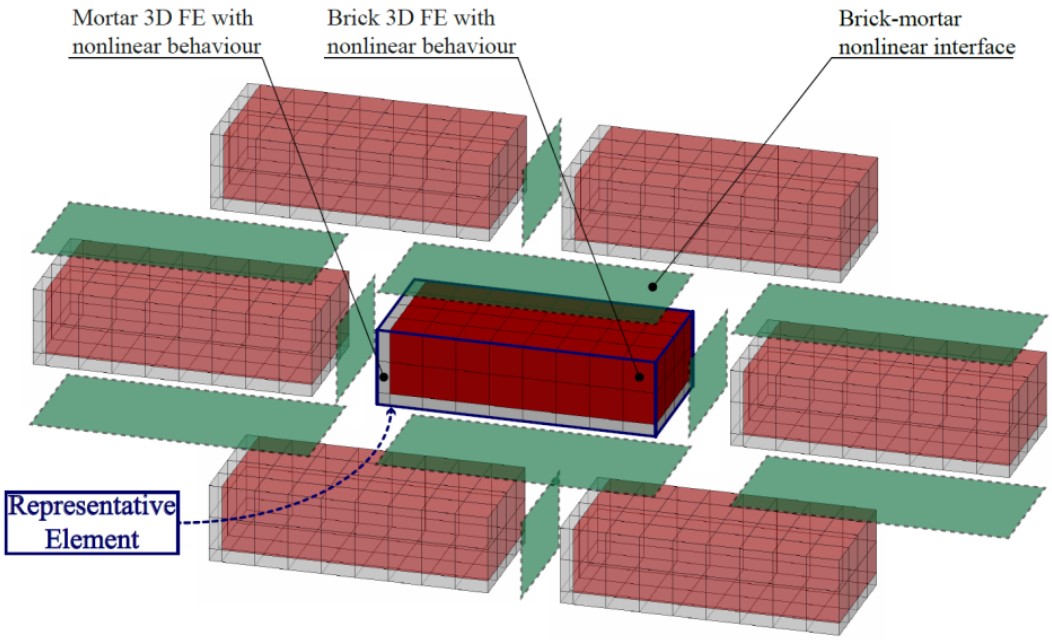

Figure 4.3. Detailed micro-modelling approach

4.2. Constitutive law of materials and brick-mortar interface

4.2.1. Brick-mortar interface behavior

In the normal direction, the contact stress $\boldsymbol{\sigma}$ is computed by means of the linear relationship:

$$\boldsymbol{\sigma} = \boldsymbol{k}^{\boldsymbol{n}}_{\boldsymbol{penalty}}\boldsymbol{u} \qquad (\mathbf{4.1})$$

where $k^n_{penalty}$ is the penalty stiffness in normal direction and u is the normal displacement. Through the contact penalty method, this relation is assumed to be valid also for tensile until the tensile strength f_t of the interface is reached, see Figure 4.4(a)

In the shear direction, the tangential slip δ is linearly related to the interface shear stress with the relation:

$$\boldsymbol{\tau = k^s_{penalty}\delta} \qquad (\mathbf{4.2})$$

where $k^s_{penalty}$ is the penalty stiffness in shear. This relation is valid until the shear stress equals the shear strength f_s, see Figure 4.4(b). The shear strength f_s of the interface is assumed to be dependent on the contact stress:

$$\boldsymbol{f_s(\sigma) = c - \tan(\emptyset)\,\sigma} \qquad (\mathbf{4.3})$$

where $\tan(\emptyset)$ and c are parameters experimentally defined.

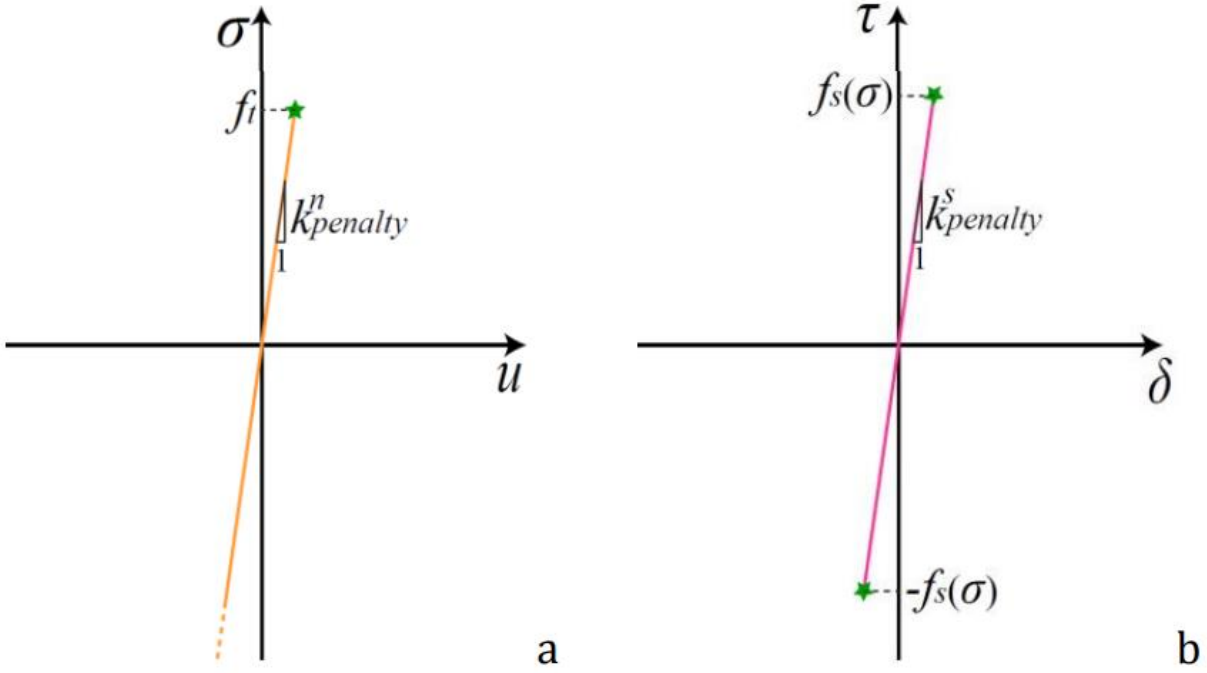

Figure 4.4. Interfacial pre-failure behavior: a) normal behavior and b) shear behavior

Interface failure occurs, i.e. the process of degradation begins, when the contact stresses at a point satisfy a failure criterion. Particularly, failure obtained when the maximum contact stress ratio intersects a Mohr-Coulomb failure surface with tension cut-off. This simple criterion can be expressed as:

$$\boldsymbol{max\left\{\frac{\langle x\rangle}{f_t}, \frac{\tau}{f_s(\sigma)}\right\} = 1} \qquad (\mathbf{4.4})$$

Where $\langle x \rangle = (|x| + x)/2$ denotes the Macaulay bracket function. The Macaulay brackets are used to signify that a purely compressive stress state does not induce interfacial failure. A sketch of the failure surface adopted for the interfacial behavior is shown in Figure 4.5. Once failure of the interface is reached, cohesive behavior in tension and cohesive-frictional in shear in activated.

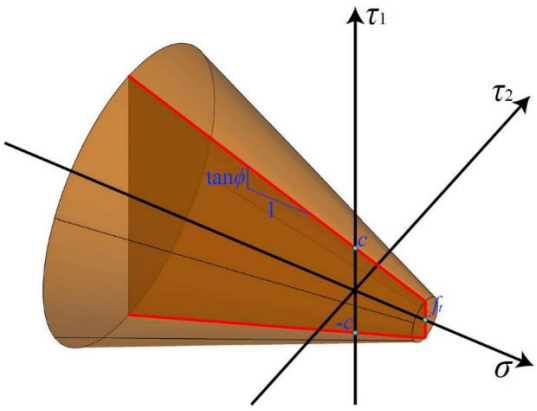

Figure 4.5. Interfacial failure surface: Morh-Coulomb surface with tension cut-off ($\boldsymbol{\tau_1}$ and $\boldsymbol{\tau_2}$ are the shear stress components along two orthogonal directions in the plane of the interface)

a) Post-failure tensile behavior

After reaching tensile strength f_t, an interfacial cohesive behavior is activated in normal direction and the stress σ decreases with an increasing separation u, while at $u = u_k$ stress ends to be transmitted, see Figure 4.6. The stress follows the relationship:

$$\boldsymbol{\sigma} = \begin{cases} \boldsymbol{(1-Q)f_t, u < u_k} \\ \boldsymbol{0, u \geq u_k} \end{cases} \qquad \boldsymbol{(4.5)}$$

where Q is an exponential scaling function defined as:

$$\boldsymbol{Q = \frac{1 - e^{-\beta \frac{u}{u_k}}}{1 - e^{-\beta}}} \qquad \boldsymbol{(4.6)}$$

being β a non-dimensional shape parameter. The cohesive behavior is only active for tension, whereas for pure compression stress states no failure is considered at the interfacial level (see Figure 4.5)

b) Post-failure shear behavior

Concerning the shear behavior, when the shear stress $\boldsymbol{\tau}$ reaches the shear strength $f_s(\sigma)$, a simplified cohesive-frictional behavior in activated, and the contacting

surface start sliding. After failure the shear stress is composed by a cohesive term $(1-H)f_s(\sigma)$ and a frictional one $H\mu\langle-\sigma\rangle$ (Figure 4.6(b)), according to the relationship:

$$\boldsymbol{\tau = \begin{cases} (1-H)f_s(\sigma) + H\mu\langle-\sigma\rangle, \delta < \delta_k \\ \mu\langle-\sigma\rangle, \delta \geq \delta_k \end{cases}} \quad (4.7)$$

where δ_k is the ultimate slip of the cohesive behavior, μ is the frictional coefficient and H is an exponential scaling function defined as:

$$\boldsymbol{H = \frac{1 - e^{-\gamma\frac{\delta}{\delta_k}}}{1 - e^{-\gamma}}} \quad (4.8)$$

being $\boldsymbol{\gamma}$ a non-dimensional shape parameter.

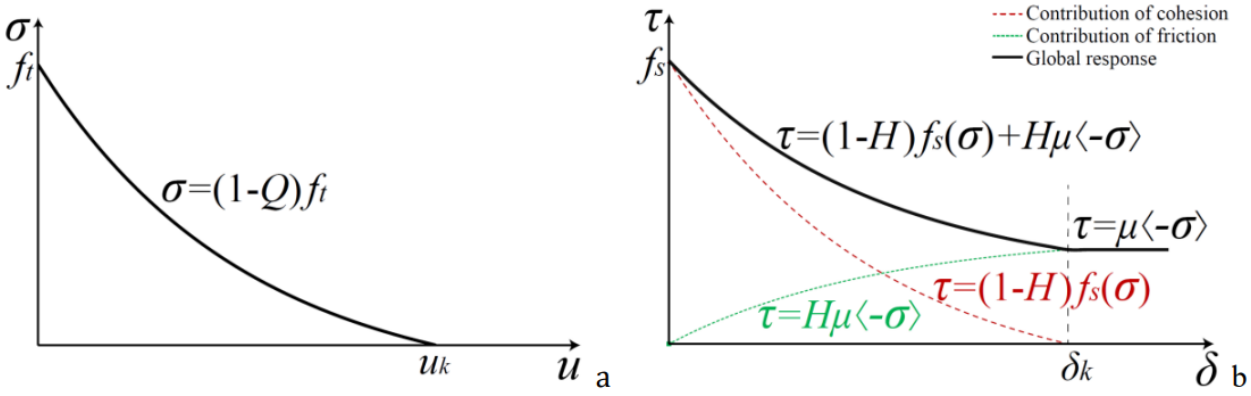

Figure 4.6. Interfacial post-failure behavior: a) tensile response and b) shear response

In this study, in DIANA software, surface-to-surface contact interfaces are used to simulate the bond between the brick and the mortar. The cohesive interface exhibits initially a linear elastic response, followed by a cracking behavior that describes the most critical failure modes, namely, tensile cracking and shear sliding. Material mode "Coulomb friction" is employed, this allows simulating the failure occurred in correspondence of the brick-mortar interfaces for the triplets in shear test. On the other hand, in bending and torsion tests, the interface mainly experiences tensile cracking. Therefore, the material model selected is discrete cracking. In the models, the surfaces of the mortar were assigned as "Target face type". Meanwhile, the surfaces of the brick were selected as "Source face type". The interfaces were modelled with 4 + 4 nodes, Q24IF – plane quadrilateral. Normal interface stiffness (K_n) and shear interface stiffness (K_s) were calculated by Equation 5.12 and 5.13.

$$k_n = \frac{E_b \times E_m}{h_m(E_u - E_m)} \qquad (4.9) \qquad\qquad k_s = \frac{k_n}{2(1-v)} \qquad (4.10)$$

where, E_b, E_m is the young's modulus of the brick and mortar; h_m is the thickness of the mortar.

4.2.2. Brick-mortar nonlinear behavior

The two components (bricks and mortar layers) are described as a continuum, and discretised using 3D eight-node element of reduced integration with orthogonal hourglass control (HX2L). The behavior of the brick unit and mortar is described using a Total-strain based crack model in all three experiments, available in DIANA software. DIANA's total strain based constitutive model defines the tensile and compressive behavior of a material by a stress-strain relationship. The tensile and compression behavior of the units and the mortar was assumed to be linear-ultimate crack strain, parabolic model, respectively, see Figure 4.7.

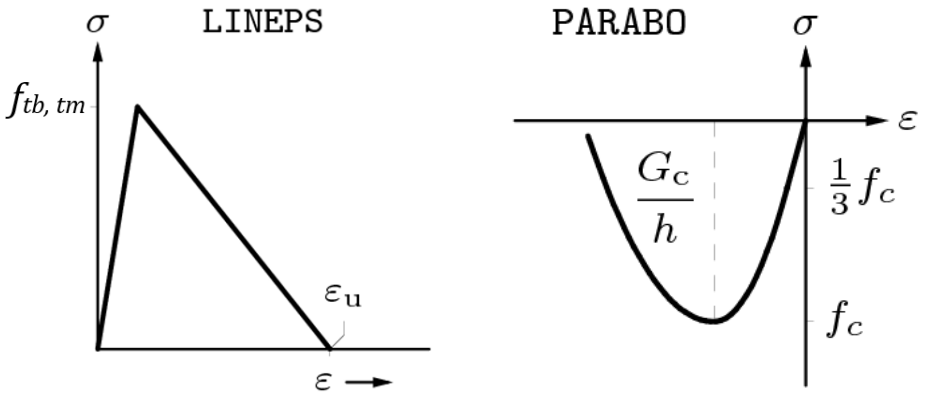

(a) Tensile behavior (b) Compression behavior

Figure 4.7. Constitutive models for brick and mortar

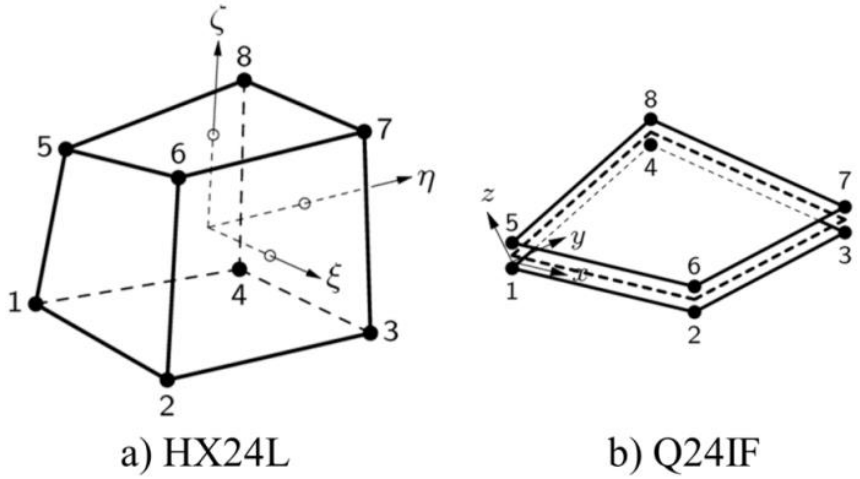

Figure 4.8. Finite elements of the numerical model (Brick, mortar (HX2L) and Interface (Q24IF))

Table 4.1 and Table 4.2 illustrate the main parameters of the brick units, the mortar layer, and the interface. It is noteworthy that most of these values have been taken from the characterization tests carried out on the specimens of brick and mortar. Some parameter values (e.g., ultimate strain of brick and tensile fracture energy of mortar) have been calibrated to achieve a better fit to experimental results. Nevertheless, all the parameter values are within the ranges recommended in the literature.

4.2.3. PP band linear and the PP band-Steel washer behavior

PP band is modeled as beam element using conventional plastic constitutive law connected toghther with the masonry by elastic by spring representing the polypropylen band to brick connector (Table 4.3). Additionally, the properties of the contact PP band-Steel washer also were listed in table 4.4

Table 4.1. Mechanical properties of the brick unit and mortar

Mechanical properties	Shear, bending and torsion tests		Source
	Brick unit	Mortar	
Young's modulus, E	15700	2400	Material tests
Poison's ratio,	0.16	0.2	-
Peak tensile strength,	5.2	4.7	Material tests
Ultimate strain	18	10	Best fit to test results
Compressive strength	36	23	Material tests

Table 4.2. Properties of the contact interfaces describing the brick-mortar joints

Brick-mortar interface properties	Shear test	Bending and torsion test	Source
	Coulomb friction	Discrete cracking	
k_n, N/mm^3	238	238	Calculated from material results
k_s; k_t, N/mm^3	99	99	Calculated from material results
Cohesion, N/mm^2	0.288	-	Triplet test
Friction angle, rad	1.469	-	Triplet test
Dilatancy angle, rad	-	-	-
Tensile strength, N/mm^2	0.33-0.36	0.33-0.36	Bending test
Model for gap appearance	Brittle	-	DIANA software
			DIANA software
Mode-I tension softening	-	Hordijk et al.	-
Fracture energy	-	0.04	Best fit to results

Table 4.3. Mechanial properties of the PP band

Mechanical properties	Shear, bending and torsion tests	Source
	PP band	
Young's modulus, E	15700	Material tests
Poison's ratio,	0.16	-
Peak tensile strength,	180	Material tests
Ultimate strain	0.13	-

Table 4.4. Properties of the contact PP band-Steel washer

PP band-Steel washer interface properties	Bending, shear, and torsion test	Source
	Discrete cracking	
k_n, N/mm^3	6	Calculated from material results
k_s; k_t, N/mm^3	3.5	Calculated from material results
Tensile strength, N/mm^2	80	Direct tensile test
Relative displacement-Tensile traction	Multi-linear	- Direct tensile test
Model-I unloading/reloading model	Secant	Bending test DIANA software
Model-II shear criterion for crack development	Zero shear traction	DIANA software Best fit to results

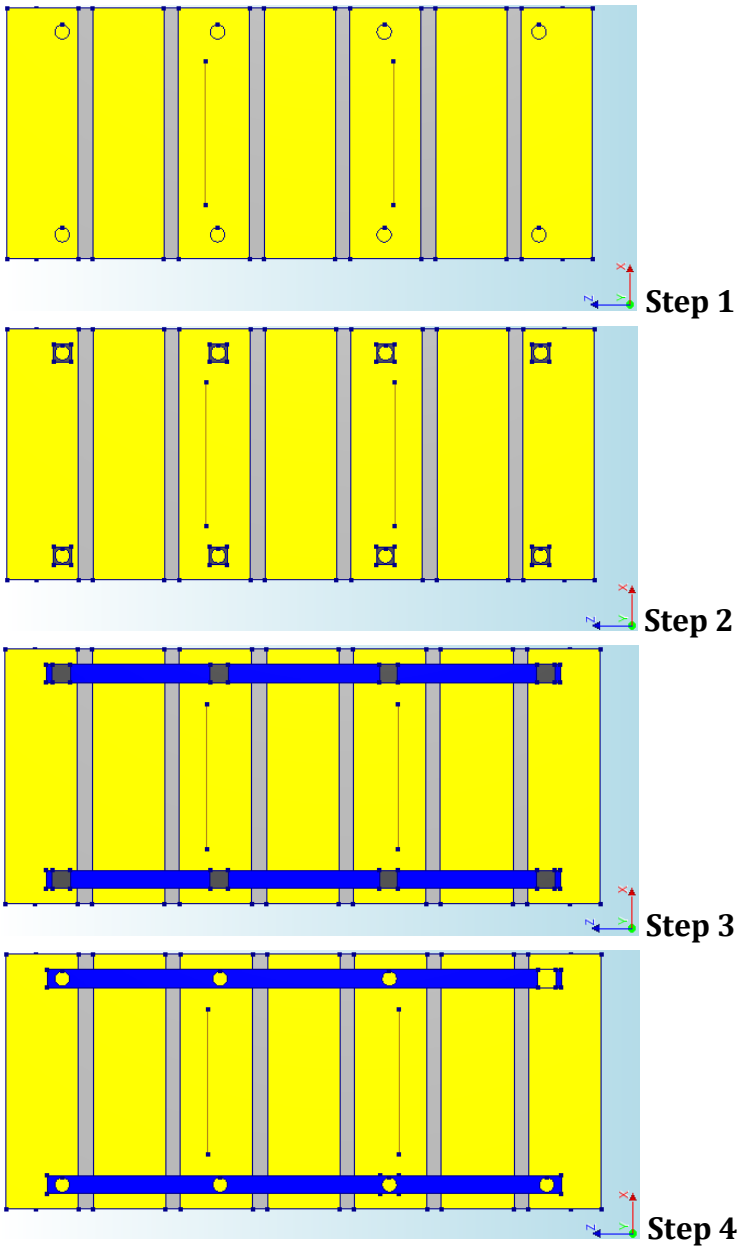

Figure 4.9. Procedue for modeling PP band specimens in bending tests

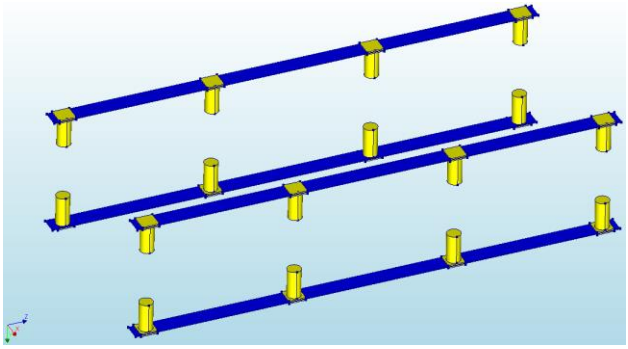

Figure 4.10. Steel washer and PP band system in model

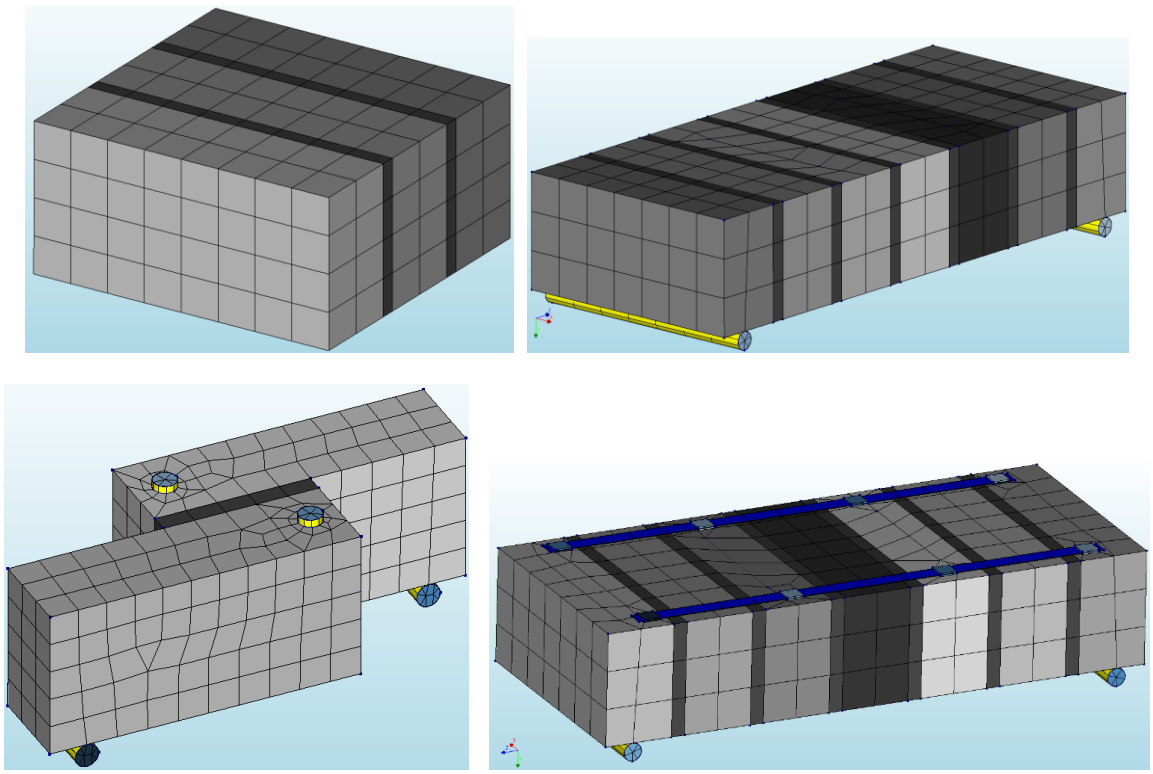

Figure 4.11. Finite element model with refined mesh in shear, flexural, and torsion test

4.3. Numerical analysis of flexural tests

4.3.1. Effect of mesh size and flexural strength of brick-mortar interface without PP band

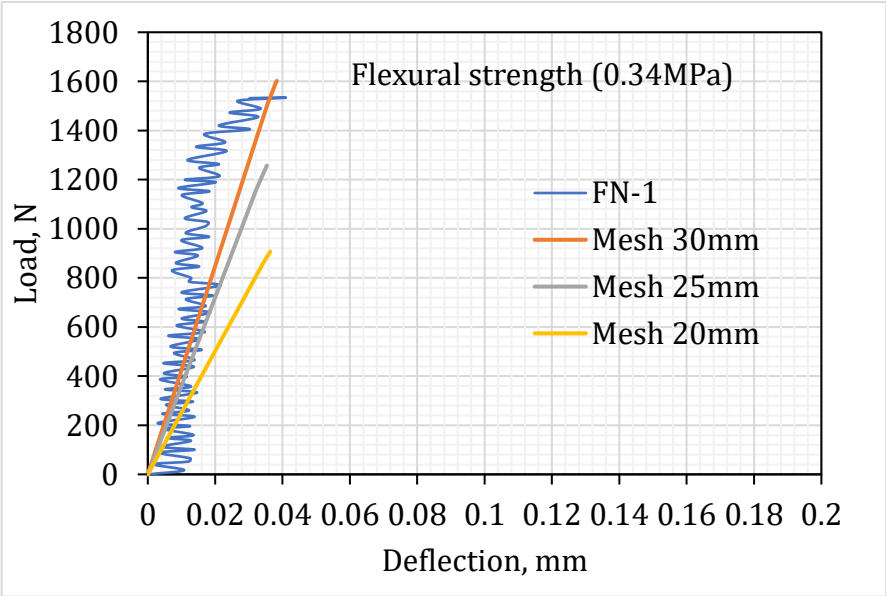

Effect of mesh size

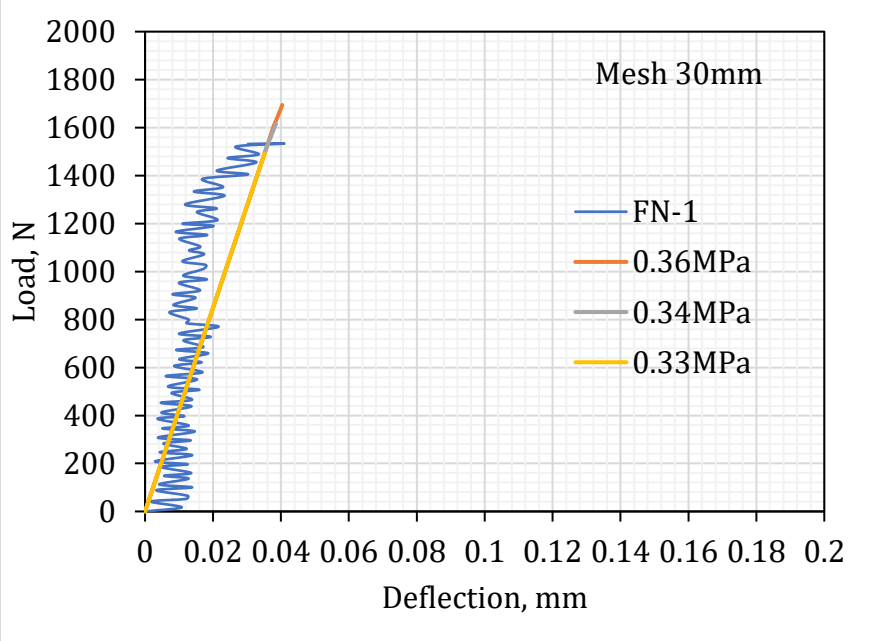

Effect of flexural strength

Figure 4.12. Comparative assessment between experiment and numerical results in flexural test without PP band

From the results in Figure 4.12, it can be seen that mesh size and bending strength have a great influence on the accuracy of the results. When increasing the mesh size from 20 to 30 mm, the load value gradually increases, and when compared with the experimental results, the mesh size of 30 mm is the most suitable. In all three cases, the bending stress is evenly distributed at the lower edge of the brick-mortar joint, and the relative displacement also originates from the corner of the brick-mortar joint. Then extend into the middle of the interface. This shows that the destruction mechanism in experiment and analysis is the same.

However, for the results explained in Figure 4.13, the description of the model's behavior after reaching the maximum load has not been achieved. This will be explored further in further studies. The failure mechanism at the first crack is similar to that in the specimen without PP bands.

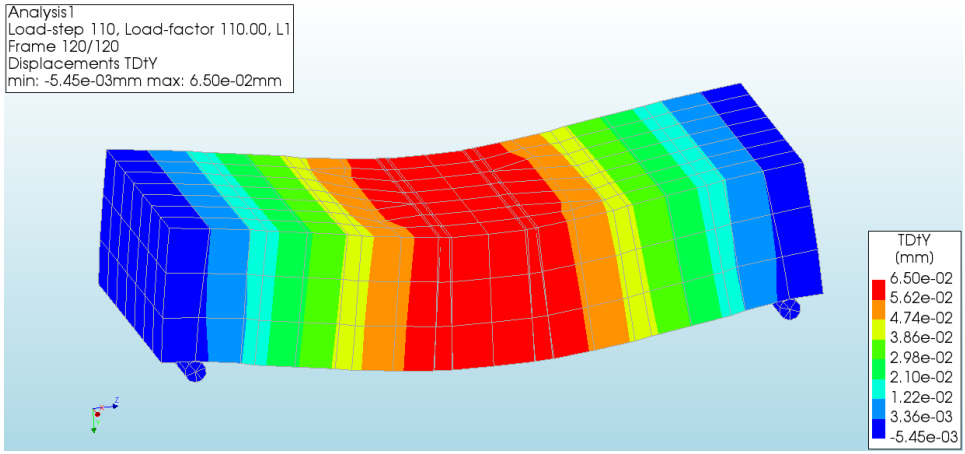

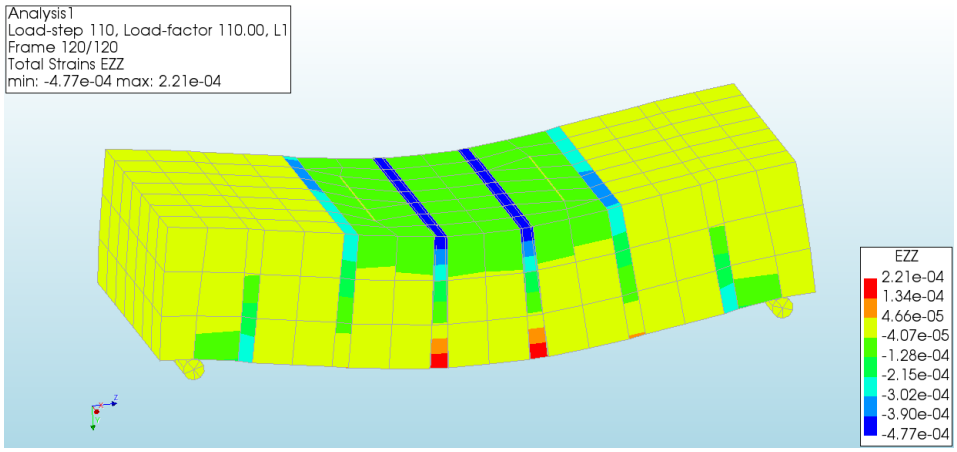

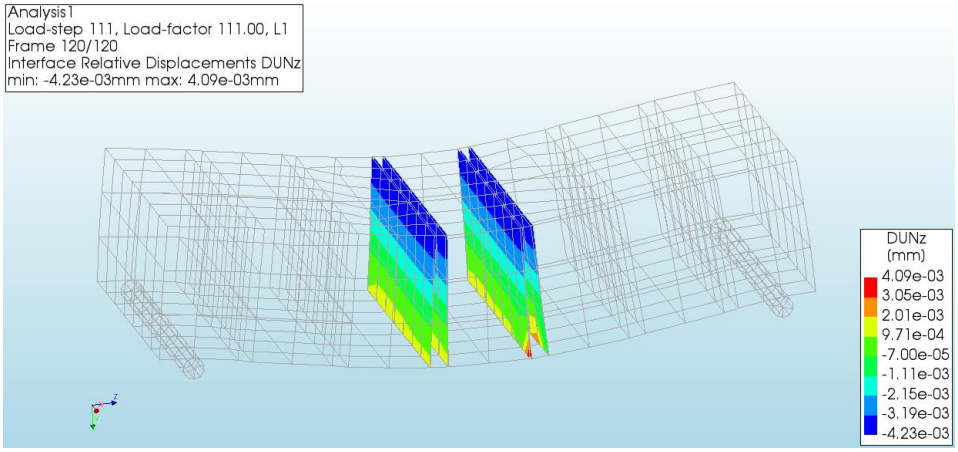
Analysis 1
Load-step 111, Load-factor 111.00, L1
Frame 120/120
Interface Relative Displacements DUNz
min: -4.23e-03mm max: 4.09e-03mm
DUNz
(mm)
4.09e-03
3.05e-03
2.01e-03
9.71e-04
-7.00e-05
-1.11e-03
-2.15e-03
-3.19e-03
-4.23e-03

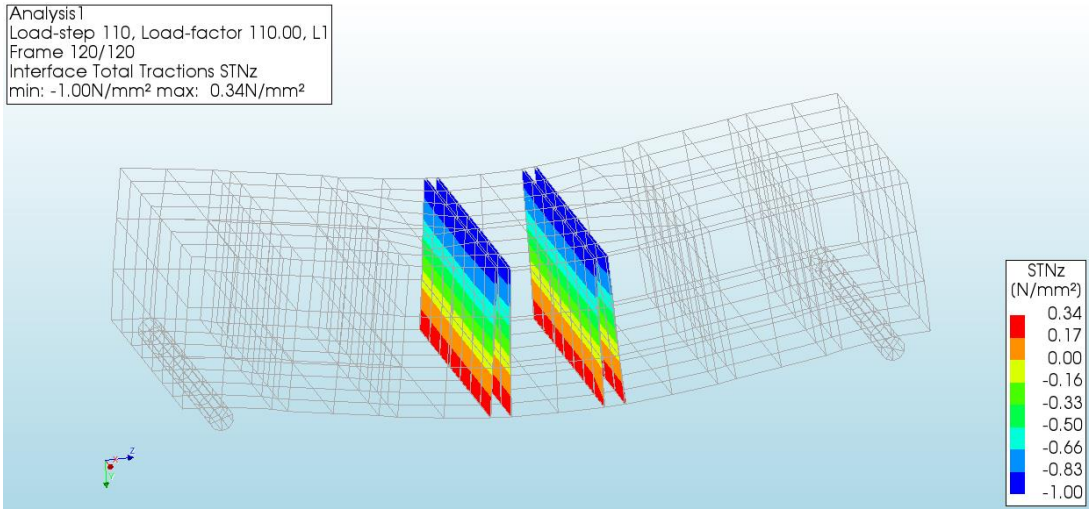
Analysis 1
Load-step 110, Load-factor 110.00, L1
Frame 120/120
Interface Total Tractions STNz
min: -1.00N/mm² max: 0.34N/mm²
STNz
(N/mm²)
0.34
0.17
0.00
-0.16
-0.33
-0.50
-0.66
-0.83
-1.00

a. (30mm)

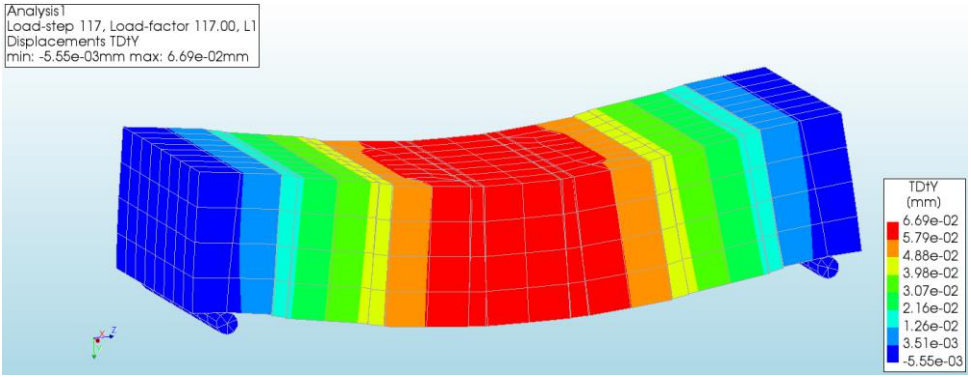
Analysis 1
Load-step 117, Load-factor 117.00, L1
Displacements TDtY
min: -5.55e-03mm max: 6.69e-02mm
TDtY
(mm)
6.69e-02
5.79e-02
4.88e-02
3.98e-02
3.07e-02
2.16e-02
1.26e-02
3.51e-03
-5.55e-03

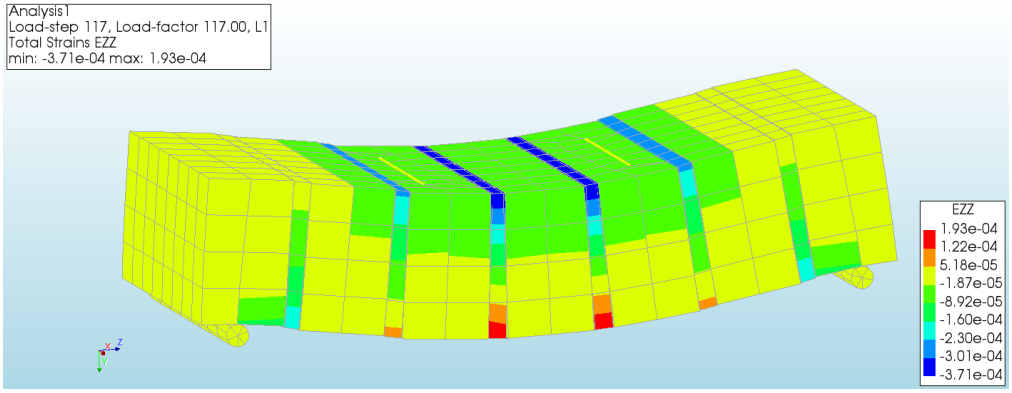
Analysis1
Load-step 117, Load-factor 117.00, L1
Total Strains EZZ
min: -3.71e-04 max: 1.93e-04
EZZ
1.93e-04
1.22e-04
5.18e-05
-1.87e-05
-8.92e-05
-1.60e-04
-2.30e-04
-3.01e-04
-3.71e-04

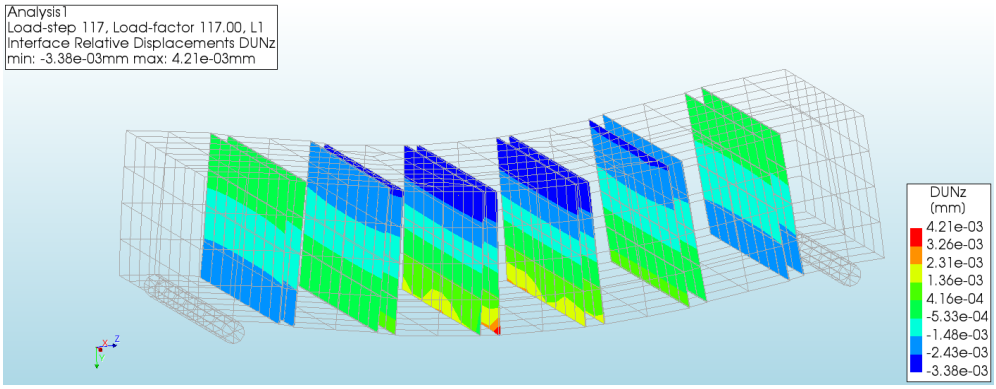
Analysis1
Load-step 117, Load-factor 117.00, L1
Interface Relative Displacements DUNz
min: -3.38e-03mm max: 4.21e-03mm
DUNz
(mm)
4.21e-03
3.26e-03
2.31e-03
1.36e-03
4.16e-04
-5.33e-04
-1.48e-03
-2.43e-03
-3.38e-03

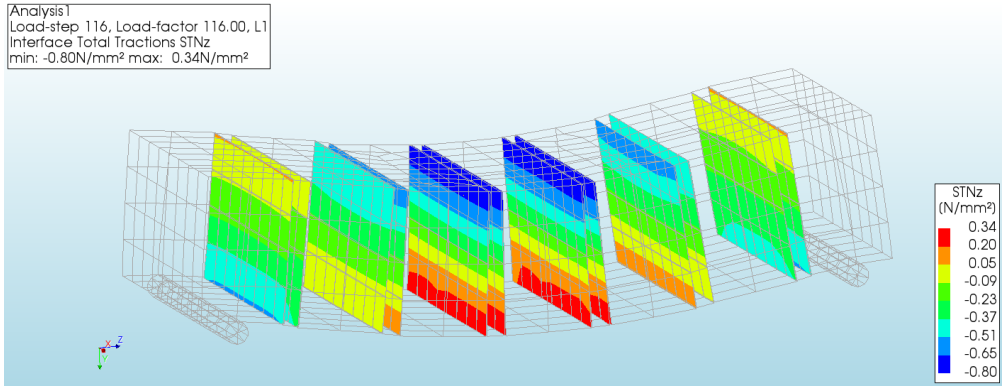
Analysis1
Load-step 116, Load-factor 116.00, L1
Interface Total Tractions STNz
min: -0.80N/mm² max: 0.34N/mm²
STNz
(N/mm²)
0.34
0.20
0.05
-0.09
-0.23
-0.37
-0.51
-0.65
-0.80

b. 25mm

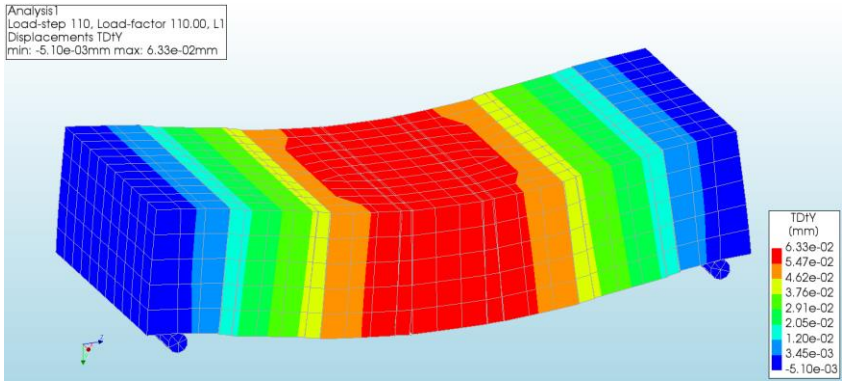
Analysis1
Load-step 110, Load-factor 110.00, L1
Displacements TDtY
min: -5.10e-03mm max: 6.33e-02mm
TDtY
(mm)
6.33e-02
5.47e-02
4.62e-02
3.76e-02
2.91e-02
2.05e-02
1.20e-02
3.45e-03
-5.10e-03

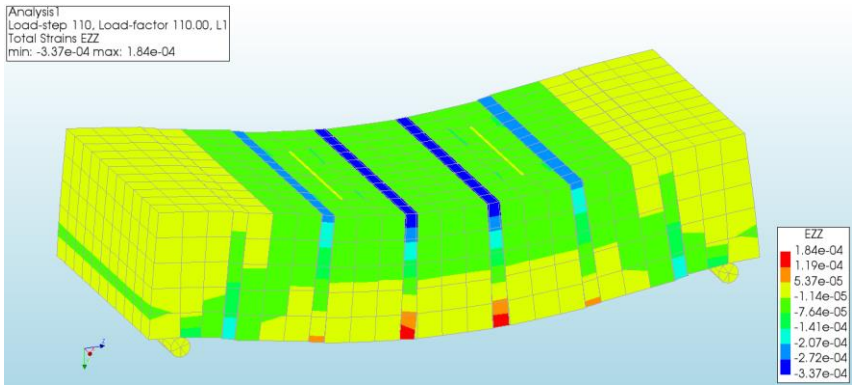
Analysis1
Load-step 110, Load-factor 110.00, L1
Total Strains EZZ
min: -3.37e-04 max: 1.84e-04
EZZ
1.84e-04
1.19e-04
5.37e-05
-1.14e-05
-7.64e-05
-1.41e-04
-2.07e-04
-2.72e-04
-3.37e-04

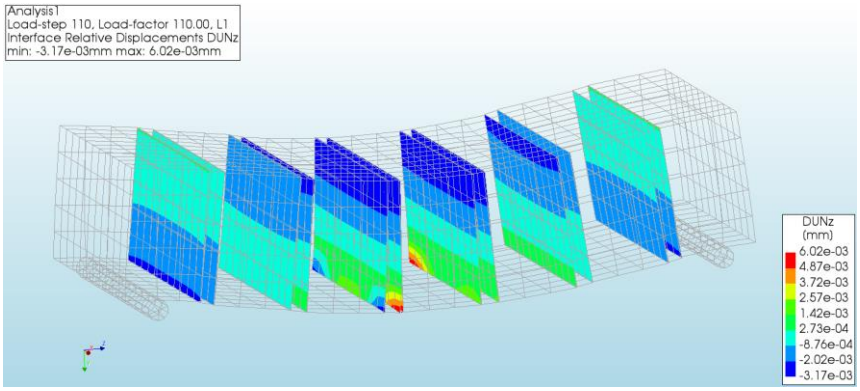
Analysis1
Load-step 110, Load-factor 110.00, L1
Interface Relative Displacements DUNz
min: -3.17e-03mm max: 6.02e-03mm
DUNz
(mm)
6.02e-03
4.87e-03
3.72e-03
2.57e-03
1.42e-03
2.73e-04
-8.76e-04
-2.02e-03
-3.17e-03

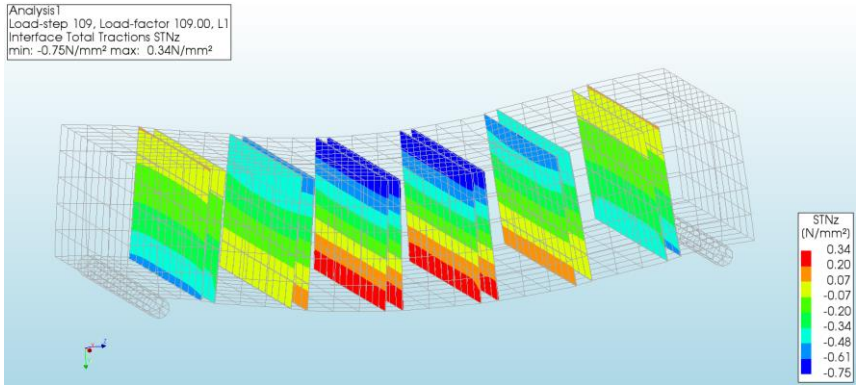
Analysis1
Load-step 109, Load-factor 109.00, L1
Interface Total Tractions STNz
min: -0.75N/mm² max: 0.34N/mm²
STNz
(N/mm²)
0.34
0.20
0.07
-0.07
-0.20
-0.34
-0.48
-0.61
-0.75

c. 20mm

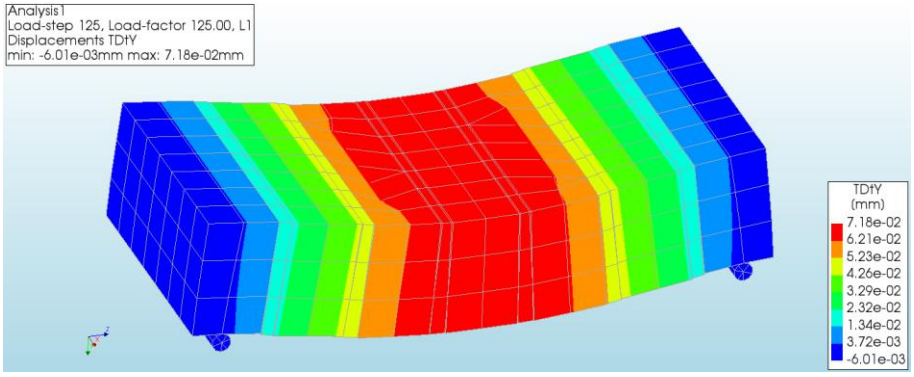
Analysis1
Load-step 125, Load-factor 125.00, L1
Displacements TDtY
min: -6.01e-03mm max: 7.18e-02mm
TDtY
(mm)
7.18e-02
6.21e-02
5.23e-02
4.26e-02
3.29e-02
2.32e-02
1.34e-02
3.72e-03
-6.01e-03

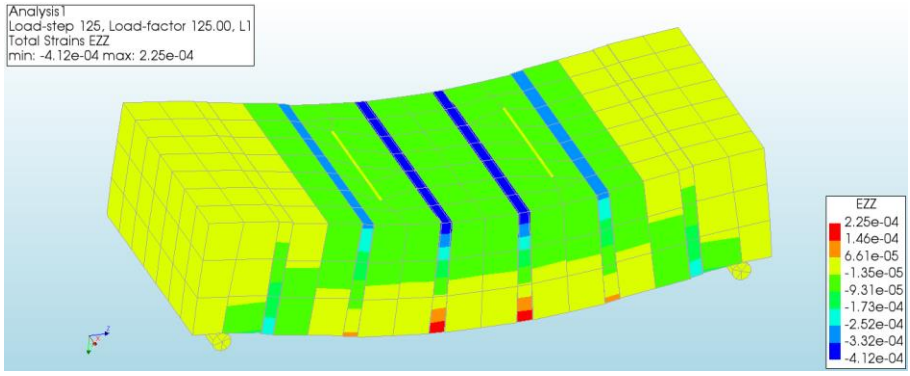

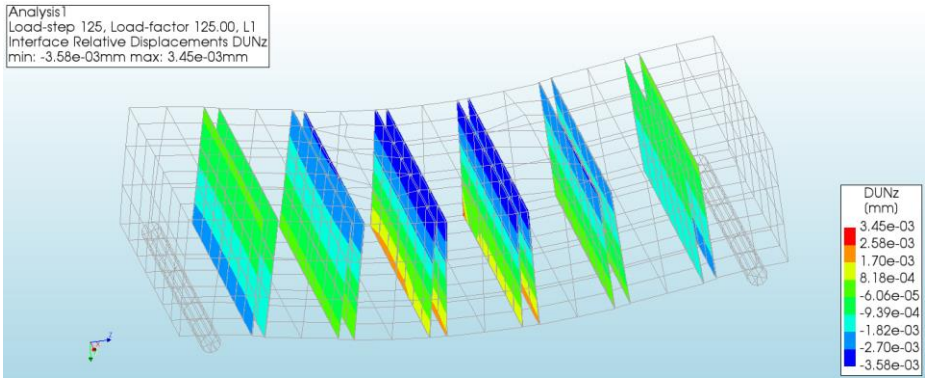

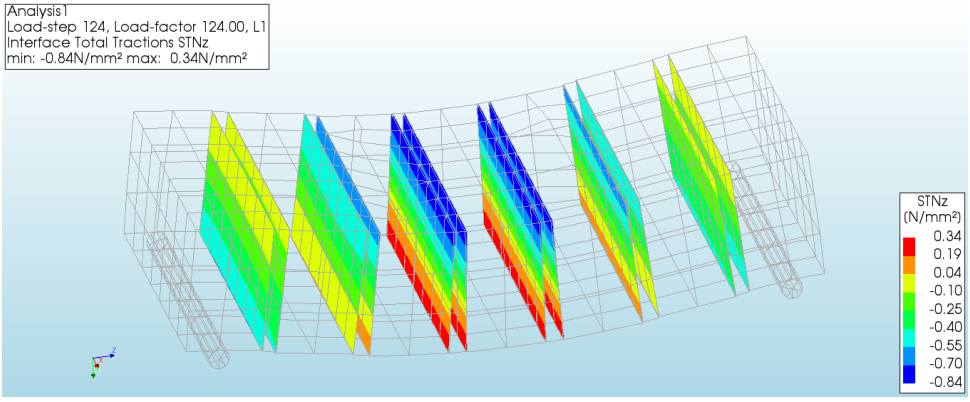

a. 30mm, 0.34MPa

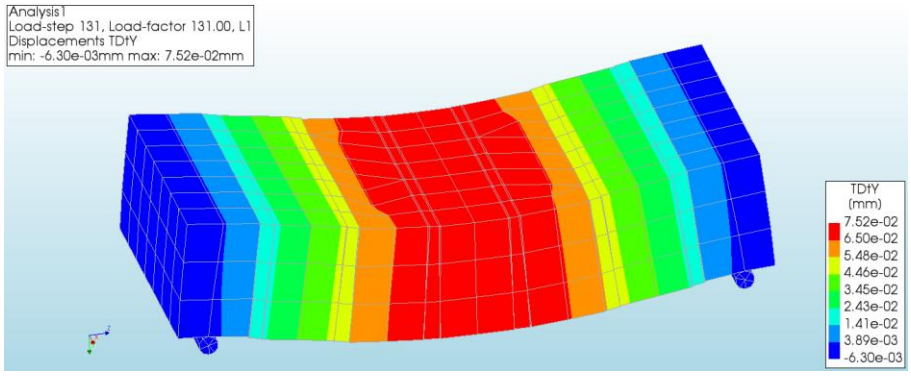

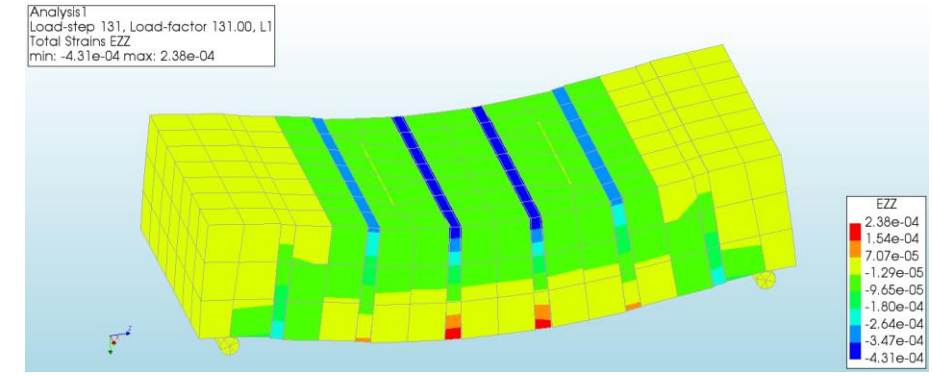

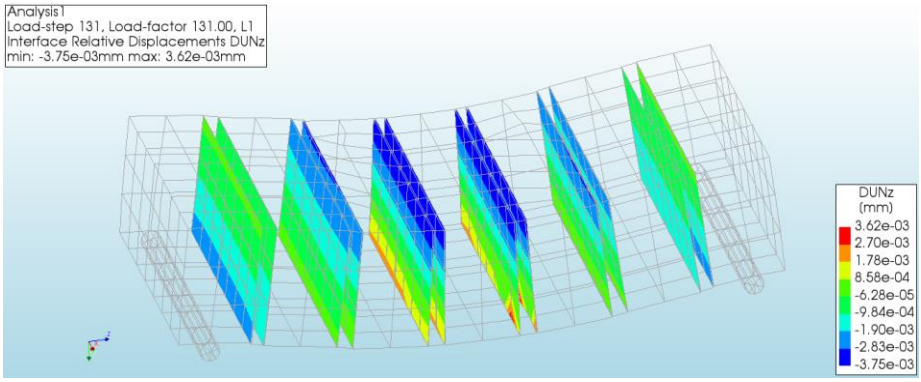

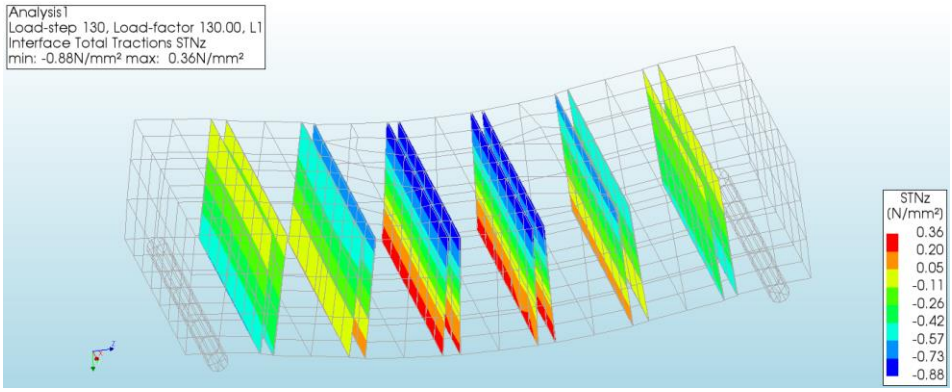

b. 30mm, 0.36MPa

4.3.2. Effect of mesh size and flexural strength of brick-mortar interface with PP band

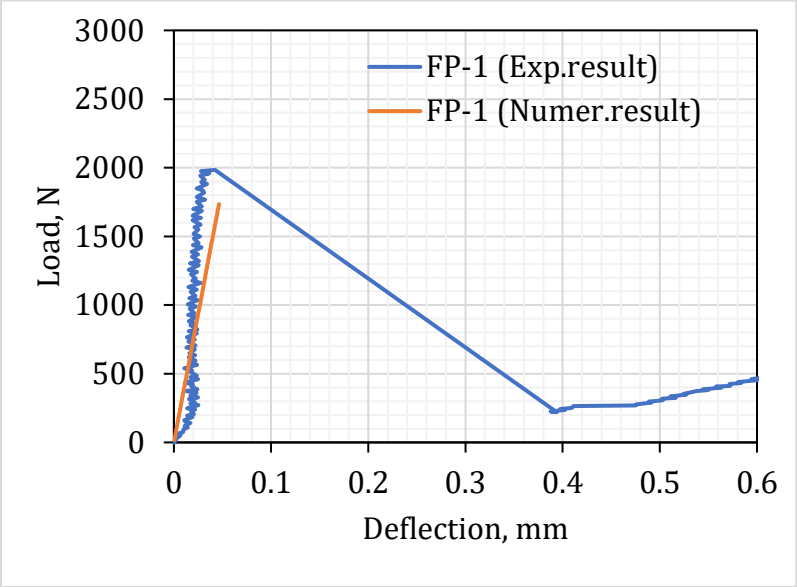

Figure 4.13. Comparative assessment between experiment and numerical results in flexural test with PP band

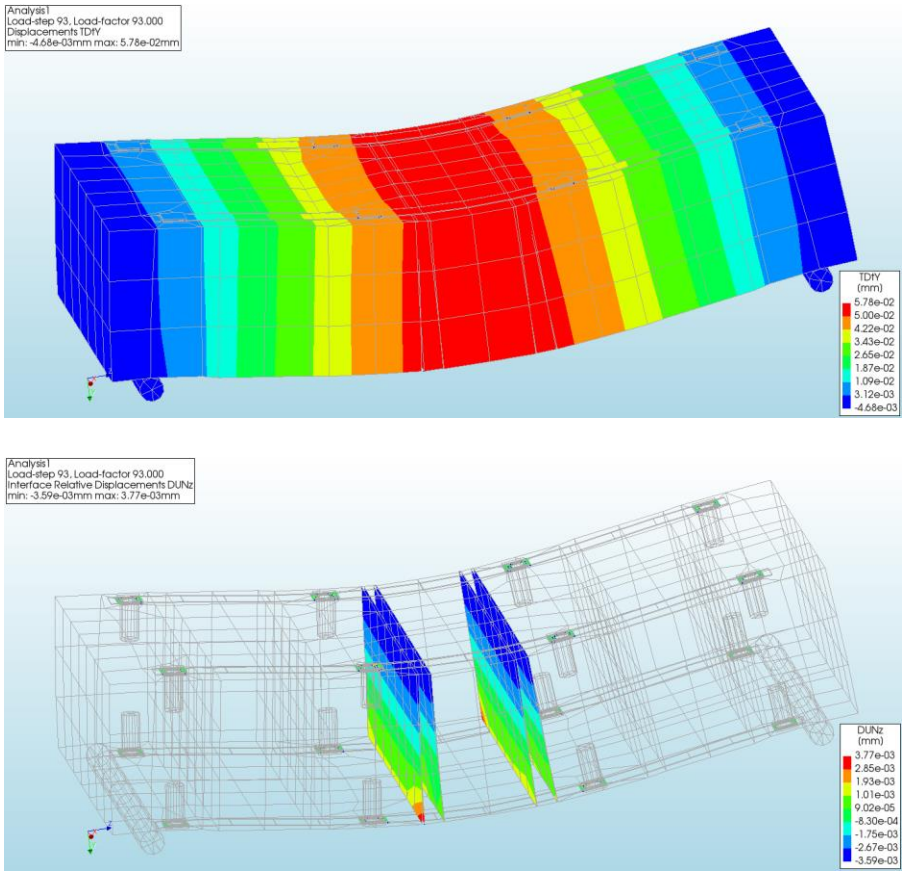

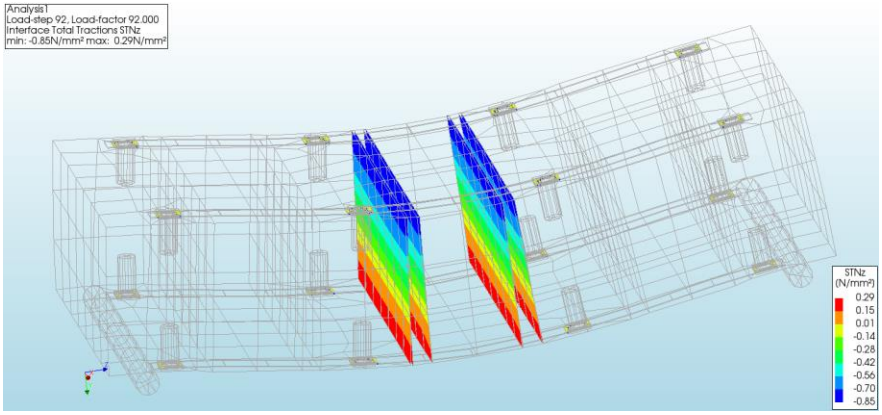

4.4. Numerical analysis of shear test

4.4.1. Effect of mesh size

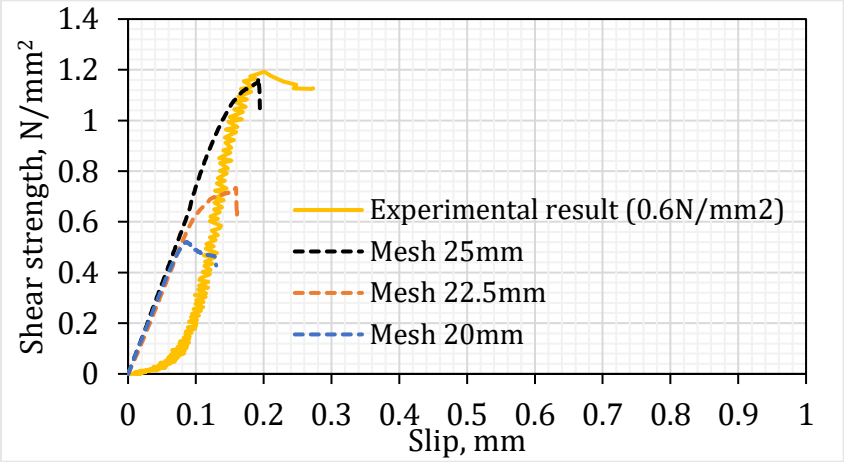

Figure 4.14. Comparative assessment between experiment and numerical results in shear test (0.6MPa)

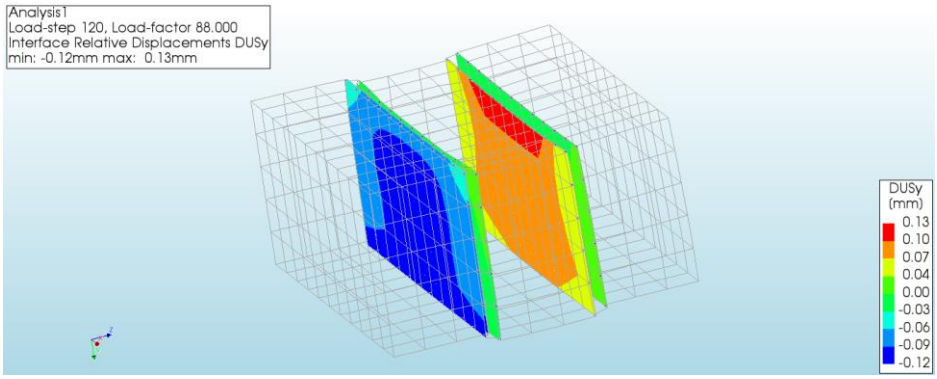

a1. 20mm, 0.6MPa

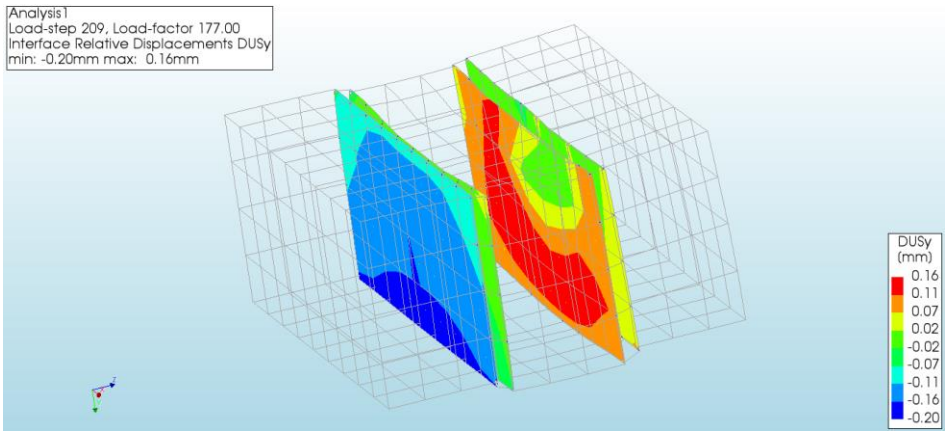

b1.22.5mm, 0.6MPa

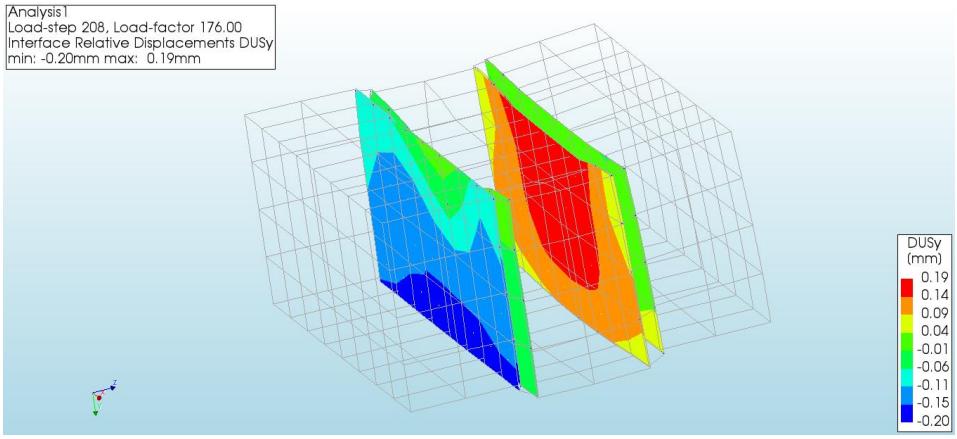

c1.25mm, 0.6MPa

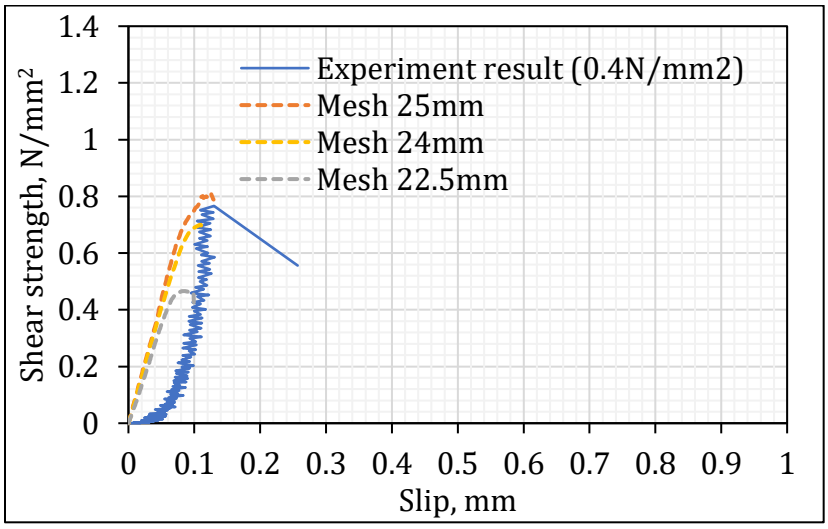

Figure 4.15. Comparative assessment between experiment and numerical results in shear test (0.4MPa)

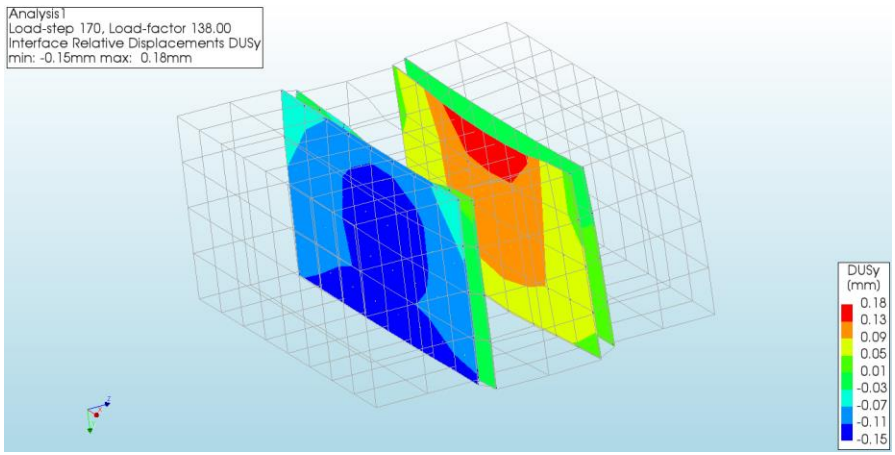

(25mm, 0.4MPa)

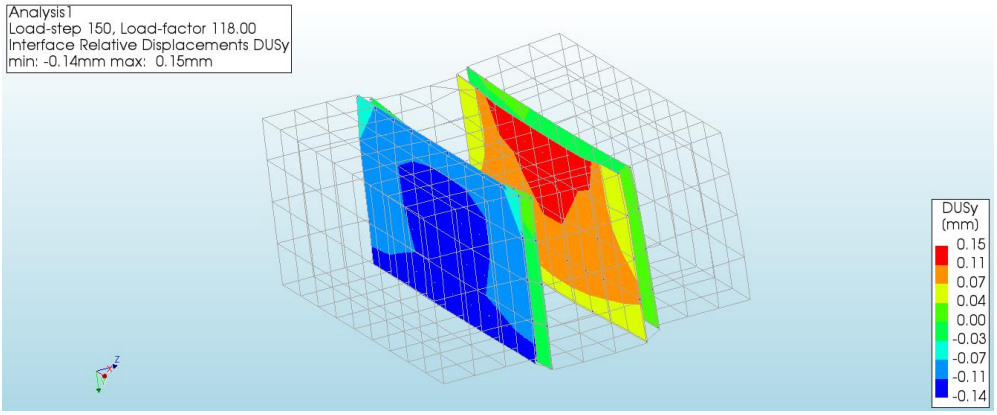

(24mm, 0.4MPa)

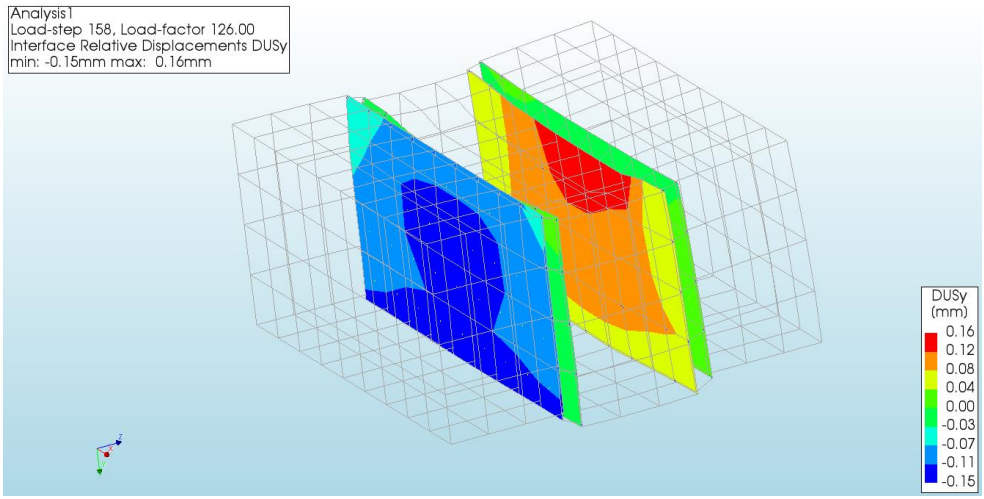

(22.5mm, 0.4MPa)

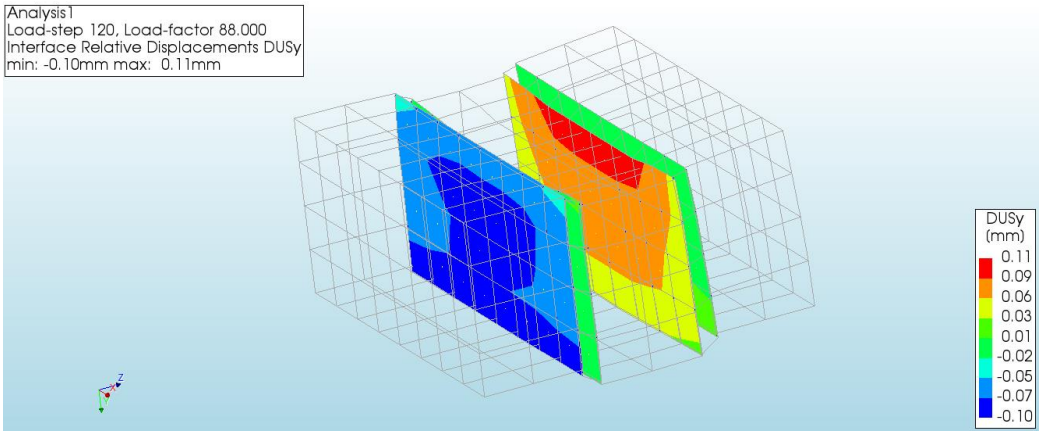

(25mm, 0.2MPa)

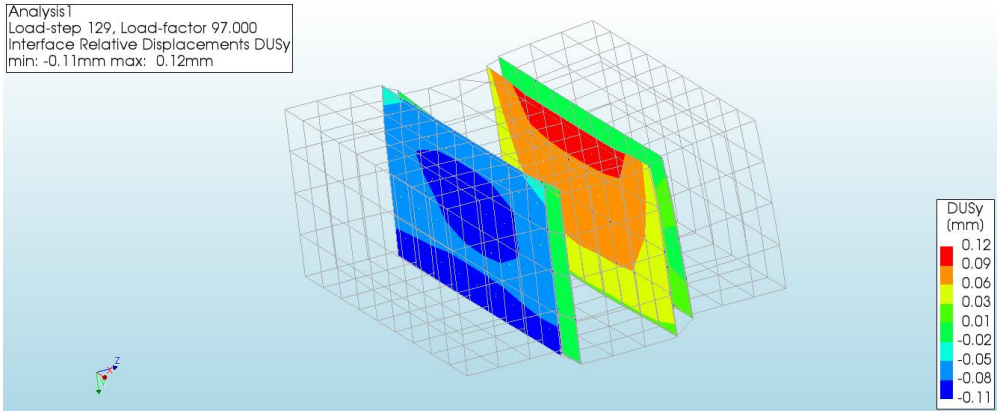

(24mm, 0.2MPa)

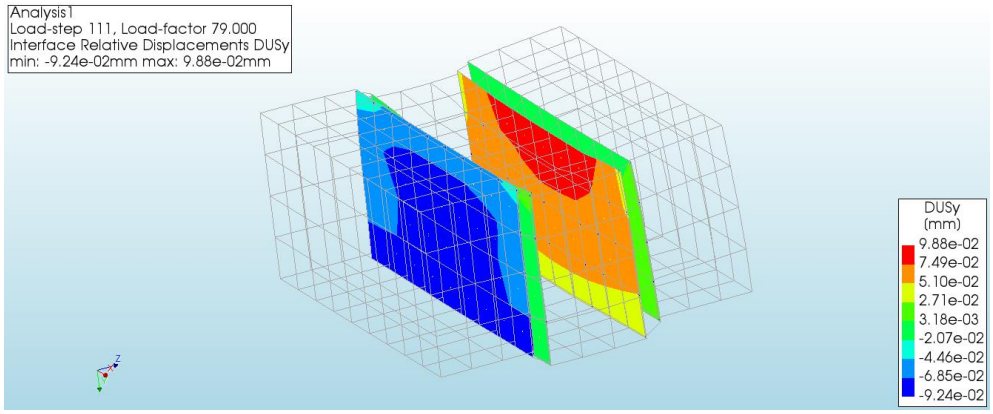

(22.5mm, 0.2MPa)

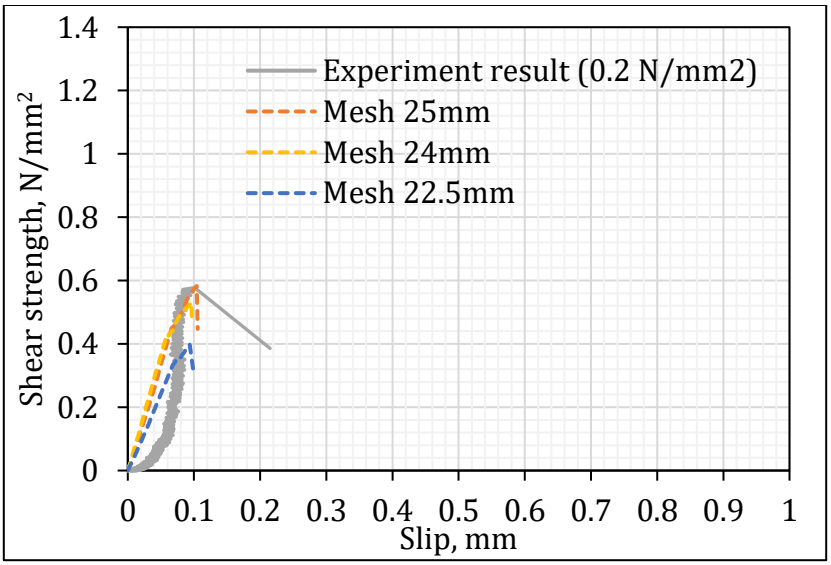

Figure 4.16. Comparative assessment between experiment and numerical results in shear test (0.2MPa)

When looking at all three cases of evaluating how the mesh size affects the results, it was found that the appropriate mesh size was 25 mm. The destruction mechanism in all three cases (0.2 MPa, 0.4 MPa, and 0.6 MPa) is similar and true to the behavior in the experiment. First, one of the two brick-mortar joints, the one with the lower adhesion, it will show the first crack. Then the crack widens in the direction from bottom to top. It can be seen that the shear stress on the general surface is not evenly distributed because the surface of the steel plate does not cover the entire suface of the central brick. This leads to the relative displacement of positions on the interface, which is also irregular.

4.5. Numerical analysis of torsion test

4.5.1. Effect of mesh size and flexural strength of brick-mortar interface

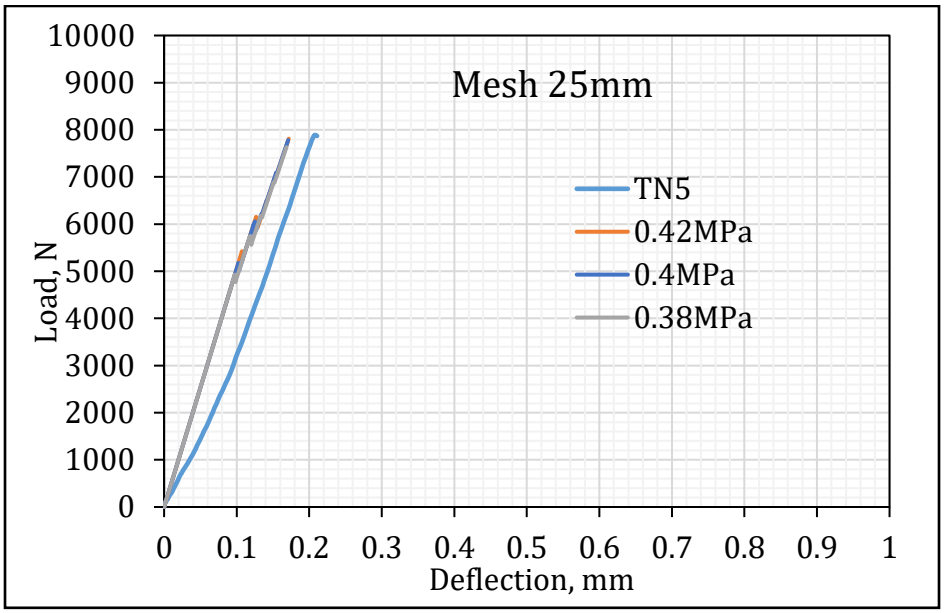

Figure 4.17. Comparative assessment between experiment and numerical results in torsion test (Effect of flexural strength of brick-mortar interface)

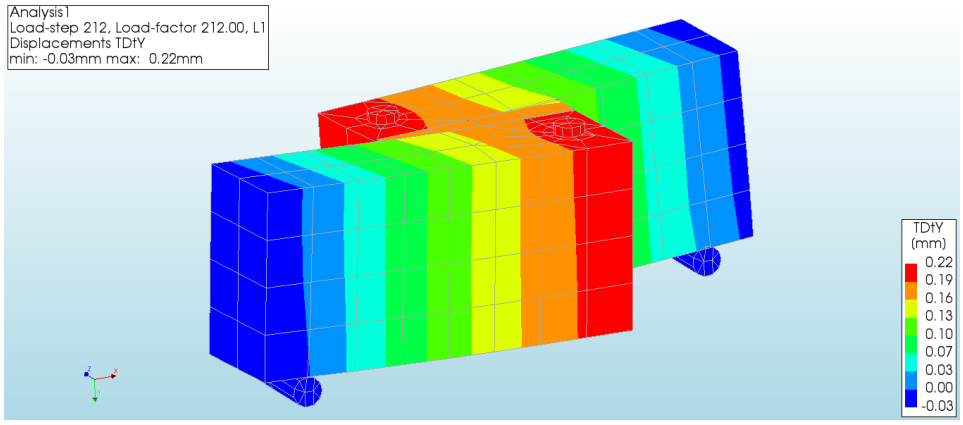

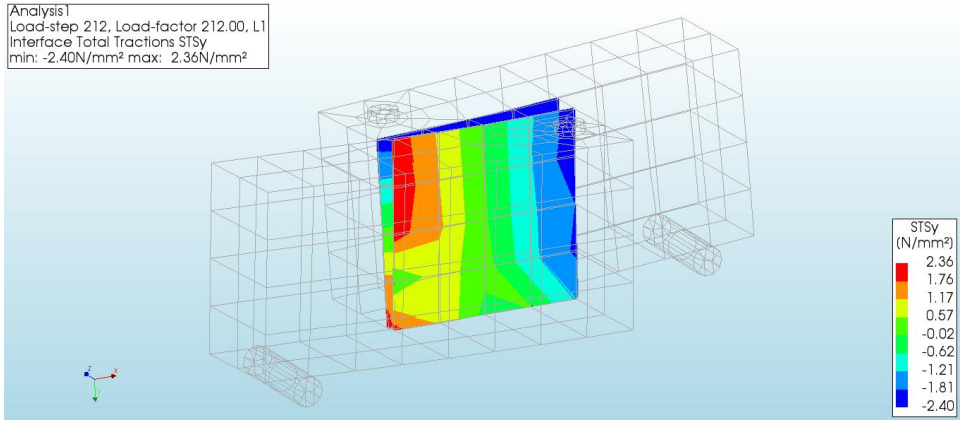

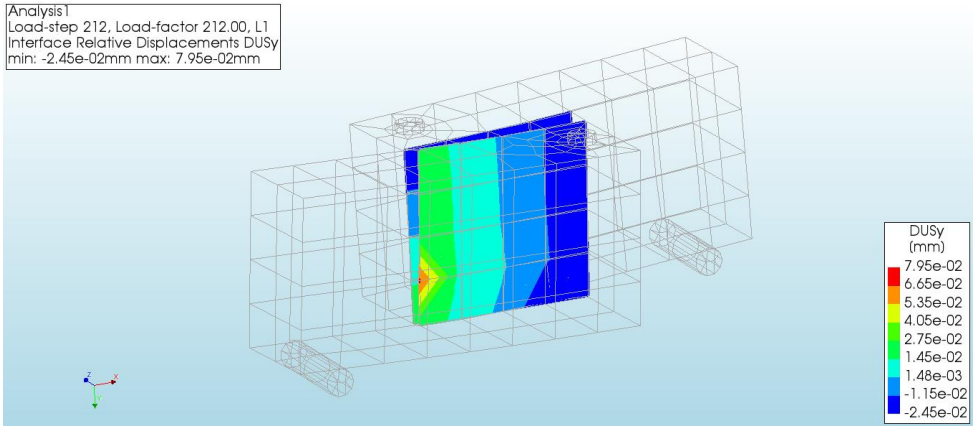

a1. 25mm, 0.4MPa

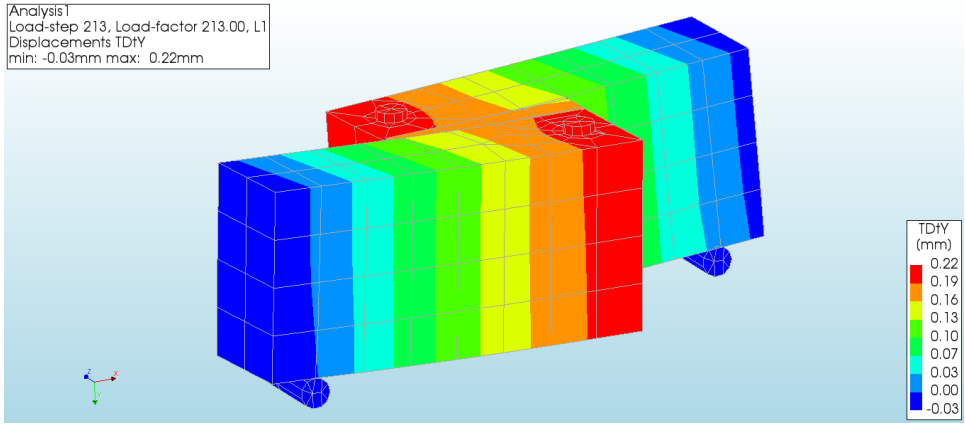

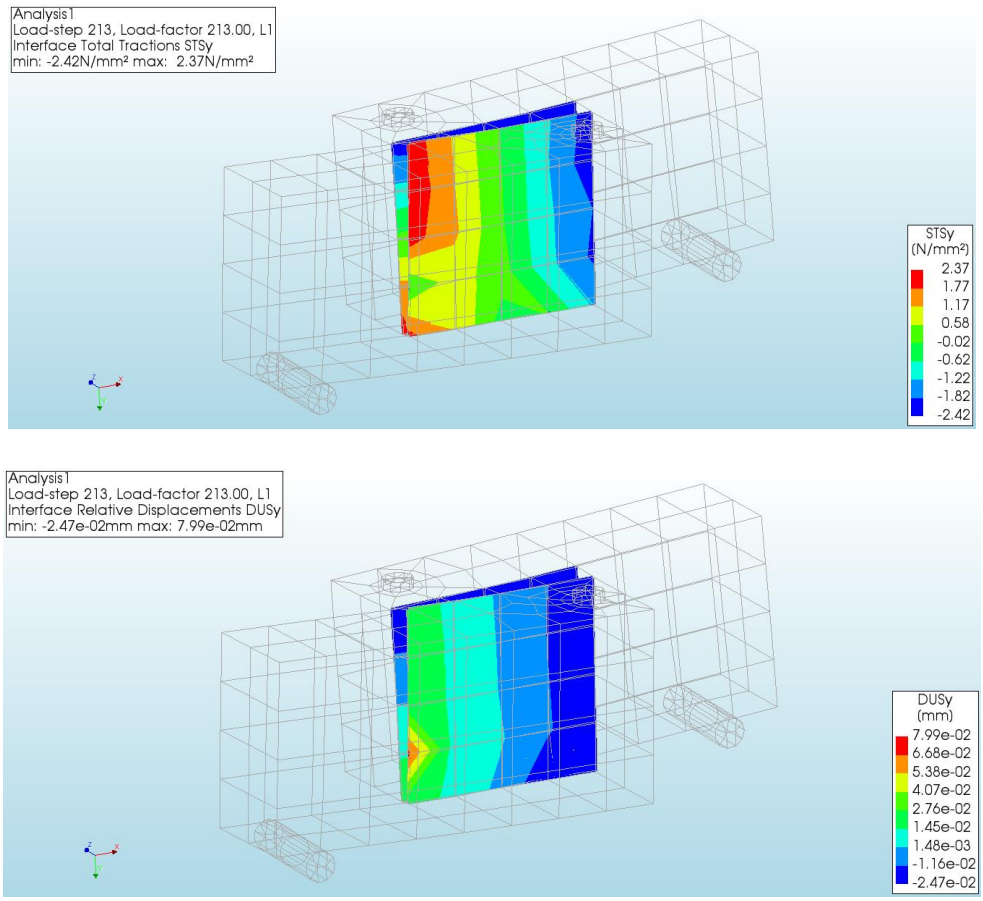

b1. 25mm, 0.42MPa

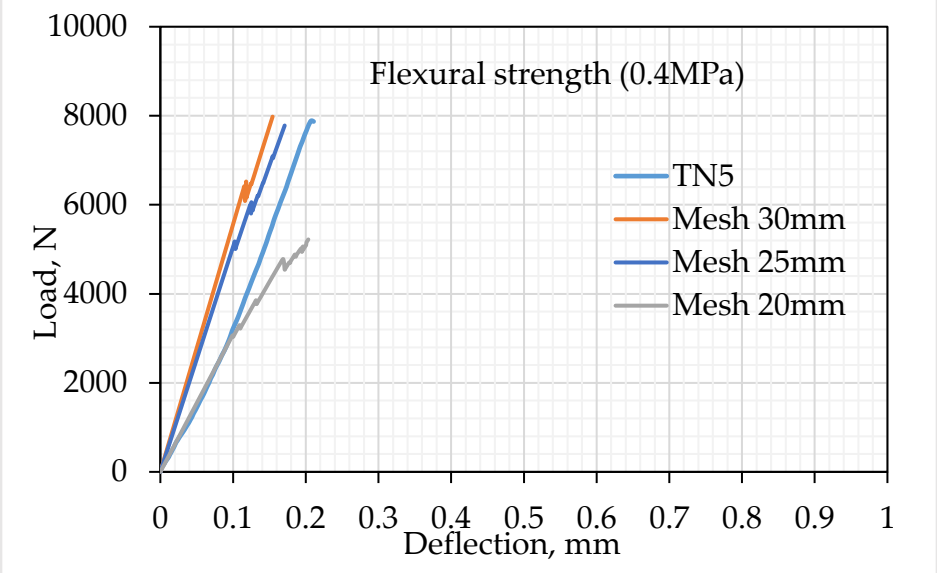

Figure 4.18. Comparative assessment between experiment and numerical results in torsion test (Effect of mesh size)

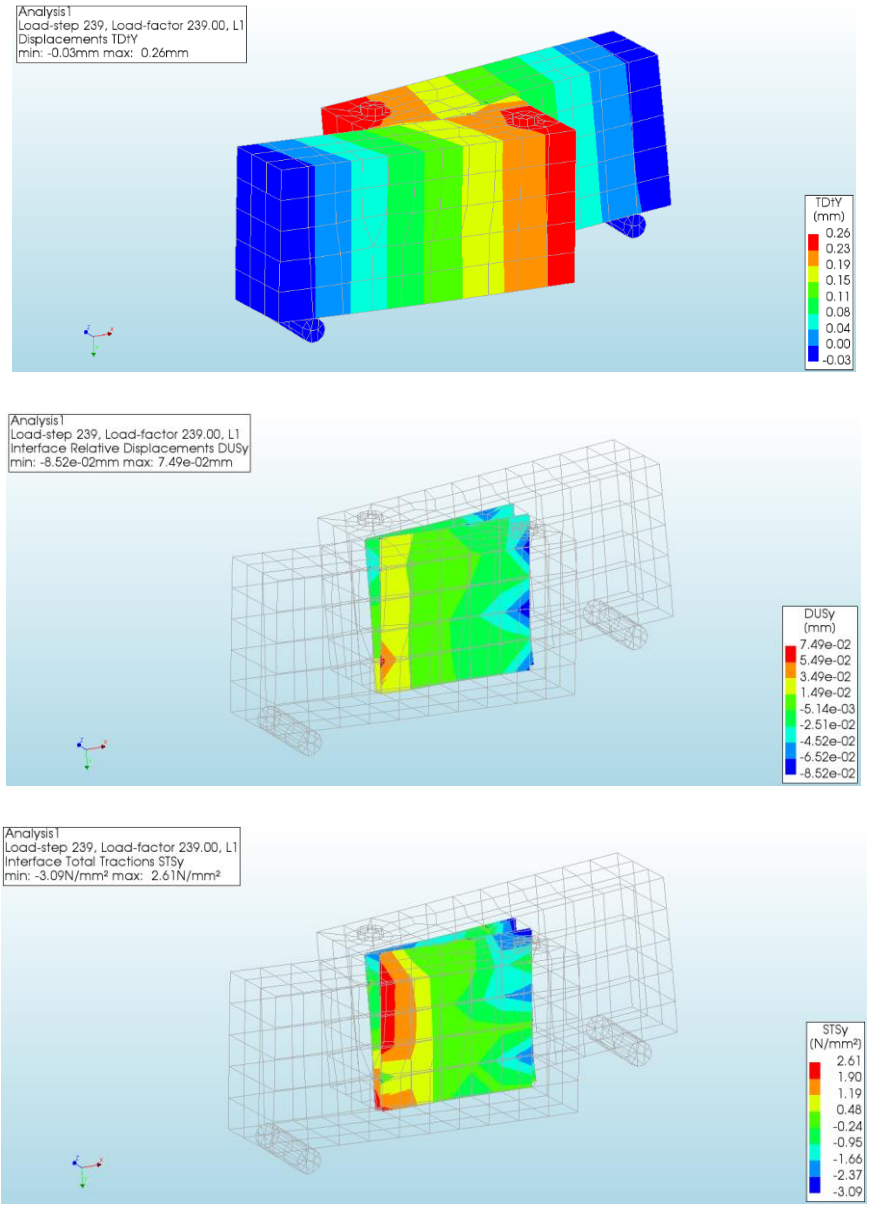

a2. 20mm, 0.4MPa

The influence of mesh size and bending strength has also been evaluated in figures a and b. The suitable mesh size and bending strength ranges are 25–30 mm and 0.4-0.42 MPa, respectively. Regarding the destruction mechanism, there is no difference in the cases, similar to the behavior in the experiment.

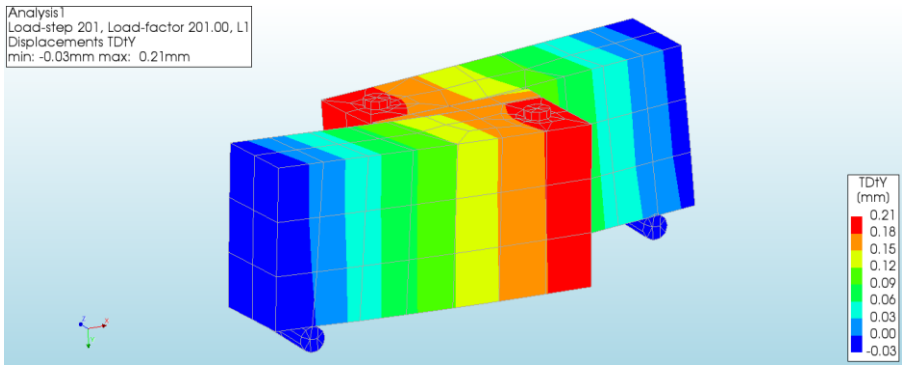

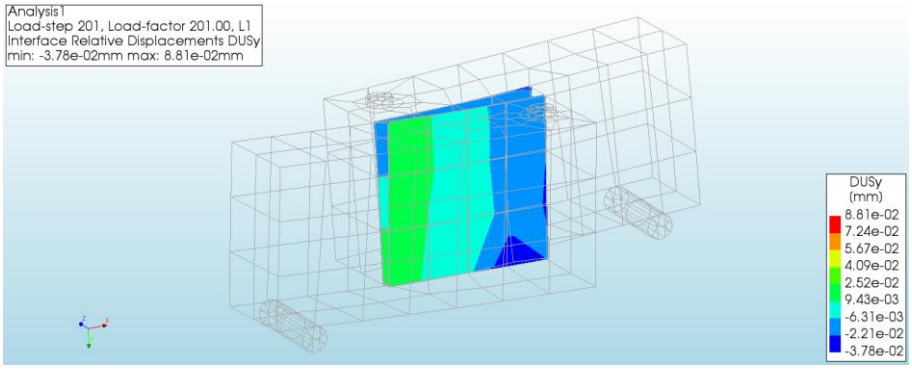

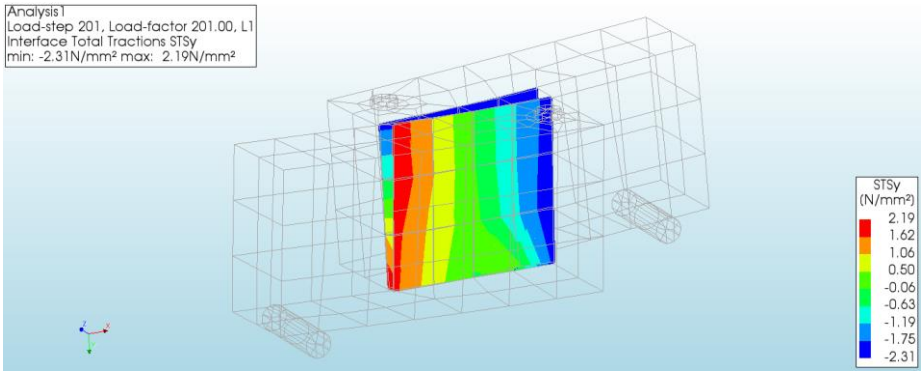

b2. 30mm. 0.4MPa

4.6. Conclusions

In this chapter, tests of bending, shear, and torsional behavior of small masonry reinforced by the proposed method were conducted. The results show that the proposed method is effective in all tests. Especially in bending behavior. In addition, numerical studies have also been performed using the results obtained from experiments. Detailed micro-modelling approach surveys on the three components of brick, mortar, and the joint surface between brick and mortar show compatibility. The influence of node size and flexural strength was investigated. The results demonstrate that the appropriate node size range in the model is between 25 and 30 mm, and the bending strength of 0.34 MPa is suitable for the model. In addition, the failure model of specimens without the PP band in the experiment and analysis tests showed similarities at positions and damaged shapes. In almost all of them, the failure appeared at the brick-mortar joint.

Modeling of the specimen with the PP band was also performed with the bending test as a representative. However, the effective working stage of the PP band in ultimate failure has not been reached. This will be resolved in the following research by focusing on the bond model between steel washers and PP bands.

CHAPTER 5. SUMMARY AND CONCLUSIONS

5.1. SUMMARY

In order to develop a PP band fixing method for strengthening unreinforced brick masonry, a new method was proposed. An applicability of the proposed method for small specimens was investigated by conducting flexural, shear, and torsion tests. The objectives of this research are threefold. First, to evaluate the correctness of the proposed method and the suitability of using two steel plates to clamp the PP band. The second objective is to study the applicability of PP strips on small samples. The third objective is to verify the destruction model using numerical modeling. Then, draw conclusions.

A total of 49 small specimens were test in the course of this research, nine specimens in flexural test, thirty triplet masonry specimens in shear tests, and ten specimens in torsion test

The analytical portion of the research is employed to describe the flexural, shear and torsion behavior of all tested specimens and for comparison with the experimental results.

5.2. CONCLUSIONS

Based on the observations of the experimental investigations, the following conclusions were drawn.

1. Strengthening the prism specimens with PP bands in the flexural tests significantly improved their performances in terms of load-carrying capacities and deflections at the first crack and ultimate failure that were the findings in this study. The PP band specimens showed 1.70 times and 1.62 times higher than those of the non PP band specimens. Improvements in the load-carrying capacity and deflection capacity were observed.
2. In the shear tests, the strengthened specimens represented negligible increases in the shear strength at the peak load, for all pre-compression ranges of 0 – 0.6 N/mm^2. After the specimens were damaged, the load did not increase and gradually decreased.

Therefore, the use of the PP band is not yet effective for strengthening triplet specimens under pre-compression.

3. In the torsion tests, improvements in the load-carrying capacity and deformation capacity at the first crack were observed as 1.21 times and 1.47 times, respectively. Nevertheless, at ultimate failure, the load-carrying capacity was lower than that at the first crack even though PP bands were also effective in increasing load. Thanks to PP band strengthening, the collapse times of the specimens were extended.
4. The proposed fixing method was effective in improving performances, restricting separation at the brick-mortar interface, and maintaining specimen's integrity particularly in the flexural tests.
5. In numerical analysis work, the use of a detailed micro-modelling approach accurately described the behavior of the small sample. However, for a more detailed view, in-depth assessments need to be performed.

REFERENCES

1. UNDP 2015, Strengthening disaster risk governance. UNDP Support during the HFA Implementation
2. CRED, EM-DAT 2015, The international Disaster Database
3. GSO. 2009. Vietnam Population and Housing Census 2009. Migration and Urbanisation in Vietnam: Conditions, Trends, and Differences. Ministry of Planning and Investment, General Statistics Office, Hanoi.
4. ADPC. 2007. Promoting safer housing construction through CBDRM: Community-designed safe housing in PostXangsane Da Nang City. Safer Cities 19. Thailand.
5. Central Population and Housing Census Steering Committee, Socialist Republic of Vietnam, the 2009 Vietnam Population and Housing Census Major Findings, 2009, Table 9.2, 122.
6. Davis, I. 1978. Shelter after disaster. Oxford Polytechnic.
7. Chantry, G. and Norton, J. 2008. Vaccinate your home against the storm – reducing vulnerability in Vietnam. Open House International 33, 26–31
8. Charlesworth, E. 2011. Home, sustainable home. Making Cities Work. Melbourne: RMIT University.
9. CCFSC. 2011. Disaster data in Vietnam. Central Committee for Flood and Storm Control (CCFSC) website. See www.ccfsc.gov.vn/kw6f2b34/disaster-database.aspx. Accessed September 2011
10. Hoang, V.H. 2011. Housing and Climate Change: Adaptation Strategies in Vietnam. In: Kumssa, B.Y.A.A. (ed.) Climate Change and Sustainable Urban Development in Africa and Asia. Springer Science+Business Media
11. MONRE. 2012. Scenarios of Climate Change and Sea Level Rise in Vietnam. Ministry of Natural Resource and Environment (MONRE), Hanoi
12. EM-DAT. 2012. The International Disaster Database. See www.emdat.be/database.
13. Ly, P., Birkeland, J. and Demirbilek, N. 2010. Applying environmentally responsive characteristics of vernacular architecture to sustainable housing in Vietnam. Sustainable Architecture & Urban Development, CSAAR Press, Amman, 287–306. See www.irbnet.de/daten/iconda/CIB_DC22717.pdf

14. Susanta Banerjee et al 2018. Enhancing shear capacity of masonry wallet using PP band and steel wire mesh. TOP Conf.Series: Materials Sience and Engineering 431.
15. Susanta Banerjee et al 2019, Enhancing the flexural behavior of masonry wallet using PP band and Steel wire mesh. Construction and Building Materials 194, 179-191.
16. Susanta Banerjee et al 2020, Augmenting the seismic performance of masonry models using polypropylene band and steel wire mesh through shaking table testing, Structure 26, 340-347.
17. Susanta Banerjee et al 2021. Seismic performance enhancement of masonry building models strengthened with the cost-effective materials under bi-directional excitation, Engineering Structure 242, 112516
18. Sanket Nayak and Sekhar Chandra Dutta 2015. Improving seismic performance of masonry structures with openings by polypropylene bands and L-shaped reinforcing bars, Performane of Constructed Facilities 30(2).
19. Sanket Nayak and Sekhar Chandra Dutta 2016. Failure of masonry structures in earthquake: A few simple cost-effective techniques as possible solutions. Engineering Structures 106:53-67.
20. Jamshid Zohreh Heydariha et al 2019. Experimental and field performance of PP band-retrofitted masonry: evaluation of seismic behavior. Performance of Constructed Facilities 33.
21. S. Ebrahimzadeh and K. Nasrollahzadeh 2023. Experimental study on performance of repaired and strengthened unreinforced masonry walls using polypropylene bands. Transactions on Civil Engineering 30, 918-935.
22. Zhao Wenyang et al 2023. Experimental study on the seismic performance of masonry wall reinforced by cement mortar and polypropylene band. Earthquake Engineering and Engineering Vibration 22, 469-479.
23. Sathiparan, Mayroca, Meguro 2010. Experimental study on static and dynamic behavior of PP band mesh retrofitted adobe masonry structure. 7th International Conference on Urban Earthquake Engineering (7CUEE) & 5th International Conference on Earthquake Engineering.

24. Navaratnarajah Sathiparan, Meguro 2012. Shaking Table Tests on ¼ Scale PP-band Retrofitted Model of Low Earthquake Resistant Masonry Houses. Earthquake Spectra 28, 277-299.
25. Sathiparan, Meguro 2013. Experimental investigation on the seismic performance of PP band strengthening stone masonry houses. Bulletin of Earthquake Engineering 11, 2177-2196.
26. Sathiparan, Meguro 2013. Shear and flexural bending strength of masonry wall retrofitted using PP band mesh. ConstructII Journal 14, 3-12.
27. Sathiparan, Meguro 2014. Seismic evaluation of earthquake resistance and retrofitting measures for two story masonry houses. Bulletin of Earthquake Engineering 12, 1805-1826.
28. Dar, Umair, Meguro 2014. Reduction of PP band mesh connectivity for masonry structure retrofitting. Japan Society of Civil Engineers Ser A1 70, 586-595.
29. Sathiparan and Meguro 2015. Strengthening of adobe houses with arch roofs using tie-bars and polypropylene band mesh. Construction and Building Materials 82, 360-375.
30. SM Umair, M Numada, Meguro 2015. Fiber reinforced polymer and Polypropylene composite retrofitting technique for masonry structures. Polymers 7, 963-984.
31. M.Umair Saleem et al. 2016. Seismic response of PP band and FRP retrofitted house models under shake table testing. Construction and Building Materials 111, 298-316.
32. Pranoy Debnath, Sekhar Chandra Dutta 2023. In plane and out of plane strength of different masonry bonds along with the effect of some waste materials for strengthening masonry wallets. Bulding Engineering 73, 106766.
33. Navaratnarajah Sathiparan and Kimiro Meguro 2011. Seismic behavior of low earthquake resistant arch shaped roof masonry houses retrofitted by PP band meshes. Practice Periodical on Structural Design and Construction 17, 54-64.
34. Navaratnarajah Sathiparan et al 2013. Experimental investigation on the seismic performance of PP band strengthening stone masonry houses. Bulletin of Earthquake Engineering 11, 2177-2196.

35. Zhao Wenyang et al 2023. Study on bending tensile performance of brick masonry reinforced with PP band. Engineering Mechanics 190, 158-166.
36. Santhosh. L. S et al 2019. Review on performance of polypropylene band-Retrofitted masonry: Evaluation of seismic behavior. International Research Journal of Engineering and Technology 6.
37. Architectural Institute of Japan (AIJ). Technical Information for Disaster Mitigation of Masonry Structure, March 2017.
38. Willis, C.R. Design of unreinforced masonry walls for out-of-plane loading. Ph.D. Thesis, University of Adelaide, Australia, November 2004.
39. Lang-Zi, C.; Jan, G.R.; Rita, E. Influence of aspect ratio and pre-compression on force capacity of unreinforced masonry wall in out-of-plane two-way bending. *Journal of Engineering Structures* 2021, 249, 113350.
40. Vasconcelos, G.; Lourenco, P. Experimental characterization of stone masonry in shear and compression. *Journal of Construction and building Materials 2009*, 23, 3337-3345.
41. JIS R 1250. Common bricks and facing bricks. Japanese Industrial Standards Committee, Tokyo, Japan, 2011.
42. JIS R 2213. Test method for modulus of rupture of refractory bricks. Japanese Industrial Standards Committee, Tokyo, Japan, 1995.
43. JIS R 5201. Physical testing methods for cement. Japanese Industrial Standards Committee, Tokyo, Japan, 2015.
44. JIS Z 1527. Polypropylene band. Japanese Industrial Standards Committee, Tokyo, Japan, 2002.
45. ASTM E518-03. Standard test methods for flexural bond strength of masonry. American Society for Testing and Materials: West Conshohocken, PA, USA, 2010.
46. RILEM TC 127-MS. Tests for masonry materials and structures. Material and Structures 1996, 29, 459-475.
47. Hansen, K.F.; Pedersen, C.M. Torsion testing of bed joints. *International Masonry Society* 2008, 21.
48. Hansen, K.F.; Pedersen, C.M. Shear and Torsion testing of brick-mortar joints. *International Masonry Society* 2009, 22, 31-38.

49. P. B. Lourenço and J. G. Rots, “Multisurface Interface Model for Analysis of Masonry Structures,” Journal of Engineering Mechanics, vol. 123, no. 7, p. 660–668, 1997.
50. R. Weyler, J. Oliver, T. Sain and J. Cante, “On the Contact Domain Method: A Comparison of Penalty and Lagrange Multiplier Implementations,” Computer Methods in Applied Mechanics and Engineering, vol. 205–208, p. 68–82, 2012
51. R. van der Pluijm, “Shear behaviour of bed joints,” in 6th North American Masonry Conference, 6-9 June 1993, Philadelphia, Pennysylvania, USA, 1993.
52. R. Serpieri, M. Albarella and E. Sacco, “A 3D Microstructured Cohesive–frictional Interface Model and Its Rational Calibration for the Analysis of Masonry Panels,” International Journal of Solids and Structures, vol. 122–123, p. 110–127, 2017.
53. M. Godio, I. Stefanou and K. Sab, “Effects of the dilatancy of joints and of the size of the building blocks on the mechanical behavior of masonry structures,” Meccanica, 2017.
54. R. van der Pluijm, H. Rutten and M. Ceelen, “Shear behaviour of bed joints,” in Proceedings of the Twelfth International Brick/Block Masonry Conference, 2000.
55. J. Lee and G. L. Fenves, “Plastic-Damage Model for Cyclic Loading of Concrete Structures,” Journal of Engineering Mechanics, vol. 124, no. 8, p. 892–900, 1998.
56. M. Petracca, L. Pelà, R. Rossi, S. Zaghi, G. Camata and E. Spacone, “Micro-Scale Continuous and Discrete Numerical Models for Nonlinear Analysis of Masonry Shear Walls,” Construction and Building Materials, vol. 149, p. 296–314, 2017.
57. P. B. Lourenço, “Computations on Historic Masonry Structures,” Progress in Structural Engineering and Materials, vol. 4, no. 3, p. 301–319, 2002.